ChemComm

FEATURE ARTICLE

Cite this: *Chem. Commun.*, 2016, 52, 4418

Research progress on polyoxometalate-based transition-metal–rare-earth heterometallic derived materials: synthetic strategies, structural overview and functional applications†

Jun-Wei Zhao,*[a] Yan-Zhou Li,[a] Li-Juan Chen[a] and Guo-Yu Yang*[b]

Received 21st December 2015,
Accepted 5th February 2016

DOI: 10.1039/c5cc10447e

www.rsc.org/chemcomm

With the rapid development of science and technology and the trend of multidisciplinary pervasion, POM-based TM–RE heterometallic chemistry (POM = polyoxometalate, TM = transition-metal, RE = rare-earth) has become one of the most rapidly growing and challengeable areas of inorganic chemistry due to the impressive structural diversities, various chemical compositions and potential applications of these materials in magnetism, optics, electrochemistry, electrocatalysis and materials science. Over the past several years, continuous interest and persisting efforts have been dedicated to the preparation and exploration of POM-based TM–RE heterometallic derived materials (PTRHDMs), which have led to more than two hundred PTRHDMs. In this review, we summarize the structural types of reported PTRHDMs together with synthetic strategies, structural motifs and relevant functional applications. The exciting array of this emerging research theme presages continuous growth and great vitality. In the last section, some prospects of this branch are also presented and possible guidance for future work is outlined.

1. Introduction

Polyoxometalates (POMs) are a unique and important class of metal–oxygen anionic clusters of early transition-metals (TMs) usually in their d^0 or d^1 electronic configurations (such as V^V, Nb^V, Ta^V, Mo^{VI}, Mo^V, or W^{VI}) bridged by oxygen atoms (formally O^{2-} or occasionally HO^- ions).[1–5]

The history of POM chemistry has been known for nearly two centuries since the first report of what we term a POM dates back to the 19th century, as it is generally admitted that the first compound of this class (the ammonium salt of $PMo_{12}O_{40}^{3-}$) was discovered by Berzelius in 1826.[6,7] In 1934, the first structural determination of phosphotungstic acid $H_3[PW_{12}O_{40}]\cdot 29H_2O$ was reported by Keggin by means of a powder X-ray diffraction study.[8] From then on, the worldwide interest in the POM

[a] Henan Key Laboratory of Polyoxometalate Chemistry, Institute of Molecular and Crystal Engineering, College of Chemistry and Chemical Engineering, Henan University, Kaifeng, Henan 475004, P. R. China. E-mail: zhaojunwei@henu.edu.cn
[b] MOE Key Laboratory of Cluster Science, School of Chemistry, Beijing Institute of Technology, Beijing 100081, P. R. China. E-mail: ygy@bit.edu.cn; Fax: +86-10-68918572

† Electronic supplementary information (ESI) available. See DOI: 10.1039/c5cc10447e

Jun-Wei Zhao

Jun-Wei Zhao received his PhD in 2008 under the supervision of Prof. Guo-Yu Yang in the Fujian Institute of Research on the Structure of Matter, Chinese Academy of Sciences. After that, he joined the faculty of Henan University and was promoted to a full Professor of chemistry in 2014. Currently, he is mainly engaged in the synthesis and preparative chemistry of POM-based functional materials and the relevant optical, electrical, magnetic and biological properties.

Yan-Zhou Li

Yan-Zhou Li received her BS degree from Henan University in 2014. Then she joined the Fujian Institute of Research on the Structure of Matter, Chinese Academy of Sciences, as a graduate student.

discipline and the rate of discovering novel species have steadily increased. Historically, the successful industrialization of the production of isopropylalcohol by hydration of propylene catalyzed by $H_4SiW_{12}O_{40}$ in Japan in 1972 further ignited the extensively increasing interest throughout the world.[9] The research surge in the structural assembly chemistry and the potential of POMs was further driven by a comprehensive review article written by Pope and Müller in 1991.[10] In 1998, a special issue of Chemical Reviews reviewed a collection of articles involving an in-depth coverage of selected topics of intellectual or technical significance and simultaneously defined the breadth of research impacted by POMs.[11] This special issue contains several fundamental and practical aspects of the research of POM chemistry: (1) elucidation of the history of POM chemistry until 1998;[12] (2) the nomenclature of POMs;[13] (3) POM derivative chemistry of main-group elements, organic and organometal groups;[14] (4) electron transfer processes in POM systems;[15] (5) POM catalytic problems;[16–18] (6) functional materials chemistry of POMs;[19–22] (7) pharmaceutical chemistry of POMs,[5] and (8) the application aspects of POMs.[23] Hitherto, POMs have developed as a rapidly growing library of inorganic oxide clusters bearing more commercial applications than other cluster compounds.[24,25] The contemporary tremendous impetus in systematic design and controllable syntheses of POM-based multifunctional materials has been provoked not only because of their stunning compositions, diversified architectures and fascinating topologies, but also by their numerous versatile potential applications in various areas such as catalysis, medicine, materials science, nanotechnology, molecular magnetism and photochemistry, and so on.[26–38]

To date, several classical structural types of POM anions have been established such as Keggin, Wells–Dawson, Lindqvist, Anderson–Evans, Weakley, Finke, Silverton, and Stranberg.[1,9,12] In the phylogeny of POM chemistry, Keggin-, Dawson- and Lindqvist-type species have long played a crucial role and occupied a special status because they can function as excellent candidates for the multistep elaboration of POM-based derived materials. Generally speaking, Keggin- and Dawson-type POMs are popular largely in the form of derivatives of polyoxotungstates (POTs) and polyoxomolybdates (POMBs), whereas Lindqvist-type ones chiefly prevail among polyoxoniobates. Since the first TM-substituted POM (TMSP) was reported by Simmons at the 1962 (Stockholm) International Conference on Coordination Chemistry (ICCC)[39] and its structure (it is an 11-tungstosilicate wherein one tungsten atom of the Keggin structure was replaced by a Co^{2+} ion) was determined at the 1966 (St. Moritz) ICCC,[40] the TMSP synthetic chemistry has undergone a great deal of development and has generally dominated the research forefront of POM science. The vast growth in the number of assembled TMSPs with an unmatched range of physical and chemical properties may originate from thousands of combinatorial possibilities between POM fragments and relevant ingredients, in which each POM building block can adopt variable isomers. During the course of assembling TMSPs, lacunary POT precursors were widely employed as the starting materials due to their easy availability in one- or two-step processes in high yield.[41] The commonly used lacunary POT precursors can be classified into four major categories according to the number of tungsten atoms removed compared to their plenary parent structures: (a) monovacant precursors such as $[\alpha\text{-}XW_{11}O_{39}]^{7/8-}$ ($X = P^V$, Si^{IV}, Ge^{IV}) that are derived from the α-Keggin $[\alpha\text{-}XW_{12}O_{40}]^{3/4-}$ parent polyoxoanion (POA) with T_d symmetry by the removal of a $W{=}O_t$ group,[42a] $[\beta_1\text{-}SiW_{11}O_{39}]^{8-}$, $[\beta_2\text{-}SiW_{11}O_{39}]^{8-}$ and $[\beta_3\text{-}SiW_{11}O_{39}]^{8-}$ that originate from the β-Keggin $[\beta\text{-}SiW_{12}O_{40}]^{4-}$ POA with C_{3V} symmetry by respectively removing a $W{=}O_t$ group at three

Li-Juan Chen

Li-Juan Chen gained her BS and MS degrees in chemistry from Henan University in 2005 and obtained her PhD in 2009 under the supervision of Prof. Jian-Min Chen at the Lanzhou Institute of Chemical Physics, Chinese Academy of Sciences. In 2009, she joined Henan University. In 2013, she was promoted to an associate professor. Her research interest is principally focused on coordination chemistry of POMs and photophysical properties of POM-based materials.

Guo-Yu Yang

Guo-Yu Yang graduated from Jilin University in 1988, and received his MS and PhD from Jilin University in 1991 and 1998, respectively. In 1991, he joined the faculty at Jilin University. From 1998 to 2001, he worked as a postdoctoral fellow in the University of Notre Dame and Stockholm University successively. Since 2001, he has been working at the Fujian Institute of Research on the Structure of Matter, Chinese Academy of Sciences, as a professor of chemistry. In 2014, he joined the Beijing Institute of Technology. His research interest is focused on (1) oxo cluster chemistry, including transition-metal, main-group, and rare-element clusters, as well as cluster–organic frameworks; and (2) the functionality of oxo clusters, including nonlinear optical properties, magnetic properties, and catalytic properties.

different positions,[42b] $[\alpha_1\text{-}P_2W_{17}O_{61}]^{10-}$ and $[\alpha_2\text{-}P_2W_{17}O_{61}]^{10-}$ that result from the Wells–Dawson $[\alpha\text{-}P_2W_{18}O_{62}]^{6-}$ POA with D_{3h} symmetry by respectively removing a W=O$_t$ group at the belt position and at the cap position;[42a] (b) divacant precursors such as $[\gamma\text{-}XW_{10}O_{36}]^{7/8-}$ (X = P^V, Si^{IV}, Ge^{IV}) that can be visualized as a derivative of the γ-Keggin $[\gamma\text{-}XW_{12}O_{40}]^{3/4-}$ POA with C_{2v} symmetry by the removal of a W_2O_4 unit,[43–45] and $[As_2W_{19}O_{67}(H_2O)]^{14-}$ derived from the parent $[As_2W_{21}O_{69}(H_2O)]^{6-}$ with C_{2v} symmetry *via* removing two WO bridging units;[46] (c) trivacant precursors such as $[A\text{-}\alpha\text{-}XW_9O_{34}]^{9/10-}$ (X = P^V, As^V, Si^{IV}, Ge^{IV}) generated by removing three WO_6 octahedra from three different W_3O_{13} units in a saturated Keggin $[\alpha\text{-}XW_{12}O_{40}]^{3/4-}$ POA, $[B\text{-}\alpha\text{-}XW_9O_{34}]^{9/10-}$ (X = P^V, As^V, Si^{IV}, Ge^{IV}) formed by the removal of a W_3O_{13} unit from a plenary Keggin $[\alpha\text{-}XW_{12}O_{40}]^{3/4-}$ POA,[47,48] $[A\text{-}\alpha\text{-}XW_9O_{33}]^{8/9-}$ and $[B\text{-}\alpha\text{-}XW_9O_{33}]^{8/9-}$ (X = Te^{IV}, As^{III}, Sb^{III}, Bi^{III}),[49–52] and $[\alpha\text{-}P_2W_{15}O_{56}]^{12-}$ formed by the removal of a W_3O_6 unit from a saturated Wells–Dawson $[\alpha\text{-}P_2W_{18}O_{62}]^{6-}$ POA;[53] (d) multivacant precursors: the metastable hexavacant Dawson $[\alpha\text{-}H_2P_2W_{12}O_{48}]^{12-}$ POA made by the degradation of [α- or β-$P_2W_{18}O_{62}]^{6-}$ under alkaline conditions,[54] which can be considered to be formed by the symmetrical removal of two $\{WO_6\}$ octahedra at two cap positions and four corner-sharing $\{WO_6\}$ octahedra at the belt position in the D_{3h} Wells–Dawson $[\alpha\text{-}P_2W_{18}O_{62}]^{6-}$ POA; the D_{4h} symmetric $[H_7P_8W_{48}O_{184}]^{33-}$ POA synthesized by making use of dilute $[\alpha\text{-}H_2P_2W_{12}O_{48}]^{12-}$ solution,[55] which may be viewed as a condensed tetramer of $[\alpha\text{-}H_2P_2W_{12}O_{48}]^{12-}$ moieties, alternatively, which can be regarded as a cyclic octamer of hexavacant $[PW_6O_{23}]^{5-}$ fragments that are derived from the Keggin POA by the removal of two corner-sharing triads of $\{WO_6\}$ octahedra;[19] and the D_{3h} symmetric $[NaSb_9W_{21}O_{86}]^{18-}$ POA that consists of three $[SbW_7O_{28}]^{11-}$ subunits linked to a central core of two $\{Sb_3O\}$ groups encapsulating a sodium cation,[56] where the $[SbW_7O_{28}]^{11-}$ units can be considered as pentavacant derivatives of the hypothetical $\{\beta\text{-}SbW_{12}\}$ anion. These lacunary POM precursors can often work as excellent multidentate inorganic ligands to coordinate to TM electrophiles for the design and construction of TMPS aggregates with different dimensionalities by judicious selection of appropriate TM centers and functional organic ligands.[7,38,57,58] Especially, due to the synergistic effect of the strong Lewis acidity, Brønsted acidity and reversible redox activity, POM components and electrophilic TM cations serve as effective solid acid catalysts and electron transfer catalysts for diverse organic reactions.[38,59–61] TMSPs are oxidative, hydrolytically stable and have different types of catalytically active sites, which can generally influence the catalytic activity and selectivity for epoxidation.[62] Thus, various H_2O_2-based epoxidation systems catalyzed by various TMSPs have been extensively developed. It has been proven that Zn, Ti, Fe and Mn-substituted POMs can function as effective catalysts for H_2O_2-based epoxidation reactions.[62–66] For example, Yamase's group put forward that the η^2-peroxo Ti(O_2) species produced by reacting $[PTi_xW_{12-x}O_{40}]^{(3+2x)-}$ with H_2O_2 was an active intermediate for epoxidation of olefins.[67,68] Neumann *et al.* discovered that the nickel-substituted polyfluorooxometalate $[Ni(H_2O)H_2F_6NaW_{17}O_{55}]^{9-}$ was the most active for H_2O_2-based epoxidation of olefins and allylic alcohols among polyfluorooxometalates.[69] Hill *et al.* reported the methyltricaprylammonium salt of $[((Mn^{II}OH_2)Mn^{II}_2PW_9O_{34})_2(PW_6O_{26})]^{17-}$ that can effectively catalyze the epoxidation of cyclooctene, cyclohexene and 1-hexene.[70] Mizuno and coworkers found that the di-Fe^{III} substituted silicotungstate $[\gamma\text{-}SiW_{10}\{Fe(OH_2)\}_2O_{38}]^{6-}$ can catalyze the selective epoxidation of olefins as well as alkanes with highly efficient utilization of hydrogen peroxide.[71–74] Furthermore, diamagnetic POM matrices can accommodate a large number of spin-coupled magnetic TM clusters at specific sites, which not only guarantee an effective magnetic isolation of TM clusters from each other so that intermolecular interactions are usually negligible, providing a good opportunity for investigating magnetic exchange interactions at the molecular and atomic levels, but also can control the magnitude of magnetic couplings.[75–77] Müller, Coronado and Kortz reviewed the magnetic chemistry of some TMSPs in 1998,[19] 1999[75] and 2009,[78] respectively. In 2012, Mialane's group and Yang's group also summarized synthetic conditions and magnetic properties of some TMSPs from different aspects.[34,79] In other words, reports on TMSPs are too numerous to mention one by one herein. Compared with TM cations, RE cations possess the following characteristics: (i) the lanthanide (Ln) series display a Ln contraction effect; (ii) because 4f orbitals of Ln cations are efficiently shielded by outer fully occupied 5s and 5p orbitals, the ligand field stabilization energies of the Ln-based complexes are lower than those of TM-based complexes; (iii) according to the Hard and Soft Acids and Bases (HSAB) theory,[80] RE ions are oxyphilic and can easily coordinate to oxygenic ligands; (iv) the ligand field has a weak effect on 4f electronic configuration, thus the absorption spectra are line-shaped whereas the d-block TM absorption spectra are band-shaped; (v) RE ions have fascinating photophysical properties such as strong fluorescence and long lifetime and usually can be used to manufacture luminescent materials and laser medium;[81] (vi) due to the existence of spin–orbit coupling and the crystal field effect, the orbital contribution of the magnetic moment is much more important for RE ions compared to TM ions, unquenched orbital angular momentum results in magnetic anisotropy and a large number of unpaired 4f electrons lead to high spin, as a result, lanthanide complexes are being vigorously utilized as molecular magnetic materials including magnetic refrigeration, ultra high-density data storage and quantum computation.[82a] Therefore, it is extremely significant to introduce RE ions to POMs to construct RE substituted POMs (RESPs).[82b] The first RESP $[H_6CeMo_{12}O_{42}]^{2-}$ was discovered by Barbieri in 1914.[83] In 1971, Peacock and Weakley successively separated a family of 1 : 2 series RESPs $[RE(W_5O_{18})_2]^{9-}$, $[RE(SiW_{11}O_{39})_2]^{17-}$ and $[\alpha_2\text{-}RE(P_2W_{17}O_{61})_2]^{17-}$, which completely opened up the way to the in-depth development of RESP chemistry.[84] Subsequently, diverse 1 : 1 and 1 : 2 series RESP species were synthesized.[85–88] Liu *et al.* obtained a series of Anderson-type derivatives $[RE(H_2O)_4]_2[TeMo_6O_{24}]\cdot 3H_2O$ (RE = La^{III}, Ce^{III}, Nd^{III}),[89] $\{[Eu(H_2O)_7]_2(TeMo_6O_{24})\}\cdot 5H_2O$,[90] and $\{[Sm(H_2O)_5]_2(TeMo_6O_{24})\}\cdot 6H_2O$[90] by reaction of precursor $[TeMo_6O_{24}]^{6-}$ with RE cations. Xu *et al.* not only reported the first crystal structures for 1 : 2 type RE-substituted germanotungstate,[91] but also discovered the tetra-Ln dimers $[Ln_4(\alpha(1,4)GeW_{10}O_{38})_2(H_2O)_6]^{12-}$ (Ln = Dy^{III}, Er^{III}).[92] In 2010–2011, Hussain's group isolated a series of acetate-bridging

2 : 2-type RE-substituted germanotungstates $[\{Y(\alpha\text{-}GeW_{11}O_{39})(H_2O)\}_2(\mu\text{-}CH_3COO)_2]^{12-}$ and $[\{Ln(CH_3COO)GeW_{11}O_{39}(H_2O)\}_2]^{12-}$ (Ln = Eu^{III}, Gd^{III}, Tb^{III}, Dy^{III}, Ho^{III}, Er^{III}, Tm^{III}, Yb^{III}).[93,94] Niu *et al.* prepared inorganic–organic hybrid RESPs such as $[\{RE(NMP)_6\}(\alpha\text{-}PMo_{12}O_{40})]_n$ (RE = La^{III}, Ce^{III}, Pr^{III}),[95] $[Nd_{1.50}(\alpha\text{-}GeW_{11}O_{39})(H_2O)_6]^{3.5-}$,[96] $[Sm_2(\alpha\text{-}GeW_{11}O_{39})(DMSO)_3(H_2O)_6]^{2-}$,[96] $\{[Sm(H_2O)_{5.5}(DMF)_{0.5}]_2[Sm(H_2O)_2(DMF)][Sm(H_2O)_3(\alpha\text{-}SiW_{11}O_{39})]_2\}^{-}$,[7] and $[\{(\alpha\text{-}PW_{11}O_{39})Ln(H_2O)(\eta^2,\mu\text{-}1,1)\text{-}CH_3COO\}_2]^{10-}$ (Ln = Sm^{III}, Eu^{III}, Gd^{III}, Tb^{III}, Ho^{III}, Er^{III}; n = 6, 8).[98] Recently, on one hand, the design and assembly of large RESP aggregates have become a challenging topic. In 1997, Pope *et al.* reported a Ce_{16}-containing POT $[As_{12}Ce_{16}W_{148}O_{524}(H_2O)_{36}]^{76-}$.[99] In 2001, a unique tetrameric phosphotungstate $[(PEuW_{10}O_{38})_4(W_3O_{14})]^{30-}$ was discovered by Francesconi *et al.*[100] In 2003, two crown-shaped europium containing arsenotungstates $[K\subset\{Eu(H_2O)_2(\alpha\text{-}AsW_9O_{33})\}_6]^{35-}$ and $[Cs\subset\{Eu(H_2O)_2(\alpha\text{-}AsW_9O_{33})\}_4]^{23-}$ were communicated by Yamase.[101a] In 2005–2008, Fedin *et al.* addressed a class of 1-D, 2-D and 3-D polymeric frameworks based on nanosized molybdenum-oxide $[Mo_{36}O_{108}(NO)_4(H_2O)_{16}]^{12-}$ clusters and RE linkers.[101b–d] In 2007, an unprecedented Ce_{20}-containing decameric germanotungstate $[Ce_{20}Ge_{10}W_{100}O_{376}(OH)_4(H_2O)_{30}]^{56-}$ was prepared by Kortz's group.[102] In 2009, the longest RESP molecule $[Gd_8As_{12}W_{124}O_{432}(H_2O)_{36}]^{60-}$ was discovered by Patzke *et al.*[103] In 2013, a series of arsenotungsates $[RE_6(H_2O)_x\{As_4W_{44}(OH)_2(proline)_2O_{151}\}]^{10-}$ (Ln = Tb^{III}, Dy^{III}, x = 22; Ln = Nd^{III}, x = 26) were isolated by Wang's group.[104] A series of Ln-containing octameric peroxoisopolyoxomolybdates $[H_3RE_6(H_2O)_{26}(MoO_4)\{Mo_7O_{22}(O_2)_2\}_4]^{5-}$ (RE = Ce^{III}, Pr^{III}, Sm^{III}, Eu^{III}, Nd^{III}) and $[H_4La_5(H_2O)_{21}(MoO_4)\{Mo_7O_{22}(O_2)_2\}_4]^{7-}$ were separated by Niu *et al.*[105] On the other hand, the applications of RESPs were also explored. For example, in 1988, the antitumor activity of $[IPrNH_3]_6[Mo_7O_{24}]\cdot 3H_2O$[106] and the antiviral activity of $K_{13}[Pr(BW_{11}O_{39})_2]\cdot nH_2O$ and $K_{13}[Pr(GeW_{11}O_{39})_2]\cdot nH_2O$[107] were evaluated. In 2002, Lu *et al.* addressed an antiferromagnetic (AFM) 3-D RESP $[Gd(H_2O)_3]_3[GdMo_{12}O_{42}]\cdot 3H_2O$.[108] In 2012, Song and collaborators found that $Na_7H_2LaW_{10}O_{36}\cdot 32H_2O$ can work as the very efficient desulfurization catalyst in the $[bmim]BF_4$ ionic liquid system.[109] Recently, with the comprehensive research drive of POM chemistry, the interpenetrating trend of multidisciplines and the urgent requirement of science progress, the exploration and assembly of multifunctional PTRHDMs (Fig. 1 shows the distribution of the main constituent elements of PTHRDMs in the periodic table of elements) have become a crucial research topic. As is known to us, oxyphilic RE cations have high reactivity with POM precursors, which usually leads to precipitation instead of crystallization,[108,110] whereas the reactive activity between TM ions and POM precursors is relatively weak, and thus there exist the unavoidable competitive reactions among highly negative POM precursors, strongly oxyphilic RE cations and less active TM cations in the same reaction system.[111] As a result, it is comparatively difficult to find appropriate synthetic conditions to prepare PTRHDMs. Hitherto, more than two hundred PTRHDMs have been obtained under the persisting efforts of synthetic chemists albeit the rational design and synthesis of functional PTRHDMs are still considerably challenging issues. Our recent great efforts have been considerably dedicated to this branch. Herein, we provide the state-of-the-art progress in this area involving synthetic strategies, structural motifs and related potential applications and try to offer readers a fairly complete perspective, hoping that this current review can shed light on some useful enlightenment for the design and preparation of desired PTRHDMs with specific functionalities. The first two sections of this article are devoted to synthetic strategies and structural architectures of PTRHDMs. Important synthetic information and synthetic strategies on PTRHDMs are collected in Table S1 (ESI†) with the chronological order.[112–169] The reported PTRHDMs display a variety of stable or metastable POM secondary structural blocks primarily including Keggin, Dawson, Anderson and Evans–Showell types (Fig. 2). Amongst these secondary structural blocks, some stem from the self-assembly of simple oxometalates and others

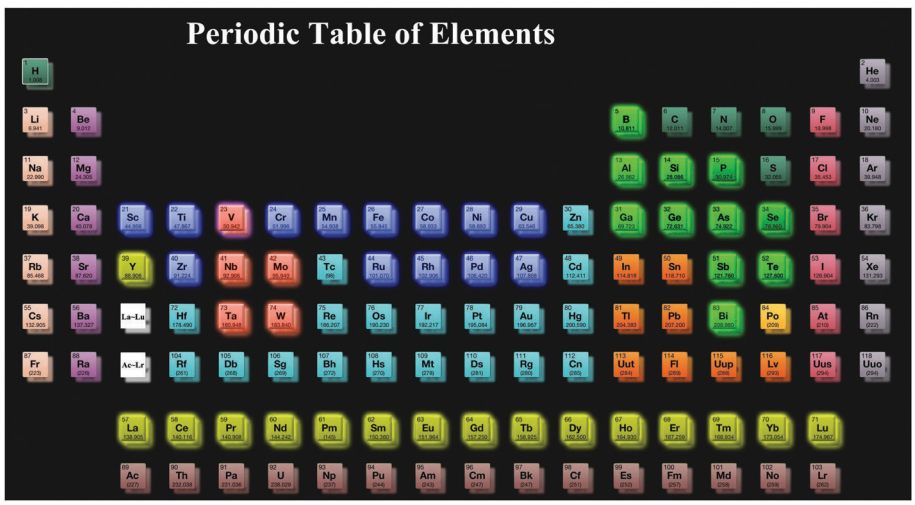

Fig. 1 The distribution of the main constituent elements of PTHRDMs in the periodic table of elements. (Skeletal elements: rose; heteroatomic elements: bright green; RE elements: gold; TM elements: bluish violet. Notably, some skeletal elements of Nb/Ta, heteroatomic elements of B/Ga/Bi/Se/Te and TM elements of Sc/Ti/Zr/Ru/Rh/Pd have not been used in the PTHRDM field to date, which offers us a great opportunity for developing new PTHRDMs.)

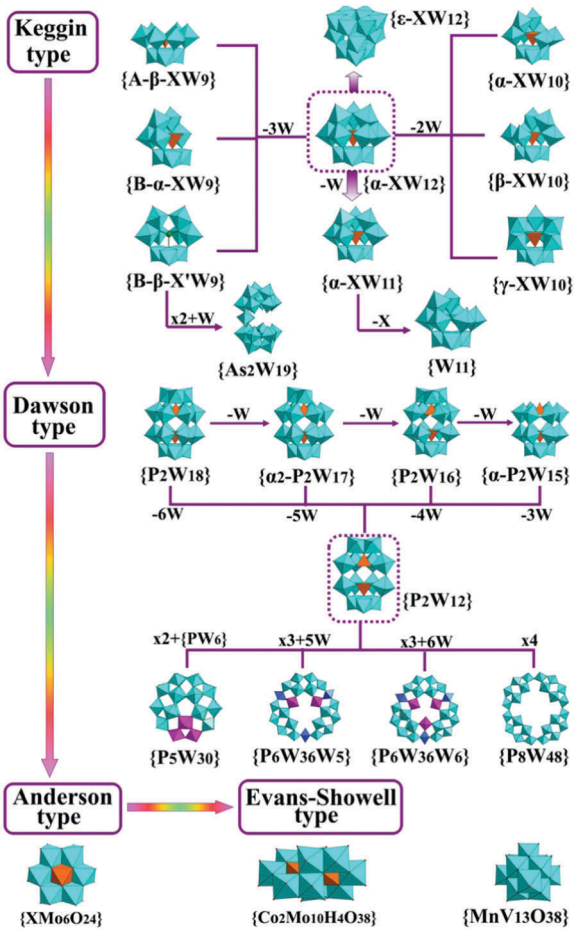

Fig. 2 Various stable or meta-stable POM secondary structural blocks indwelling in reported PTRHDMs.

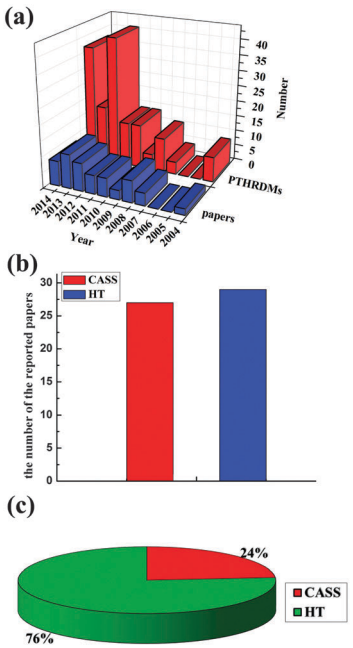

Fig. 3 (a) The statistic histogram of the numbers of reported papers and as-synthesized PTRHDMs between 2004 and July, 2015. (b) The distribution of the already reported papers based on two synthetic methods. (c) The pie chart of the percentage of reported PTRHDMs based on two synthetic methods. (CASS: conventional aqueous solution synthesis; HT: hydrothermal technique.)

originate from the degradation or rearrangement of POM precursors during the course of the reaction. In addition, from Fig. 3a we can see that the synthesis and exploration of PTRHDMs have shown great potential in this field since 2004, which suggests that PTRHDMs are also a promising field with continuous and fast development that attracts much more interest of many researchers (Fig. 3b). In the third section, we briefly discuss the latent application fields of PTRHDMs such as the magnetic, luminescence, electrocatalytic and photoocatalytic properties. The last section focuses on the outlook of this branch.

2. Synthetic strategies

In the beginning of exploring the design and synthesis of PTRHDMs, the conventional aqueous solution synthesis (CASS) route certainly is the first chosen method for chemists in that it is the world-widely employed and accepted facile synthetic method all over the world and is easily manipulated in any routine laboratory. The commonly used soluble POM precursors are the most selected starting materials to interact with TM and RE ions in the absence of organic constituents.[111–122] In the following years, the appearance of some gigantic PTRHDMs also prove that this method is very effective.[127,130,131,143,144,146] In 2008, the hydrothermal technique (HT) was introduced for the first time to prepare novel PTRHDMs by Wang *et al.*, where a trimeric Cu^{II}–Dy^{III} heterometallic germanotungstate $\{[Cu(en)_2]_2[Na_2(H_2O)_{1.75}][K(H_2O)_3][Dy_2(H_2O)_2(GeW_{11}O_{39})_3]\}^{11-}$ with the $Dy^{3+}/[\alpha\text{-}GeW_{11}O_{39}]^{8-}$ ratio of 2:3 was prepared by a mixture of $K_8[\alpha\text{-}GeW_{11}O_{39}]\cdot nH_2O$, $DyCl_3$, $Cu(NO_3)_2\cdot 3H_2O$, en and water in a 165 °C hydrothermal environment.[122] Subsequently, this technique was extensively applied to the preparation of organic–inorganic hybrid PTRHDMs using various N-, O-, N,O-organic ligands.[125,126,128,132,134–141,145,147,148,151–158,160,161,165,167,168] During the course of the preparation of PTHRDMs, both synthetic methods have their own advantages. The merits of CASS include:

(1) In a conventional aqueous solution system, all the reaction components interact with each other in a beaker, tube or flask under bench conditions at ambient pressure and lower temperature, which can reduce the requirements of experimental conditions and are very convenient for most synthetic manipulators;

(2) All the reactants or raw materials need to be dissolved in a homogeneous system, which are favorable to the mutual diffusion of different chemical components and thus increase the collision probability between atoms or molecules, whereby provide for great combination opportunities of different components;

(3) Most of the reaction processes performed under conventional aqueous solution are thermodynamically controlled and require long reaction time. After that, a slow evaporation process is beneficial for the crystallization of good-quality crystals;

(4) The long crystallization time offers good opportunity for the growth and formation of water soluble larger aggregates

and gigantic poly(POM) clusters under gentle thermodynamic conditions.

Based on these advantages of CASS, four types of synthetic strategies of PTHRDMs have been developed:

(a) The one-pot self-assembly reaction of simple initial materials (Fig. 4i);[111,115,127]

(b) The combinatorial reaction of RE-substituted POMs with TM cations or TM complexes (TMCs) (Fig. 4ii);[117,123,146,164]

(c) The combinatorial reaction of lacunary POM precursors with TM–RE heterometallic clusters (Fig. 4iii);[119,120,142,143]

(d) The combinatorial reaction of TM-substituted POMs with RE cations (Fig. 4iv).[129,133,163,164]

Comparable to CASS, HT also has its own preponderances:

(1) Under hydrothermal conditions, the reaction system can be a heterogeneous system, as a result, the starting materials aren't dissolved (such as some organic ligands and metal oxides, *etc.*) can be introduced since the high pressure and temperature can effectively enhance the solubility of the starting chemicals by forming soluble phases;[34,170a,b]

(2) The high pressure and temperature generated under hydrothermal conditions can break the normal chemical equilibrium that is kept under conventional aqueous conditions and drive a chemical reaction from the thermodynamically controlled process to the dynamically controlled process and give rise to some metastable or intermediate phases,[170c–e] which will create favorable preconditions for the formation of new materials;

(3) The reaction medium, water, is an important constituent for the hydrothermal system. Its physicochemical properties such as its density, surface tension, lower viscosity and higher vapor pressure can be significantly changed under high temperature and pressure hydrothermal conditions,[170f] which provide a highly reactive environment for the formation of novel species.

Taking advantage of HT, a variety of organic–inorganic hybrid PTHRDMs with interesting structures and potential properties have been prepared by the synthetic strategy of POM precursors, TM and RE (or RE oxides) cations in the presence of organic ligands (Fig. 4v).[122,125,126,128,132,134–141,145,148,150–153,155–158,160,161,165,167–169] In conclusion, CASS and the HT can be viewed as two main methods of cultivating and growing PTHRDM crystals by controlling reaction conditions.[111–169] Therefore, adjusting and controlling synthetic reaction conditions are the key to the successful preparation of PTRHDMs. The controllable conditions can be classified as the interior reaction system conditions and the exterior reaction environment conditions. The interior reaction system conditions play a decisive role in the formation of PTRHDMs. Generally speaking, TM cations, such as Cr, Mn, Fe, Co, Ni and Cu, can easily coordinate with N, O and S atoms while RE cations are more oxyphilic, indeed, which has been proved by the experimental results of reported PTRHDMs. However, the exterior reaction system conditions (such as concentration, temperature, pH value, time, pressure, organic or inorganic additives) can also have an important influence on the formation of PTRHDMs. Table S1 (ESI†) summarizes some major reactants, temperature, pH value, time, synthetic methods and product phases of all the reported PTRHDMs. Hitherto, more than fifty papers on PTRHDMs have been reported and their distribution situation and proportion based on two synthetic methods are shown. From Fig. 3 and 4 we can see that both methods are effective for the preparation of PTHRDMs.

Currently, the used synthetic strategies of PTRHDMs can be mainly divided into five types: (i) the one-pot reaction of simple initial materials,[111,115,127] (ii) the reaction of RE-substituted POMs with TM cations or TM complexes,[117,123,146,164] (iii) the reaction of TM-substituted POMs with RE cations,[113,114,129,130,133,154,163] (iv) the reaction of POM precursors, RE cations and TM cations,[112,116,118,121,122,124–126,128,131,132,134–141,144,145,147–153,155–162,165–169] and (v) the reaction of lacunary POM precursors with TM–RE heterometallic clusters.[119,120,142,143] Fig. 4 illustrates the typical reaction procedures from initial reactants to final products in the five synthetic routes. Hitherto, more than fifty papers on PTRHDMs have been reported and their distribution situation and proportion based on two synthetic methods are shown in Fig. 3c and d. From Fig. 3 and 4 we can see that both methods are effective for the preparation of PTRHDMs.

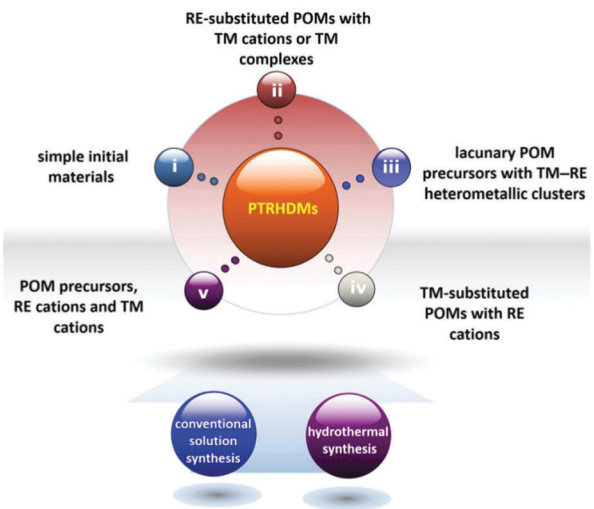

Fig. 4 Five synthetic strategies of PTRHDMs based on CASS and TH methods.

3. Structural diversities

In this section, various PTRHDMs will be successively described in detail on the basis of the types of versatile POM building units. For the sake of saving space, only one representative PTRHDM will be discussed or described for each kind of structural type. According to our statistical results of the published articles with regard to PTRHDMs, most of the PTRHDMs encapsulate a variety of lacunary POM fragments derived from classical plenary Keggin, Dawson polyoxoanions, which mainly contain monovacant, divacant, trivacant and multivacant POM fragments. From the origin of these lacunary POM fragments, some come from the *in situ* reaction during the course of the self-assembly of simple starting materials, others are derived from the rearrangement and degradation of plenary

or lacunary POM precursors. From the already reported PTRHDMs, we can make several conclusions:

(1) from the number of reported PTRHDMs, the majority are based on monovacant POM fragments because the pH environments in which monovacant POM fragments exist are also suitable for the existence of RE ions, which are convenient for the incorporation of RE ions into the defect site of POM fragments;

(2) from synthetic approaches of PTRHDMs, hydrothermal reactions favor the preparation and formation of organic–inorganic hybrid PTRHDMs based on monovacant POM fragments since hydrothermal environments favor the combination of organic ligands with TM or RE ions, in contrast, the conventional solvent evaporation method is beneficial to grow and cultivate PTRHDMs containing divacant, trivacant and multivacant POM fragments due to the slow phase diffusion process;

(3) from the functionalities of TM and RE cations, RE cations are often implanted to the defect sites of POM fragments forming RESP units and TMs function as pendants or bridging groups to construct high-dimensional structures in the monovacant-POM-involving PTRHDMs, and TM cations are usually embedded into the lacunary positions of POM fragments forming TMSP units and RE cations serve as connectors to proliferate high-dimensional architectures in the di/trivacant-POM-embracing PTRHDMs, while TM and RE cations usually simultaneously graft to the defect locations of POM fragments or simultaneously connect different POM fragments together to generate orderly extended architectures in the multivacant-POM-containing PTRHDMs;

(4) from the viewpoint of chemical compositions, on one hand, the majority of PTRHDMs are based on POT building units, in contrast, POMB and polyoxovanadate(POV)-based TM–RE heterometallic derivatives are rather rarely reported, mainly because lacunary POT fragments are more stable than those of POMBs and POVs either in the conventional aqueous solution or under hydrothermal conditions; on the other hand, for mono- and di-vacant PTRHDMs, the most used TM cations is the copper ion, which is closely correlated with the fact that the Jahn–Teller effect of the octahedral geometry and the pseudo-Jahn–Teller effect of the square pyramidal geometry of the copper cation may effectively overcome the large steric hindrance and greatly contribute to stabilize *in situ* formed PTRHDMs; for tri- and multi-vacant PTRHDMs, manganese cations are the preferred option since they own active redox catalytic activities that can be used to synthesize high-efficiency POM-based catalysts and they possess relatively high spin values and negative single-axis magnetic anisotropy that make them widely applicable in the construction of neotype magnetic materials, especially single molecule magnets (SMMs);[149]

(5) from the role of organic components, most of the reported PTRHDMs embrace organic components, especially *N*-containing organic ligands since organic components not only act as the charge compensation cations in the form of protonated organic cations, but also work as the multidentate chelating agents to coordinate TM or/and TM cations, which make organic components become important structure-stabilizing agents in the formation of organic–inorganic hybrid PTRHDMs.

3.1 PTRHDMs based on monovacant POM fragments

On the basis of the previously reported results on RESPs,[93,94,96–98] in comparison with di-, tri- and multi-vacant POM fragments, the monovacant POM fragment is liable to incorporate the RE center to the lacunae sites because the appropriate "bite angle" in the packet of a monovacant POM fragment matches the magnitude of the RE center. According to the ratios of RE/POM, the RESP units can be classified into 1 : 1-, 1 : 2- and 2 : 2-type. 1 : 1-type RESP units refer to the combination of a RE ion with one monovacant POM fragment, 1 : 2-type RESP units are that two monovacant POM fragments share a RE ion and 2 : 2-type RESP units are formed by two monovacant POM fragments *via* two RE linkers. Among the classical 1 : 1-, 1 : 2- and 2 : 2-type RESP units, 1 : 1-type RESP units can be decorated or connected by TM complexes (TMCs) or together produce novel PTRHDMs with interesting structures and particular properties. Now, we begin to discuss this section from 1 : 1-type RESP units. We hydrothermally prepared two isomorphic organic–inorganic hybrid monolacunary Keggin PTRHDMs with supporting Cu–en complexes $[Cu(en)_2(H_2O)]_2[Tb(\alpha\text{-}HSiW_{11}O_{39})(H_2O)_3]\cdot 12H_2O$ and $[Cu(en)_2(H_2O)]_2[Eu(\alpha\text{-}HGeW_{11}O_{39})(H_2O)_3]\cdot 12H_2O$ (Fig. 5a),[152] which exhibit the rare 1-D linear chain arrangement built by mono-Ln substituted Keggin 1 : 1-type $[Ln(\alpha\text{-}HXW_{11}O_{39})(H_2O)_3]^{4-}$ ($Ln = Tb^{III}$, Eu^{III}; $X = Si^{IV}$, Ge^{IV}) units *via* W–O–Ln–O–W bridges (Fig. 5c). This linear chain building mode is very similar to that observed in an organic–inorganic RESP hybrid $[Sm(H_2O)_6]_{0.25}[Sm(H_2O)_5]_{0.25}H_{0.5}\{Sm(H_2O)_7[Sm(H_2O)_2(DMSO)(\alpha\text{-}SiW_{11}O_{39})]\}\cdot 4.5H_2O$ discovered by Niu *et al.* in 2006.[97] Additionally, the pendant TMCs on the unusual 1 : 1 $[Ln(\alpha\text{-}XW_{11}O_{39})]^{4/5-}$ units can act as the bridging groups resulting in dimeric structural $\{[Cu(dap)_2(H_2O)]_2[Cu(dap)_2][\alpha\text{-}XW_{11}O_{39}Ln(H_2O)_3]_2\}^{4-}$ fragments (Fig. 5b),[147,156,165] and then further create the 1-D double-chain pattern by means of the bridging role of RE cations (Fig. 5d), which represent the first organic–inorganic hybrid 1-D double-chain Cu–Ln heterometallic POMs. However, such a 1-D double-chain is completely distinct from the germanotungstate-based Sm^{III}-containing hybrid 1-D double-chain observed in $[Sm_2(\alpha\text{-}GeW_{11}O_{39})(DMSO)_3(H_2O)_6]^{2-}$.[96] The most obvious discrepancy between them is that two 1-D chains in the 1-D double chain alignment in $\{[Cu(dap)_2(H_2O)]_2[Cu(dap)_2][\alpha\text{-}XW_{11}O_{39}Ln(H_2O)_3]_2\}^{4-}$ are joined together by $[Cu(en)_2]^{2+}$ bridges whereas those in $[Sm_2(\alpha\text{-}GeW_{11}O_{39})(DMSO)_3(H_2O)_6]^{2-}$ are connected by $[Sm(DMSO)_2(H_2O)_2]^{3+}$ linkers.

Besides 1 : 1-type $[Ln(\alpha\text{-}XW_{11}O_{39})]^{4/5-}$ units ($X = P^V$, As^V, Si^{IV}, Ge^{IV}), the 1 : 2-type $[Ln(\alpha\text{-}XW_{11}O_{39})_2]^{10/11-}$ units, which were first discovered by Peacock and Weakley in 1971,[171] can also induce TMCs to form hybrid PTRHDMs.[123,125,128,135,136,138–140,145,148,157,158,161] Compared with those PTRHDMs containing $[Ln(\alpha\text{-}XW_{11}O_{39})]^{4/5-}$ units, the well-known 1 : 2-type $[Ln(\alpha\text{-}XW_{11}O_{39})_2]^{10/11-}$ units not only generate the monomer $[Cu(en)_2Ln(\alpha\text{-}PW_{11}O_{39})_2]^{9-}$ (Fig. 6a)[125] and the dimers $[Cu_2(2,2'\text{-}bpy)_2(\mu\text{-}ox)Ln(\alpha\text{-}PW_{11}O_{39})_2]^{9-}$ (Fig. 6b)[123] and $\{[Cu(en)_2]_{1.5}Ln(\alpha\text{-}SiW_{11}O_{39})_2\}_2^{20-}$ (Fig. 6c),[139] but also give rise to the 1-D infinite chain fashions (Fig. 6e–h). It should be pointed out that the 1-D chain of $\{Cu(en)_2Ln(\alpha\text{-}PW_{11}O_{39})_2\}^{9-}$ is constructed

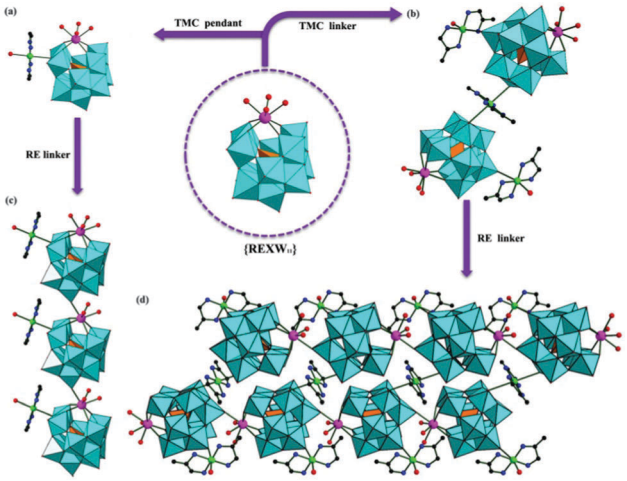

Fig. 5 (a) Polyhedral/ball-and-stick view of the structural unit of $[Cu(en)_2(H_2O)]_2[Ln(\alpha\text{-}HXW_{11}O_{39})(H_2O)_3]\cdot 12H_2O$; (b) the dimeric unit of $\{[Cu(dap)_2(H_2O)]_2[Cu(dap)_2][\alpha\text{-}XW_{11}O_{39}Ln(H_2O)_3]_2\}^{4-}$; (c) the 1-D linear chain built by $[Cu(en)_2(H_2O)]_2[Ln(\alpha\text{-}HXW_{11}O_{39})(H_2O)_3]$ unit *via* W–O–Ln–O–W linkers; (d) the 1-D double-chain motif based on dimeric $\{[Cu(dap)_2(H_2O)]_2[Cu(dap)_2]\text{-}[\alpha\text{-}XW_{11}O_{39}Ln(H_2O)_3]_2\}^{4-}$ fragments by means of the bridging role of Ln cations. (WO_6: turquoise, XO_4: light orange, Ln: pink, O: red, Cu: bright green, N: blue.)

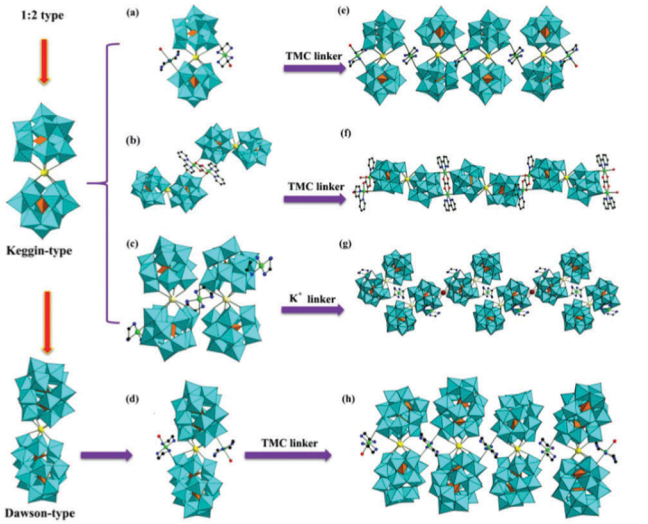

Fig. 6 (a) The monomeric $[Cu(en)_2Ln(\alpha\text{-}PW_{11}O_{39})_2]^{9-}$ segment. (b) The dimeric $[Cu_2(2,2'\text{-}bpy)_2(\mu\text{-}ox)Ln(PW_{11}O_{39})_2]^{9-}$ segment. (c) The dimeric $\{[Cu(en)_2]_{1.5}\text{-}Ln(\alpha\text{-}SiW_{11}O_{39})_2\}_2^{20-}$ segment. (d) The 1 : 2-type Dawson $[Cu(en)_2Ln\text{-}(\alpha_2\text{-}P_2W_{17}O_{61})_2]^{15-}$ segment. (e) The 1-D chain made by 1 : 2-type $[Ln(\alpha\text{-}PW_{11}O_{39})_2]^{11-}$ units and $[Cu_2(2,2'\text{-}bpy)_2(\mu\text{-}ox)]^{2+}$ complexes. (f) The 1-D chain built by 1 : 2-type $[Ln(\alpha\text{-}PW_{11}O_{39})_2]^{11-}$ units and $[Cu(en)_2]^{2+}$ bridges. (g) The 1-D chain established by $\{[Cu(en)_2]_{1.5}Ln(\alpha\text{-}SiW_{11}O_{39})_2\}_2^{20-}$ dimers connected by K^+ ions. (h) The 1-D chain of $[Cu(en)_2][Ln\text{-}(\alpha_2\text{-}P_2W_{17}O_{61})_2]^{15-}$ along the *c*-axis. (WO_6: turquoise, Ln: yellow, XO_4: light orange, O: red, Cu: bright green, N: blue.)

from 1 : 2-type $[Ln(\alpha\text{-}PW_{11}O_{39})_2]^{11-}$ units bridged by $[Cu(en)_2]^{2+}$ cations (Fig. 6e),[125] the 1-D chain-like $[Cu_2(2,2'\text{-}bpy)_2(\mu\text{-}ox)Ln(\alpha\text{-}PW_{11}O_{39})_2]^{9-}$ is built by alternate 1 : 2-type $[Ln(\alpha\text{-}PW_{11}O_{39})_2]^{11-}$ units and dinuclear copper–oxalate $[Cu_2(2,2'\text{-}bpy)_2(\mu\text{-}ox)]^{2+}$ complex ions (Fig. 6f),[123] and the 1-D zigzag chain-like motif of $\{K[Cu(en)_2]_{1.5}Ln(\alpha\text{-}SiW_{11}O_{39})_2\}_2^{19-}$ is formed by dimeric $\{[Cu(en)_2]_{1.5}Ln(\alpha\text{-}SiW_{11}O_{39})_2\}_2^{20-}$ units connected by square anti-prismatic K^+ ions (Fig. 6g).[139] Furthermore, the combination of 1 : 2-type $[Ln(\alpha_2\text{-}P_2W_{17}O_{61})_2]^{17-}$ dimers (Fig. 6d) with $[Cu(en)_2]^{2+}$ linkers leads to a series of 1-D organic–inorganic hybrid Dawson-type phosphotungstate-based TM–RE heterometallic derived materials (TRHDMs) $[Cu(en)_2Ln(\alpha_2\text{-}P_2W_{17}O_{61})_2]^{15-}$ (Fig. 6h) found by us in 2014,[161] which represent the first family of 1-D TM–Ln Dawson-type POTs built by 1 : 2-type mono-Ln substituted Dawson phosphotungstates and copper–en linkers.

Apart from the above-mentioned 1-D chain alignments, some PTRHDMs consisting of 1 : 2-type $[Ln(\alpha\text{-}XW_{11}O_{39})_2]^{10/11-}$ units as fundamental building blocks and TMCs as bridges can also form unprecedented 2-D and 3-D extended structures. For example, in 2011, Niu's group communicated isomorphous 2-D layer phosphotungstate-based TRHDMs with mixed ligands $\{[Cu(en)_2]_2(H_2O)[Cu(en)(2,2'\text{-}bipy)]Ln[(\alpha\text{-}HPW_{11}O_{39})_2]\}^{4-}$ (Ln = Gd^{III}, Tb^{III}, Er^{III}) built by $[Ln(\alpha\text{-}PW_{11}O_{39})_2]^{11-}$ units *via* $[Cu(en)_2]^{2+}$ and $[Cu(en)(2,2'\text{-}bpy)]^{2+}$ cations (Fig. 7a), which exhibit the (4,4)-topological network with the Schläfli symbol of $(4^4\cdot 6^2)$ (Fig. 7b).[138] The next year, we addressed three kinds of 2-D sheet arsenotungstate-based TRHDMs,[145] in which $[Cu(en)_2(H_2O)]_4\text{-}[Cu(en)_2]_2[Cu(H_2O)_4]_{0.5}\{Cu(en)_2[H_2Ce^{IV}(\alpha\text{-}AsW_{11}O_{39})_2]_2\}\cdot 10H_2O$ illustrates the first 4-connected 2-D TM–Ln hetero-metallic sheet architecture established by tetrameric $[Cu(H_2O)_4\{Cu(en)_2[H_2Ce\text{-}(\alpha\text{-}AsW_{11}O_{39})_2]_2\}_2]^{26-}$ units through $[Cu(en)_2]^{2+}$ connectors (Fig. 7c and d); $[Cu(en)_2(H_2O)][Cu(en)_2]_{1.5}[H_3Ln(\alpha\text{-}AsW_{11}O_{39})_2]^{3-}$ (Ln = Pr^{III}, Nd^{III}, Sm^{III}, Eu^{III}, Tb^{III}) reveals a particular 2-D (6,3)-network constructed from 1 : 2-type $[H_3Ln(\alpha\text{-}AsW_{11}O_{39})_2]^{8-}$ units *via* $[Cu(en)_2]^{2+}$ linkers (Fig. 7e and f); $[Cu(dap)_2]_{5.5}[Ln(\alpha\text{-}AsW_{11}O_{39})_2]$ (Ln = Tb^{III}, Dy^{III}) manifests the unprecedented 2-D sheet built by 1 : 2-type $[Ln(\alpha\text{-}AsW_{11}O_{39})_2]^{11-}$ units and $[Cu(dap)_2]^{2+}$ bridges, in which $[Ln(\alpha\text{-}AsW_{11}O_{39})_2]^{11-}$ subunits act as 5-connected nodes and adjacent 2-D sheets are stacked in the packing mode of –AAA– (Fig. 7g and h).

Moreover, some 3-D organic–inorganic hybrid PTRHDMs with peculiar topologies were also reported by Niu *et al.*[138,139] For instance, $\{[Cu(en)_2]_{1.5}[Cu(en)(2,2'\text{-}bipy)]Nd[(\alpha\text{-}H_5PW_{11}O_{39})_2]\}^{3-}$ displays the scarce 3-D framework with a $(4^6\cdot 6^4)$ topology (Fig. 7i and j).[138] Additionally, in 2012, they got three types of 3-D organic–inorganic hybrid Keggin silicotungstate-based THRDMs $\{[Cu(en)_2]_{1.5}Ln[(\alpha\text{-}SiW_{11}O_{39})]\}^{2-}$ [Ln = La^{III}, Ce^{III}] (Fig. 7k), $\{[Cu(en)_2(H_2O)][Cu(en)_2]_2Pr[(\alpha\text{-}SiW_{11}O_{39})_2]\}^{7-}$ (Fig. 7m) and $\{[Cu(en)_2(H_2O)][Cu(en)_2]_3Ln[(\alpha\text{-}SiW_{11}O_{39})_2]\}^{5-}$ (Fig. 7o).[139] In $\{[Cu(en)_2]_{1.5}Ln[(\alpha\text{-}SiW_{11}O_{39})]\}^{2-}$, [Ln = La^{III}, Ce^{III}] if each $\{La[(\alpha\text{-}HSiW_{11}O_{39})]\}^{4-}$ subunit acts as a 5-connected node, its 3-D framework can be described as a 5-connected network with the Schläfli symbol of $(4^8\cdot 6^2)$ (Fig. 7l). In $\{[Cu(en)_2(H_2O)]\text{-}[Cu(en)_2]_2Pr[(\alpha\text{-}SiW_{11}O_{39})_2]\}^{7-}$, if each $\{[Cu(en)_2(H_2O)]\,[Cu(en)_2]_2\text{-}Pr[(\alpha\text{-}H_{1.5}SiW_{11}O_{39})_2]\}^{4-}$ subunit is viewed as a 4-connected node, its 3-D framework is a 4-connected 3-D network with the Schläfli symbol of (6^6) (Fig. 7n). In $\{[Cu(en)_2(H_2O)]\text{-}[Cu(en)_2]_3Ln[(\alpha\text{-}SiW_{11}O_{39})_2]\}^{5-}$, if each $[Sm(\alpha\text{-}SiW_{11}O_{39})_2]^{13-}$ subunit acts as a heptadentate ligand to link seven $[Cu(en)_2]^{2+}$ groups giving rise to a fascinating 6-connected 3-D framework with the Schläfli notation of $(4^8\cdot 5^4\cdot 6^3)$ (Fig. 7p).

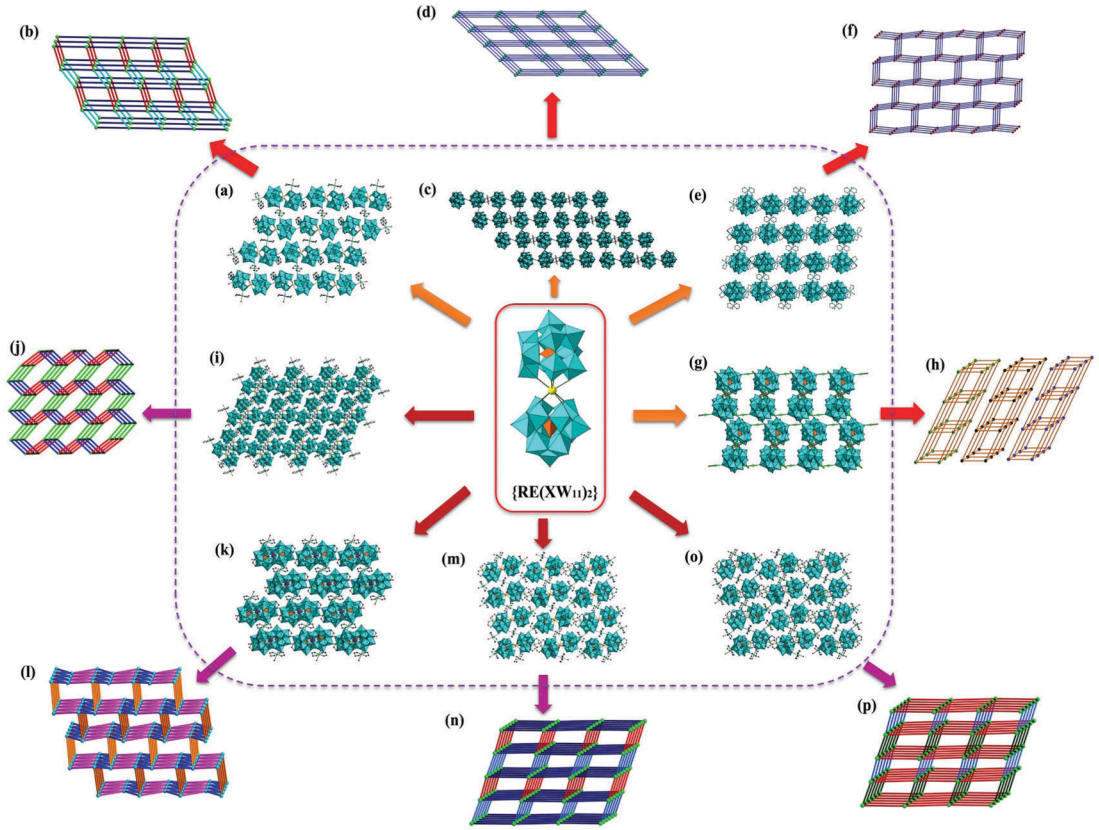

Fig. 7 (a) The 2-D structure of $\{[Cu(en)_2]_2(H_2O)[Cu(en)(2,2'\text{-bipy})]Ln[(\alpha\text{-}HPW_{11}O_{39})_2]\}^{4-}$. (b) The (4,4)-network of $\{[Cu(en)_2]_2(H_2O)[Cu(en)(2,2'\text{-bipy})]Ln\text{-}[(\alpha\text{-}HPW_{11}O_{39})_2]\}^{4-}$ showing the –AAA– packing mode. (c) The 4-connected 2-D structure of $[Cu(en)_2(H_2O)]_4[Cu(en)_2]_2[Cu(H_2O)_4]_{0.5}\{Cu(en)_2[H_2Ce^{IV}\text{-}(\alpha\text{-}AsW_{11}O_{39})_2]_2\}\cdot 10H_2O$. (d) The (4,4)-network of $[Cu(en)_2(H_2O)]_4[Cu(en)_2]_2[Cu(H_2O)_4]_{0.5}\{Cu(en)_2[H_2Ce^{IV}(\alpha\text{-}AsW_{11}O_{39})_2]_2\}\cdot 10H_2O$. (e) The 2-D sheet of $[Cu(en)_2(H_2O)][Cu(en)_2]_{1.5}[H_3Ln(\alpha\text{-}AsW_{11}O_{39})_2]^{3-}$. (f) The (6,3)-network of $Cu(en)_2(H_2O)][Cu(en)_2]_{1.5}[H_3Ln(\alpha\text{-}AsW_{11}O_{39})_2]^{3-}$. (g) The unprecedented 2-D sheet of $[Cu(dap)_2]_{5.5}[Ln(\alpha\text{-}AsW_{11}O_{39})_2]$. (h) The 5-connected topology of $[Cu(dap)_2]_{5.5}[Ln(\alpha\text{-}AsW_{11}O_{39})_2]$. (i) The 3-D framework structure of $\{[Cu(en)_2]_{1.5}[Cu(en)(2,2'\text{-bipy})]Nd[(\alpha\text{-}H_5PW_{11}O_{39})_2]\}^{3-}$. (j) The $(4^6.6^4)$ topology framework of $\{[Cu(en)_2]_{1.5}[Cu(en)(2,2'\text{-bipy})]Nd[(\alpha\text{-}H_5PW_{11}O_{39})_2]\}^{3-}$. (k) The 3-D structure of $\{[Cu(en)_2]_{1.5}Ln[(\alpha\text{-}SiW_{11}O_{39})]\}^{2-}$. (l) The $(4^8.6^2)$ topology network of $\{[Cu(en)_2]_{1.5}Ln[(\alpha\text{-}SiW_{11}O_{39})]\}^{2-}$. (m) The 3-D structure of $\{[Cu(en)_2(H_2O)][Cu(en)_2]_2Pr[(\alpha\text{-}SiW_{11}O_{39})_2]\}^{7-}$. (n) The (6^6) topology framework of $\{[Cu(en)_2(H_2O)][Cu(en)_2]_2Pr[(\alpha\text{-}SiW_{11}O_{39})_2]\}^{7-}$. (o) The 3-D structure of $\{[Cu(en)_2(H_2O)][Cu(en)_2]_3Ln[(\alpha\text{-}SiW_{11}O_{39})_2]\}^{5-}$. (p) The $(4^8.5^4.6^3)$ topology framework of $\{[Cu(en)_2(H_2O)][Cu(en)_2]_3Ln[(\alpha\text{-}SiW_{11}O_{39})_2]\}^{5-}$. ($WO_6$: turquoise, XO_4: light orange, Ln: yellow, O: red, Cu: bright green, N: blue.)

It should be noted that the above mentioned 0-, 1- or high-dimensional PTRHDMs were synthesized by reaction of pre-fabricated POM precursors with copper and RE cations in the presence of *N*-containing organic ligands under hydrothermal conditions and their structures are constructed from 1 : 1-type Keggin $[Ln(\alpha\text{-}XW_{11}O_{39})]^{4/5-}$, 1 : 2-type Keggin $[Ln(\alpha\text{-}XW_{11}O_{39})_2]^{10/11-}$ or 1 : 2-type Dawson $[Ln(\alpha_2\text{-}P_2W_{17}O_{61})_2]^{17-}$ *via* TMCs. When O-containing organic ligands or N,O-containing organic ligands were utilized to replace *N*-containing organic ligands, another class of dimeric PTRHDMs with $RE : XW_{11} = 2 : 2$ (denoted as 2 : 2-type) were found.[126,132,140,141,150,159] Typically, Su *et al.* used the trivacant precursor $[\alpha\text{-}SiW_9O_{34}]^{10-}$ to react with Ln ions and copper ions in the presence of en in the acetate/acetic acid buffer solution under hydrothermal conditions leading to the isolation of three inorganic–organic hybrid 2 : 2-type silicotungstate-based TRHDMs $[Cu(en)_2H_2O]_6[(\alpha\text{-}SiW_{11}O_{39})Nd\text{-}(H_2O)(\eta^2,\mu\text{-}1,1)\text{-}CH_3COO]_2\cdot 7H_2O$, $[Cu(en)_2H_2O]_6[(\alpha\text{-}SiW_{11}O_{39})Sm(H_2O)(\eta^2,\mu\text{-}1,1)\text{-}CH_3COO]_2\cdot 6H_2O$ and $H_2[Cu(en)_2H_2O]_8[Cu(en)_2]_3[\{(\alpha\text{-}SiW_{11}O_{39})Ce\text{-}(H_2O)(\eta^2,\mu\text{-}1,1)\text{-}CH_3COO\}_4]\cdot 22H_2O$ (Fig. 8a).[132] Their common structural feature is that they consist of a dimeric $[(\alpha\text{-}SiW_{11}O_{39})Ln(H_2O)\text{-}(\eta^2,\mu\text{-}1,1)\text{-}CH_3COO]_2^{12-}$ unit, which can be perceived as the fusion of two mono-Ln substituted $[(\alpha\text{-}SiW_{11}O_{39})Ln(H_2O)(\eta^2,\mu\text{-}1,1)\text{-}CH_3COO]^{6-}$ subunits bridged by two $(\eta^2,\mu\text{-}1,1)$-acetate ligands. This 2 : 2-type structural type was first discovered by Mialane *et al.* in $[\{(\alpha\text{-}SiW_{11}O_{39})Ln(COOCH_3)(H_2O)\}_2]^{12-}$ (Ln = Gd^{III}, Yb^{III}) during the course of investigating the Ln/monovacant silicotungstate system.[110] More interestingly, in $[Cu(en)_2H_2O]_8[Cu(en)_2]_3[\{(\alpha\text{-}SiW_{11}O_{39})Ce(H_2O)(\eta^2,\mu\text{-}1,1)\text{-}CH_3COO\}_4]^{2-}$, adjacent $[(\alpha\text{-}SiW_{11}O_{39})\text{-}Ln(H_2O)(\eta^2,\mu\text{-}1,1)\text{-}CH_3COO]_2^{12-}$ units are further combined together by $[Cu(en)_2]^{2+}$ groups forming the first 1-D ladder-like chain consisting of monovacant Keggin-type fragments, Ln complexes and TMCs in POM chemistry (Fig. 8b). By the participation of the pyrazine-2,3-dicarboxylate (pzda) ligand, Niu *et al.* separated a family of organic–inorganic hybrid TRHDMs based on silicotungstates and mixed ligands $[Cu(en)_2(H_2O)]_2\{[Cu(en)_2]_2[Cu(pzda)_2]\ [(\alpha\text{-}H_2SiW_{11}O_{39})Ce(H_2O)]_2\}\cdot 8H_2O$ (Fig. 8c) and $(enH_2)[Cu(en)_2(H_2O)]_2\{[Cu(en)_2][Cu(en)_2(H_2O)][(\alpha\text{-}SiW_{11}O_{39})RE(H_2O)(pzda)]\}_2\cdot 4H_2O$ (RE = Y^{III}, Dy^{III}, Yb^{III}, Lu^{III}) (Fig. 8e),[141] which all contain the 2 : 2-type

mono-RE substituted Keggin $[RE(\alpha\text{-}SiW_{11}O_{39})]_2^{10-}$ subunits linked by H_2pzda ligands. Interestingly, $[Cu(en)_2(H_2O)]_2\{[Cu(en)_2]_2[Cu(pzda)_2][(\alpha\text{-}H_2SiW_{11}O_{39})Ce(H_2O)]_2\}\cdot 8H_2O$ displays an unusual 1-D chain architecture by the bridging role of $[Cu(en)_2]^{2+}$ and $[Cu(pzda)_2]^{2-}$ cations (Fig. 8d). It is noteworthy that the connection role of $[Cu(pzda)_2]^{2-}$ cations leads to a 1-D Cu–Ce heterometallic organic–inorganic hybrid chain (Fig. 8d), which is for the first time observed in POM chemistry. In contrast, $(enH_2)[Cu(en)_2(H_2O)]_2\{[Cu(en)_2][Cu(en)_2(H_2O)][(\alpha\text{-}SiW_{11}O_{39})RE(H_2O)(pzda)]\}_2\cdot 4H_2O$ exhibits a discrete structure, in which the pzda ligand acts as a tetradentate ligand to bind RE and Cu cations sandwiched by two $[\alpha\text{-}SiW_{11}O_{39}]^{8-}$ fragments (Fig. 8e). By virtue of the combined action of oxalic acid and en, in 2013, Yang's group studied the hydrothermal reaction of the mixed vacant precursors $Na_9[A\text{-}\alpha\text{-}PW_9O_{34}]\cdot 7H_2O$ and $K_{12}[\alpha\text{-}H_2P_2W_{12}O_{48}]\cdot 24H_2O$ with Tb^{3+} and Cu^{2+} cations and obtained a 1-D hybrid oxalate-bridging heterometallic phosphortungstate $[Cu(en)_2(H_2O)]\ [Cu(en)_2][Tb(\alpha\text{-}PW_{11}O_{39})(H_2O)_2(ox)Cu(en)]\cdot 6H_2O$ with mixed ox and en ligands.[150] In this compound, two intriguing structural features should be pointed out: (1) two mono-Tb^{III} substituted $[\alpha\text{-}PW_{11}TbO_{39}]^{4-}$ segments are linked by an oxalate ligand, at the same time, the oxalate ligands are supported by two $[Cu(en)_2]^{2+}$ cations, and thus gives rise to the special 2 : 2-type $\{[Cu(en)_2]_2[(\alpha\text{-}PW_{11}O_{39})Tb(H_2O)_2]_2(\mu\text{-}ox)\}^{6-}$ unit (Fig. 8f); (2) contiguous $\{[Cu(en)_2]_2[(\alpha\text{-}PW_{11}O_{39})Tb(H_2O)_2]_2(\mu\text{-}ox)\}^{6-}$ units are bridged together by dicaryotic Cu(II)–oxalate $[Cu_2(en)_2(\mu\text{-}ox)]^{2+}$ complexes forming an unprecedented 1-D zigzag chain (Fig. 8g). Notably, it represents the first PTRHDM based on oxalate-bridging terbium-substituted phosphotungstate dimeric units and dinuclear Cu(II)–oxalate linkers. In 2010, Mialane *et al.* communicated a class of extraordinary $\{LnCu_3(OH)_3O\}$-cubane (Ln = La^{III}, Gd^{III}, Eu^{III}) inserted monovacant silicotungstate-based TRHDMs with the ratio of Ln : XW_{11} of 2 : 2 $[Cu(en)_2][(Cu(en)(OH))_3La(\alpha\text{-}SiW_{11}O_{39})]\cdot 20H_2O$ (Fig. 8h) and $\{[Cu(en)_2(H_2O)][(Cu(en)(OH))_3Ln(\alpha\text{-}SiW_{11}O_{39})(H_2O)]\}_2\cdot 20H_2O$ (Ln = Gd^{III}, Eu^{III}), in which two $[\alpha\text{-}SiW_{11}O_{39}]^{8-}$ subunits are joined together by two $\{LnCu_3(OH)_3O\}$-cubane clusters *via* W–O–Ln–O–W linkages.[126] Later, such structure-type germanotungstate-based TRHDMs $\{[Cu(en)_2(H_2O)][Cu_3Ln(en)_3(OH)_3(H_2O)_2](\alpha\text{-}GeW_{11}O_{39})\}_2\cdot 11H_2O$ (Ln = Eu^{III}, Tb^{III}) and $\{[Cu(en)_2(H_2O)][Cu_3Dy(en)_3(OH)_3(H_2O)_2](\alpha\text{-}GeW_{11}O_{39})\}_2\cdot 10H_2O$ were also obtained by us.[134,140] Moreover, the dimeric $[(Cu(en)(OH))_3La(\alpha\text{-}SiW_{11}O_{39})]_2^{4-}$ units can be propagated into the 2-D sheet structure with the help of $[Cu(en)_2]^{2+}$ bridges (Fig. 8i). Except for organic–inorganic hybrid mono-Ln substituted Keggin 2 : 2-type POMs units, pure inorganic mono-Ln substituted Keggin 2 : 2-type POM units have also been made in the PTRHDM field. For instance, in 2013, Peng *et al.* used the rational self-assembly of a mono-lacunary Keggin cluster $[\alpha\text{-}SiW_{11}O_{39}]^{8-}$ with 4d (Ag^+) and 4f (Ce^{3+}, Pr^{3+}) metal salts *via* a conventional method and isolated two POM-based 4d–4f heterometallic derivatives $[Ag\{Ag_2(H_2O)_4\}\{Ln(H_2O)_6\}_2H\subset\{\alpha\text{-}SiW_{11}Ln(H_2O)_4O_{39}\}_2]\cdot nH_2O$ (Ln = Ce^{III} and n = 7, Ln = Pr^{III} and n = 3) containing lacunary Keggin anions connected to ten metals (five Ag^+ and five Ln^{3+} cations) (Fig. 8j),[159] which represent the highest number of connected metals to any monovacant Keggin polyoxoanion to date. In the molecular units of these two derivatives, two $[\alpha\text{-}SiW_{11}O_{39}]^{8-}$ fragments are directly fused by two Ln cations generating the inorganic 2 : 2-type POM $[\alpha\text{-}SiW_{11}Ln(H_2O)_4O_{39}]_2^{10-}$ unit, which is very similar to the 2 : 2-type mono-Ln substituted phosphotungstate $[\{(\alpha\text{-}PW_{11}O_{39}H)Ln(H_2O)_3\}_2]^{6-}$ (Ln = Nd^{III}, Gd^{III}) reported by Niu's group in 2009.[98] More interestingly, adjoining $[\alpha\text{-}SiW_{11}Ln(H_2O)_4O_{39}]_2^{10-}$ units are linked together by Ce^{3+} cations to generate a 2-D structure and then neighbouring 2-D networks are concatenated by $\{Ag\text{–}Ag\}^{2+}$ dimers to produce a purely inorganic 3-D framework (Fig. 8k). Similarly, Chen *et al.* also discovered a purely inorganic 3-D porous framework based on mono-Ce^{III} substituted Keggin 2 : 2-type α-metatungstate units $[\{Ag_3(H_2O)_2\}\{Ce_2(H_2O)_{12}\}H_5\subset\{H_2W_{11}Ce(H_2O)_4O_{39}\}_2]\cdot 8H_2O$, in which two monovacant isopolyanion $[H_2W_{11}O_{39}]^{10-}$ fragments are combined with two Ce^{III} cations giving rise to an inorganic 2 : 2-type $[H_2W_{11}Ce(H_2O)_4O_{39}]_2^{14-}$ unit, and then $[H_2W_{11}Ce(H_2O)_4O_{39}]_2^{14-}$ units are linked by Ce^{III} and Ag^I to form 2-D networks, and these networks are further connected by $\{Ag\text{–}Ag\}^{2+}$ dimer bonds to form a purely inorganic 3-D framework.[118]

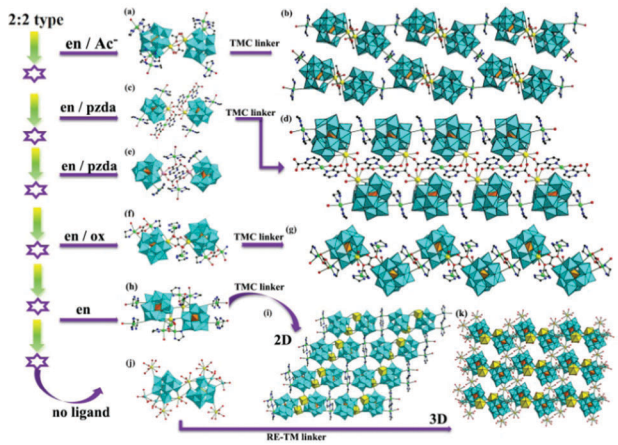

Fig. 8 (a) and (b) The dimeric structural unit of $H_2[Cu(en)_2H_2O]_8[Cu(en)_2]_3[\{(\alpha\text{-}SiW_{11}O_{39})Ce(H_2O)(\eta^2,\mu\text{-}1,1)\text{-}CH_3COO\}_4]\cdot 22H_2O$ and its 1-D ladder-like chain. (c) and (d) The structural unit of $[Cu(en)_2(H_2O)]_2\{[Cu(en)_2]_2[Cu(pzda)_2][(\alpha\text{-}H_2SiW_{11}O_{39})Ce(H_2O)]_2\}\cdot 8H_2O$ and its unusual 1-D chain architecture. (e) The molecular structure of $\{[Cu(en)_2][Cu(en)_2(H_2O)][(\alpha\text{-}SiW_{11}O_{39})RE(H_2O)(pzda)]\}_2^{6-}$. (f) and (g) The oxalate-bridging dimeric $\{[Cu_2(en)_2]_2[(\alpha\text{-}PW_{11}O_{39})Tb(H_2O)_2]_2(\mu\text{-}ox)\}^{6-}$ unit and its unprecedented 1-D zigzag chain. (h) and (i) The molecular structure of $\{[Cu(en)_2(H_2O)][Cu_3Eu(en)_3(OH)_3(H_2O)_2](\alpha\text{-}GeW_{11}O_{39})\}_2\cdot 11H_2O$; (h) and (i) the $\{LnCu_3(OH)_3O\}$-cubane-bridging dimeric unit of $[Cu(en)_2][(Cu(en)(OH))_3La(SiW_{11}O_{39})]\cdot 20H_2O$ and its 2-D sheet structure. (j) and (k) The structural unit of $[Ag\{Ag_2(H_2O)_4\}\{Pr(H_2O)_6\}_2H\subset\{SiW_{11}Pr(H_2O)_4O_{39}\}_2]\cdot 3H_2O$ and its 3-D framework. (WO_6: turquiose, XO_4: light orange, RE: yellow, O: red, Cu/Ag: bright green; N: blue.)

Apart from the aforesaid monomeric and dimeric PTRHDM units, to discover and prepare polymeric PTRHDM units are of great interest and very meaningful because they usually incorporate much more TM or RE centers and further give rise to unique and complicated PTRHDMs with intriguing extended architectures and underlying applications. In this respect, some achievements have been made in the past several years. For example, in 2008, Niu's group found a 2 : 3-type mono-Dy^{III} substituted Keggin-type trimeric subunit $[Dy_2(H_2O)_2(\alpha\text{-}GeW_{11}O_{39})_3]^{18-}$ in a germanotungstate-based TRHDM hybrid $[Cu(en)_2]_2[Cu(en)_2(H_2O)]_2H_3\{[Cu(en)_2]_2[Na_2(H_2O)_{1.75}][K(H_2O)_3][Dy_2(H_2O)_2(\alpha\text{-}GeW_{11}O_{39})_3]\}6H_2O$ (Fig. 9a), moreover, which can be polymerized to the 1-D extended architecture with the participation of $[Cu(en)_2]^{2+}$

cations (Fig. 9b).[122] In 2013, our group reported two Cu-bridged tetrahedral POM nanoclusters with tetrameric RE cores and germanotungstate vertices $[Cu(en)_2]_5[Cu(en)_2(H_2O)]_2[RE_4Ge_4W_{46}O_{164}(H_2O)_3]^{10-}$ (RE = Gd^{III}, Y^{III}),[151] in which an unprecedented 4:4-type tetrahedral $\{[(\alpha\text{-}GeW_{11}O_{39}RE)_2(\mu_3\text{-}WO_4)(\alpha\text{-}GeW_{11}O_{39}RE(H_2O))](\mu_4\text{-}WO_4)[\alpha\text{-}GeW_{11}O_{39}RE(H_2O)_2]\}^{24-}$ subunit was observed (Fig. 9c). The most prominent structural feature of this 4:4-type tetrahedral subunit consists of four mono-RE substituted Keggin $[\alpha\text{-}GeW_{11}O_{39}RE(H_2O)_n]^{5-}$ (n = 0, 1, 2) moieties combined together with the aid of two tetrahedral WO_4^{2-} connectors. More interestingly, tetrameric $\{[(\alpha\text{-}GeW_{11}O_{39}RE)_2(\mu_3\text{-}WO_4)(\alpha\text{-}GeW_{11}O_{39}RE(H_2O))](\mu_4\text{-}WO_4)[\alpha\text{-}GeW_{11}O_{39}RE(H_2O)_2]\}^{24-}$ nanoclusters can be all propagated to the 1-D extended chain under the driving force of the Jahn–Teller distortion of $[Cu(en)_2]^{2+}$ cations (Fig. 9d).

3.2 PTRHDMs based on di-vacant POM fragments

Compared to monovacant POM segments, divacant POM segments are more likely to facilitate the construction of unprecedented giant polymeric architectures by virtue of a suitable synthetic strategy that could allow the rational design of tailored assemblies. On one hand, the divacant POM segments represent one of the excellent inorganic multidentate O-donor ligands, which have been shown to display a strong potential for incorporating TM and RE ions and provide more caves for metal ions to live in. One the other hand, the encapsulated magnetic cores in bulky diamagnetic POM segments can be effectively isolated from proximal magnetic fragments, which allow the accurate determination of the intramolecular magnetic exchange interactions in a POM system. To date, only a few examples have been reported.[111,127,130,137,160] For example, in 2010, Mialane and coworkers firstly got a trinuclear $\{(Cr^{III}(OH)(H_2O))_3\}$ sandwiched precursor $[(\gamma\text{-}SiW_{10}O_{36})_2(Cr(OH)(H_2O))_3]^{10-}$ (Fig. 10a) from the reaction of the divacant $[\gamma\text{-}SiW_{10}O_{36}]^{8-}$ with the trinuclear precursor $[Cr_3(CH_3COO)_7(OH)_2]$ in aqueous solution under atmospheric pressure, and then used as-synthesized $[(\gamma\text{-}SiW_{10}O_{36})_2(Cr(OH)(H_2O))_3]^{10-}$ to react with La^{3+} cations affording a peculiar purely inorganic Cr^{III}–La^{III}double-chain 1-D system $[(\gamma\text{-}SiW_{10}O_{36})_2(Cr(OH)(H_2O))_3(La(H_2O)_7)_2]^{4-}$ (Fig. 10b).[130] Furthermore, Wang's group and Yang's group reported several Fe^{III}–Ln^{III} heterometallic aggregates $[K\subset\{Fe\text{-}Ce(\alpha\text{-}AsW_{10}O_{38})(H_2O)_2\}_3]^{14-}$,[111] $[Dy_6Fe_6(H_2O)_{12}(\alpha\text{-}SiW_{10}O_{38})_6]^{36-}$,[137] $[Tb_6Fe_6(H_2O)_{12}(\alpha\text{-}SiW_{10}O_{38})_6]^{36-}$,[137] and $[Fe_6Sm_6(H_2O)_{12}(\alpha\text{-}GeW_{10}O_{38})_6]^{36-}$,[160] and their asymmetric structural units are all made up of three divacant $[\alpha\text{-}XW_{10}O_{38}]^{11/12-}$ (X = As^V, Si^{IV}, Ge^{IV}) fragments bridged by three $\{Fe\text{–}(\mu\text{-}O)_3\text{–}RE\}$ (RE = Ce^{III}, Dy^{III}, Tb^{III}, Sm^{III}) heterometallic linkers (Fig. 10c). It is worth mentioning that their asymmetric structural units can be further dimerized to hexamers with paper-cut window grilles with a unique Chinese style by K^+ bridges (Fig. 10d). In 2010, Reinoso *et al.* reported an unprecedented giant crown-shaped POT containing Ce^{3+} and Ni^{2+} cations $\{[Ni(H_2O)_6]_3[K\subset K_7Ce_{24}Ge_{12}W_{120}O_{456}(OH)_{12}(H_2O)_{64}]\}^{46-}$ by a simple one-pot procedure containing $Na_2WO_4{\cdot}2H_2O$, $Ce(NO_3)_3{\cdot}6H_2O$, GeO_2 and $NiCl_2{\cdot}6H_2O$ in NaAc–HAc buffer solution,[127] which represents the largest tungstogermanate and the third largest POT. The giant $[Ce_{24}Ge_{12}W_{120}O_{456}(OH)_{12}(H_2O)_{64}]^{60-}$ (Fig. 10e) cluster contains a crown-shaped $[\{[Ce(H_2O)_2]_2(\beta\text{-}GeW_{10}O_{38})\}_6]^{36-}$ core including six $[\beta\text{-}Ce_2GeW_{10}O_{38}]^{6-}$ fragments, and then this crown-shaped arrangement is reinforced by six outer $[\gamma\text{-}Ce_2GeW_{10}O_{38}]^{6-}$ fragments. In this compound, only Ce^{3+} cations coordinate to the divacant germanotungstate fragments; however, discrete $[Ni(H_2O)_6]^{2+}$ cations act as countercations. As discussed above, α-, β-, and γ-Keggin POM fragments are all observed in reported divacant PTRHDMs. Obviously, the number of divacant α- or β-Keggin PTRHDMs is more than that of divacant γ-Keggin PTRHDMs, which is in good agreement with the fact that α- or β-Keggin lacunary POM fragments usually are more stable than γ-Keggin lacunary POM fragments in the construction of POM-based derivatives and divacant γ-Keggin POM fragments are easy to transform into α- or β-Keggin POM fragments in the reaction process. Therefore, in order to obtain γ-Keggin PTRHDMs, the divacant γ-Keggin $[\gamma\text{-}XW_{10}O_{36}]^{8-}$ (X = Si^{IV}, Ge^{IV}) precursors are often the primary choice and suitable reaction conditions to stabilize γ-Keggin POM fragments are required. In addition, the $[As_2W_{19}O_{67}(H_2O)]^{14-}$ POA,[172] which is derived from the plenary $[As_2W_{21}O_{69}(H_2O)]^{6-}$ POA with the removal of two {W=O} groups, can also be used as the divacant precursor to synthesize PTRHDMs. For example, Wang *et al.* got a dimeric PTRHDM $\{La[As_2W_{20}CuO_{67}(H_2O)_3]\}^{3-}$ (Fig. 11a) by the reaction of $[As_2W_{19}O_{67}(H_2O)]^{14-}$ with Cu^{2+} and La^{3+} ions.[116] In $[As_2W_{20}CuO_{67}(H_2O)_3]^{6-}$, two vacant sites are simultaneously occupied by 50% W and 50% Cu atoms. Finally, a neoteric divacant Dawson Mn^{IV}–Ce^{IV} heterometallic POM $[\{\alpha\text{-}P_2W_{16}O_{57}(OH)_2\}\{Ce^{IV}Mn_6^{IV}O_9(O_2CCH_3)_8\}]^{8-}$ (Fig. 11b)[119] was directly synthesized by Fang *et al.* from a Mn–Ce heterometallic cluster $[Ce^{IV}Mn_6^{IV}O_9(O_2CCH_3)_9(NO_3)(H_2O)_2]$[186,187] and trivacant Dawson $[\alpha\text{-}P_2W_{15}O_{56}]^{12-}$ POA. In this compound, a bowl-shaped $\{Ce^{IV}Mn_6^{IV}O_9(O_2CCH_3)_8\}^{2+}$ cluster incorporates into the divacant Dawson $\{\alpha\text{-}P_2W_{16}O_{57}(OH)_2\}^{10-}$ fragment through an additional {W=O} group grafted to the $[\alpha\text{-}P_2W_{15}O_{56}]^{12-}$ POA.

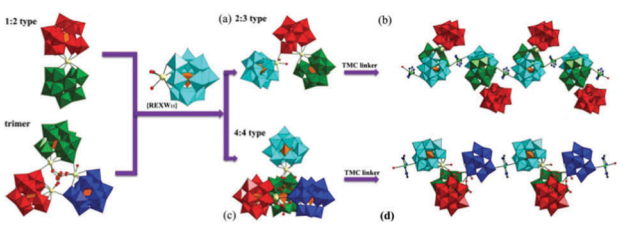

Fig. 9 (a and b) The structure unit of $[Cu(en)_2]_2[Cu(en)_2(H_2O)]_2H_3\{[Cu(en)_2]_2[Na_2(H_2O)_{1.75}][K(H_2O)_3][Dy_2(H_2O)_2(\alpha\text{-}GeW_{11}O_{39})_3]\}{\cdot}6H_2O$ and its 1-D chain motif. (c and d) The structural unit of $[Cu(en)_2]_5[Cu(en)_2(H_2O)]_2[RE_4Ge_4W_{46}O_{164}(H_2O)_3]^{10-}$ and its 1-D chain alignment. (XO_4: light orange, O: red, Re/Dy: yellow, Cu: bright green; N: blue.)

3.3 PTRHDMs based on tri-vacant POM fragments

In contrast to mono- or di-vacant POM fragments, trivacant POM fragments display more structural diversity and some typical species include (a) trivacant Keggin POM fragments with the stereoactive lone pair of electrons $[B\text{-}\alpha\text{-}XW_9O_{33}]^{8/9-}$, $[B\text{-}\beta\text{-}XW_9O_{33}]^{8/9-}$, $[A\text{-}\alpha\text{-}XW_9O_{33}]^{8/9-}$, and $[A\text{-}\beta\text{-}XW_9O_{33}]^{8/9-}$ (X = As^{III}, Sb^{III}, Bi^{III}, Se^{IV}, Te^{IV}); (b) trivacant Keggin POM fragments with the non-stereoactive lone pair of electrons $[B\text{-}\alpha\text{-}XW_9O_{34}]^{9/10-}$, $[B\text{-}\beta\text{-}XW_9O_{34}]^{9/10-}$, $[A\text{-}\alpha\text{-}XW_9O_{34}]^{9/10-}$, and $[A\text{-}\beta\text{-}XW_9O_{34}]^{9/10-}$ (X = Si^{IV}, Ge^{IV}, P^V, As^V); (c) trivacant Dawson POM fragments $[\alpha\text{-}X_2W_{15}O_{56}]^{12-}$ (X = P^V, As^V). Usually, these trivacant POM fragments are comparatively stable in a higher pH range, and therefore, they directly react with RE cations in aqueous

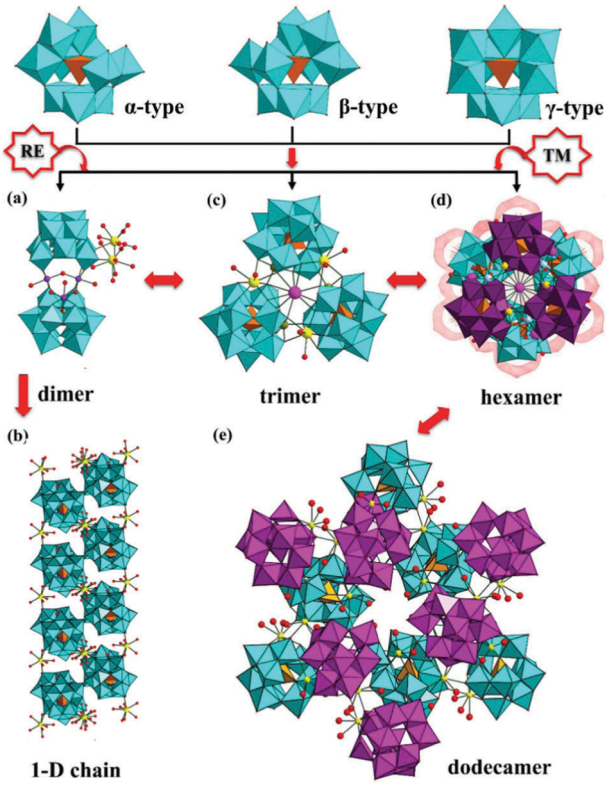

Fig. 10 (a) The structural unit of trinuclear $\{(Cr(OH)(H_2O))_3\}$ sandwiched dimeric $Cs_4[(\gamma\text{-}SiW_{10}O_{36})_2(Cr(OH)(H_2O))_3(La(H_2O)_7)_2]_3{\cdot}19H_2O$. (b) The 1-D double-chain pattern constructed by $[(\gamma\text{-}SiW_{10}O_{36})_2(Cr(OH)(H_2O))_3(La(H_2O)_7)_2]^{4-}$ units. (c) The trimeric structural unit of $[K\subset\{FeCe(X\text{-}W_{10}O_{38})(H_2O)_2\}_3]^{14/17-}$ (X = AsV, SiIV, GeIV). (d) The hexameric structure of $[Tb_6Fe_6(H_2O)_{12}(\alpha\text{-}XW_{10}O_{38})_6]^{30/36-}$ (X = As^V, Si^{IV}, Ge^{IV}). (e) The giant crown-shaped tungstogermanate $[Ce_{24}Ge_{12}W_{120}O_{456}(OH)_{12}(H_2O)_{64}]^{60-}$. ($WO_6$: turquiose, XO_4: light orange, O: red, RE: yellow, TM, bule.)

solution, which usually results in amorphous precipitation instead of crystallization. In order to obtain new trivacant PTRHDMs, currently, three main synthetic strategies have been developed: (1) the one-step aqueous assembly reaction, in which plenary or lacunary POM precursors directly react with TM cations and RE cations to prepare trivacant PTRHDMs in conventional aqueous solution; (2) the one-pot hydrothermal reaction, that is, trivacant POM precursors, TM cations and RE cations are simultaneously introduced into a reaction system and react with each other under hydrothermal conditions and thus lead to the formation of trivacant PTRHDMs; (3) the step-by-step reaction, that is to say, trivacant POM precursors are firstly combined with TM cations forming comparatively steady TM substituted POMs, and then the resulting TM substituted POMs react with RE cations thereby resulting in the desired trivacant PTRHDMs. In 2007, Müller *et al.* synthesized the first trivacant PTRHDM $[(VO)_2Dy(H_2O)_4K_2(H_2O)_2Na(H_2O)_2)(B\text{-}\alpha\text{-}AsW_9O_{33})_2]^{8-}$ that consists of two trivacant Keggin $[B\text{-}\alpha\text{-}AsW_9O_{33}]^{9-}$ units sandwiching two VO^{2+} and one Dy^{3+} cations by means of the one-step aqueous assembly reaction of $Na_2WO_4{\cdot}2H_2O$, As_2O_3, $VOSO_4{\cdot}5H_2O$ and $DyCl_3{\cdot}6H_2O$ (Fig. 12a).[115] More recently, we employed the 100 °C hydrothermal reaction of the divacant $[As_2W_{19}O_{67}(H_2O)]^{14-}$, Fe^{3+} and Ln^{3+} ions and isolated the 2-D

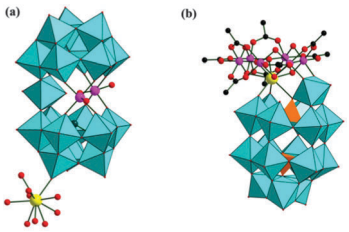

Fig. 11 (a) The structure of $\{La[As_2W_{20}CuO_{67}(H_2O)_3]\}^{3-}$. (b) The structure of $[\{\alpha\text{-}P_2W_{16}O_{57}(OH)_2\}\{Ce^{IV}Mn^{IV}_6O_9(O_2CCH_3)_8\}]^{8-}$. ($WO_6$: turquiose, XO_4: light orange, O: red, Ln: yellow, TM: pink.)

arsenotungstate-based TRHDMs $[Ln(H_2O)_6][Fe_4(H_2O)_{10}(B\text{-}\beta\text{-}AsW_9O_{33})_2]^{3-}$ (Ln = Pr^{III}, Nd^{III}) based on tetra-Fe^{III} substituted sandwich-type POM units and Ln linkers (Fig. 12b and c).[168] In 2014, we prepared the first series of Fe^{III}–RE^{III} heterometallic tungstoantimonates $[Ln(H_2O)_8][Fe_4(H_2O)_8(thr)_2][B\text{-}\beta\text{-}SbW_9O_{33}]_2{\cdot}22H_2O$ (Ln = Pr^{III}, Nd^{III}, Sm^{III}, Eu^{III}, Gd^{III}, Dy^{III}, Lu^{III}) by the one-step aqueous assembly reaction of $[B\text{-}\alpha\text{-}SbW_9O_{33}]^{9-}$, Fe^{3+} and Ln^{3+} ions in the presence of threonine (thr), which all consist of a $[Fe_4(H_2O)_8(thr)_2(B\text{-}\beta\text{-}SbW_9O_{33})_2]^{6-}$ hybrid subunit with two supporting $[Ln(H_2O)_8]^{3+}$ cations on both sides (Fig. 12d).[162] Especially, two thr ligands in the $[Fe_4(H_2O)_8(thr)_2(B\text{-}\beta\text{-}SbW_9O_{33})_2]^{6-}$ subunit substitute for two aqueous ligands in the parent $[Fe_4(H_2O)_{10}(B\text{-}\beta\text{-}SbW_9O_{33})_2]^{6-}$ POA,[173] which is tightly relevant to $[Sb_2W_{22}O_{74}(OH)_2]^{12-}$ discovered by Krebs *et al.* in 1997 that comprises two trivacant Keggin-type $[B\text{-}\beta\text{-}SbW_9O_{33}]^{9-}$ segments connected *via* two internal $[WO_2]^{2+}$ and two external $[WO_2(OH)]^{+}$ groups.[174] Then we also reported another five Fe^{III}–RE^{III} heterometallic tungstoantimonates $[Pr(H_2O)_8][Pr(H_2O)_6]Fe_4(H_2O)_{10}(B\text{-}\beta\text{-}SbW_9O_{33})_2{\cdot}16H_2O$[169] and $[RE(H_2O)_7]_2Fe_4(H_2O)_{10}(B\text{-}\beta\text{-}SbW_9O_{33})_2{\cdot}22H_2O$ [RE = Tb^{III}, Dy^{III}, Lu^{III}, Y^{III}].[169] In the former, the tetra-Fe^{III} substituted sandwich-type unit $[Fe_4(H_2O)_{10}(B\text{-}\beta\text{-}SbW_9O_{33})_2]^{6-}$ is built up of two trilacunary Keggin subunits $[B\text{-}\beta\text{-}SbW_9O_{33}]^{9-}$ sandwiching a rhomb-like $\{Fe^{III}_4\}$ cluster, and then the disordered Pr^{III} cations work as bridges to link adjacent sandwich-type units $[Fe_4(H_2O)_{10}(B\text{-}\beta\text{-}SbW_9O_{33})_2]^{6-}$ together, giving rise to the first 2-D extended sheet based on tungstoantimonate-based Fe^{III}–RE^{III} heterometallic building blocks, while the latter four are isomorphic and exhibit a discrete structure composed of a tetra-Fe^{III} substituted sandwich-type unit $[Fe_4(H_2O)_{10}(B\text{-}\beta\text{-}SbW_9O_{33})_2]^{6-}$ with two supporting $[RE(H_2O)_8]^{3+}$ cations. It is well known that the tetra-TM sandwich Weakley-type POMs $[TM_4(H_2O)_2(B\text{-}\alpha\text{-}XW_9O_{34})_2]^{n-}$ (X = P^V, As^V, Si^{IV}, Ge^{IV}) are the most representative TMSPs in POM chemistry,[175] and two external $\{TM(H_2O)\}$ groups in the sandwich belt are active and can be replaced by extraneous metal (Mn^{II}, Co^{II}, Na^{I}, *etc.*) ions forming mixed TM clusters.[176–183] Using the step-by-step reaction route, Reinoso *et al.* carried out intensive investigations on the incorporation of RE cations into active tetra-TM sandwiched Weakley-type POM skeletons and separated the first Weakley-like Mn^{III}–Ce^{III} heterometallic germanotungstate $[\{Ce^{III}(H_2O)_2\}_2Mn^{III}_2(B\text{-}\alpha\text{-}GeW_9O_{34})_2]^{8-}$ in 2010[129] from the stoichiometric reaction of the Ce^{4+} cation with the $[Mn^{II}_4(H_2O)_2(B\text{-}\alpha\text{-}GeW_9O_{34})_2]^{12-}$ precursor[184] in aqueous solution. $[\{Ce^{III}(H_2O)_2\}_2Mn^{III}_2(B\text{-}\alpha\text{-}GeW_9O_{34})_2]^{8-}$ can be described as the product of the substitution of two external Mn^{II} ions in the precursor by two extraneous $\{Ce^{III}(H_2O)_2\}$ groups

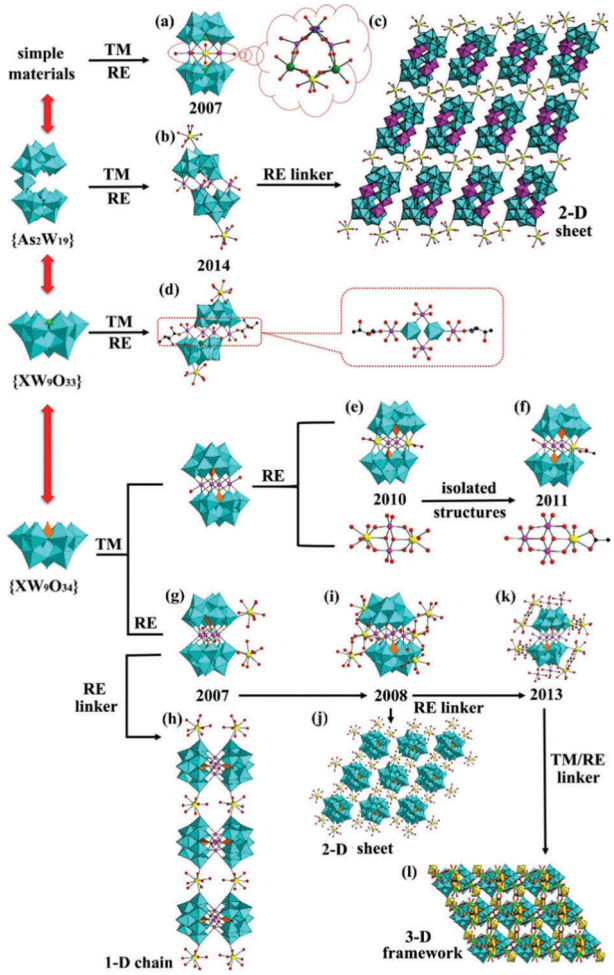

Fig. 12 (a) The structure of $[((VO)_2Dy(H_2O)_4K_2(H_2O)_2Na(H_2O)_2)(B\text{-}\alpha\text{-}AsW_9O_{33})_2]^{8-}$ consisting of two $[B\text{-}\alpha\text{-}AsW_9O_{33}]^{9-}$ trivacant Keggin units sandwiching two VO^{2+} and one Dy^{3+} cations. (b and c) The structural unit of $[Ln(H_2O)_6][Fe_4(H_2O)_{10}(B\text{-}\beta\text{-}AsW_9O_{33})_2]^{3-}$ and its 2-D sheet. (d) The structure of $[Pr(H_2O)_8]_2[Fe_4(H_2O)_8(thr)_2][B\text{-}\beta\text{-}SbW_9O_{33}]_2{\cdot}22H_2O$. (e) The structure of $[\{Ce^{III}(H_2O)_2\}_2Mn^{III}_2(B\text{-}\alpha\text{-}GeW_9O_{34})_2]^{8-}$. (f) The structure of $[\{Ce^{IV}(OAc)\}Cu^{II}_3(H_2O)(B\text{-}\alpha\text{-}GeW_9O_{34})_2]^{11-}$. (g) The structural unit of $[\{Ce(H_2O)_7\}_2Mn_4Si_2W_{18}O_{68}(H_2O)_2]^{6-}$. (h) The structural unit of $\{Nd_2(H_2O)_{12}Cu_4(H_2O)_2(SiW_9O_{34})_2\}^{6-}$. (i) The structural unit of $[Ce_2(ox)_3(H_2O)_2]_2\{[Mn(H_2O)_3]_2[Mn_4(GeW_9O_{34})_2(H_2O)_2]\}^{8-}$. (j) The 1-D chiral ladder-like chain of $[\{Ce(H_2O)_7\}_2Mn_4Si_2\ W_{18}O_{68}(H_2O)_2]^{6-}$. (k) The 2-D inorganic structure of $\{Nd_2(H_2O)_{12}Cu_4(H_2O)_2(SiW_9O_{34})_2\}^{6-}$. (l) The unseen 3-D framework of $[Ce_2(ox)_3(H_2O)_2]_2\{[Mn(H_2O)_3]_2\ [Mn_4(GeW_9O_{34})_2(H_2O)_2]\}^{8-}$. ($WO_6$: turquoise, XO_4: light orange, O: red, Mn: pink.)

accompanying the oxidation of internal Mn^{II} ions to Mn^{III} ions (Fig. 12e). The next year, the AFM Weakley-like Cu^{II}–Ce^{IV} heterometallic germanotungstate $[\{Ce^{IV}(OAc)\}Cu^{II}_3(H_2O)(B\text{-}\alpha\text{-}GeW_9O_{34})_2]^{11-}$ (Fig. 12f) was prepared using a similar approach.[133] Notably, $[\{Ce^{IV}(OAc)\}Cu^{II}_3(H_2O)(B\text{-}\alpha\text{-}GeW_9O_{34})_2]^{11-}$ can be viewed as the product of the substitution of one outer Cu^{II} cation in the $[Cu_4(H_2O)_2(B\text{-}\alpha\text{-}GeW_9O_{34})_2]^{12-}$ precursor by a $[Ce^{IV}(OAc)]^{3+}$ group, where the capping OAc^- ligand displays a κ^2-O,O′ chelating mode, together with a 60° rotation of one $[B\text{-}\alpha\text{-}GeW_9O_{34}]^{10-}$ fragment in comparison with $[\{Ce^{III}(H_2O)_2\}_2Mn^{III}_2(B\text{-}\alpha\text{-}GeW_9O_{34})_2]^{8-}$. It should be emphasized that the typical tetra-TM-substituted sandwich Weakley-type $[TM_4(H_2O)_2(B\text{-}\alpha\text{-}XW_9O_{34})_2]^{n-}$ POA, which has larger volume and more negative charge, provides an opportunity for the landing of higher coordination number metal cations (such as TM or/and RE) and is an ideal class of candidates for constructing multidimensional extended materials. Thereby, Wang's group made two extended TM–RE heterometallic sandwich-type silicotungstates $[\{Ce(H_2O)_7\}_2Mn_4Si_2W_{18}O_{68}(H_2O)_2]^{6-}$ (Fig. 12g)[114] and $\{Nd_2(H_2O)_{12}Cu_4(H_2O)_2(SiW_9O_{34})_2\}^{6-}$ (Fig. 12h),[121] respectively. The former was isolated by reaction of sandwich-type $[Mn_4Si_2W_{18}O_{68}(H_2O)_2]^{12-}$ POA, ceric sulfate and potassium citrate in an acidic aqueous solution and stands for a 1-D chiral ladder-like chain based on the sandwich-type POAs and Ln cations (Fig. 12j) while the latter is obtained by the reaction of divacant $[\gamma\text{-}SiW_{10}O_{36}]^{8-}$ POA, Cu^{2+} and Nd^{3+} cations in aqueous solution and represents the first 2-D inorganic structure composed of tetra-TM sandwiched silicotungstates and Ln linkers (Fig. 12k). Under hydrothermal conditions, Yang's team deliberately introduced the $[A\text{-}\alpha\text{-}GeW_9O_{34}]^{10-}$ precursor into the $\{Ce^{IV}/Mn^{II}/ox\}$ system and made an organic–inorganic hybrid PTRHDM $[Ce_2(ox)_3(H_2O)_2]_2\{[Mn(H_2O)_3]_2[Mn_4(GeW_9O_{34})_2(H_2O)_2]\}^{8-}$ (Fig. 12i).[153] Interestingly, each tetra-Mn^{II} substituted sandwich-type POM unit functions as a fourteen-dentate ligand to connect eight Ce^{3+} and six Mn^{2+} centers into an unseen 3-D framework (Fig. 12l). To our knowledge, it represents the first 3-D organic–inorganic hybrid TM–Ln heterometallic framework constructed by tetra-TM substituted sandwich-type POAs and mixed TM and Ln linkers in POM chemistry.

Except for the aforementioned sandwich-type PTRHDMs with TM or TM–RE clusters in the sandwich belt, notice that a tetrameric PTRHDM with a tetra-RE substituted POM component was also discovered. In 2012, Fang and co-authors utilized the preformed Mn_{12}-acetate[185] and $CeMn_6O_9(O_2CCH_3)_9(NO_3)(H_2O)_2$[186,187] clusters as Mn^{III}/Mn^{IV} sources to interact with $[A\text{-}\beta\text{-}SiW_9O_{34}]^{10-}$ in the NaAc–HAc buffer and isolated an abnormal POM-based co-crystal $\{Na_2[(A\text{-}\beta\text{-}SiW_9O_{34})_2Ce^{IV}_4O_2(CH_3COO)_2]{\cdot}[(A\text{-}\beta\text{-}SiW_9O_{34})Mn^{III}_3Mn^{IV}O_3(CH_3COO)_3]_2\}^{20-}$ (Fig. 13a) exhibiting single molecule magnet (SMM) behavior,[143] which is made up of a nonmagnetic tetra-Ce^{IV} substituted trivacant Keggin moiety $[(A\text{-}\beta\text{-}SiW_9O_{34})_2Ce^{IV}_4O_2(CH_3COO)_2]^{10-}$ (Fig. 13b) sandwiched by two magnetic $\{Mn^{III}_3Mn^{IV}\}$-capped trivacant Keggin subunits $[(A\text{-}\beta\text{-}SiW_9O_{34})Mn^{III}_3Mn^{IV}O_3(CH_3COO)_3]^{6-}$ (Fig. 13c) *via* two bridging Na^+ cations. In the diamagnetic sandwich-type $[(A\text{-}\beta\text{-}SiW_9O_{34})_2Ce^{IV}_4O_2(CH_3COO)_2]^{10-}$, two $[A\text{-}\beta\text{-}SiW_9O_{34}]^{10-}$ segments are fused together by a planar tetra-Ce^{IV} cluster (Fig. 13d and e) in the centrosymmetric pattern. The $\{Mn^{III}_3Mn^{IV}\}$-capped tri-vacant Keggin subunit $[(A\text{-}\beta\text{-}SiW_9O_{34})\ Mn^{III}_3Mn^{IV}O_3(CH_3COO)_3]^{6-}$ features an acetate-bridged tetrahedral $\{Mn_4\}$ core grafting to a $[A\text{-}\beta\text{-}SiW_9O_{34}]^{10-}$ segment (Fig. 13e and f). In addition, an inorganic octameric aggregate $\{Mn[Ce^{IV}_4As^{III}_4W_{41}O_{149}]\}^{46-}$ (Fig. 13g) was isolated by Li and co-workers *via* a step-by-step assembly process by reaction of the prefabricated sandwich-type RESP $[\{Ce_2O(H_2O)_5\}\{WO(H_2O)\}\{\alpha\text{-}AsW_9O_{33}\}_2]_2^{16-}$ precursor with Mn^{2+} ions at pH = 5.[117] Interestingly, this inorganic octamer is constituted by two cryptand-type $[Ce_4As_4W_{41}O_{149}]^{24-}$ subunits (Fig. 13h) connected together by an octahedral $[Mn(H_2O)_4]^{2+}$ linker (Fig. 13i). The cryptand-type $[Ce_4As_4W_{41}O_{149}]^{24-}$ subunit can be perceived as an assembly of a $[Ce_4W_5O_{17}]^{12+}$ cluster

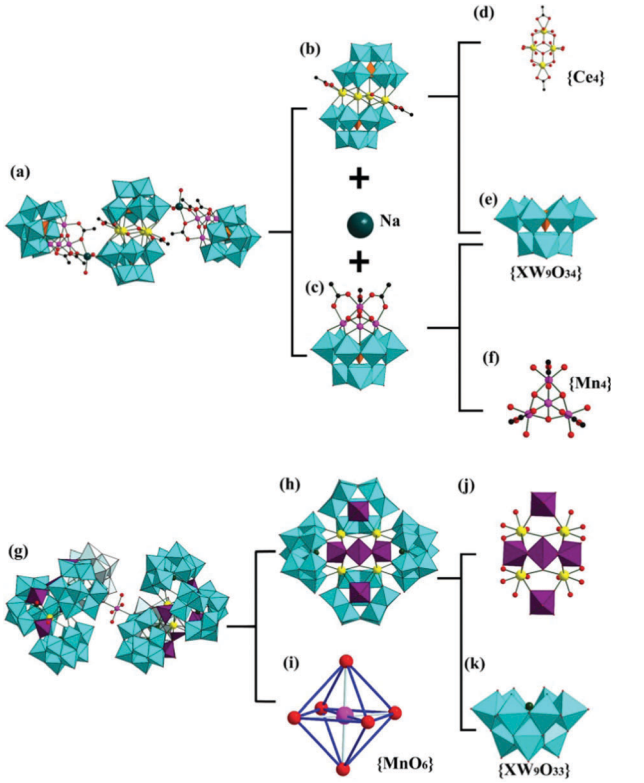

Fig. 13 (a) The 1 : 2 co-crystal $\{Na_2[(A\text{-}\beta\text{-}SiW_9O_{34})_2Ce^{IV}_4O_2(CH_3COO)_2]\text{-}[(A\text{-}\beta\text{-}SiW_9O_{34})Mn^{III}_3Mn^{IV}O_3(CH_3COO)_3]_2\}^{20-}$ with two bridging Na^+ ions. (b) The nonmagnetic tetra-Ce^{IV} substituted trivacant Keggin moiety $[(A\text{-}\beta\text{-}SiW_9O_{34})_2Ce^{IV}_4O_2(CH_3COO)_2]^{10-}$. (c) The magnetic $\{Mn^{III}_3Mn^{IV}\}$-capped trivacant Keggin subunit $[(A\text{-}\beta\text{-}SiW_9O_{34})Mn^{III}_3Mn^{IV}O_3(CH_3COO)_3]^{6-}$. (d) The planar tetra-$Ce^{IV}$ cluster. (e) The polyhedral view of the $[A\text{-}\beta\text{-}SiW_9O_{34}]^{10-}$ segment. (f) The acetate-bridged tetrahedral $\{Mn_4\}$ core. (g) The inorganic Ce–Mn-containing octamer $\{Mn[Ce^{IV}_4As^{III}_4W_{41}O_{149}]\}^{46-}$. (h) The cryptand-type $[Ce_4As_4W_{41}O_{149}]^{24-}$ subunit. (i) The octahedral $[Mn(H_2O)_4]^{2+}$ linker. (j) The $[Ce_4W_5O_{17}]^{12+}$ cluster. (k) The $[B\text{-}\alpha\text{-}AsW_9O_{33}]^{9-}$ fragment. (WO_6: turquoise, XO_4: light orange, O: red, Mn: pink, Ce: yellow, C: black.)

(Fig. 13j) and four $[B\text{-}\alpha\text{-}AsW_9O_{33}]^{9-}$ fragments (Fig. 13k). The $[Ce_4W_5O_{17}]^{12+}$ cluster is made up of five $\{WO_5\}$ square pyramids bridged by four Ce^{4+} ions.

Besides trivacant Keggin POM fragments, trivacant Dawson-type $[\alpha\text{-}P_2W_{15}O_{56}]^{12-}$ POA was also introduced into the PTRHDM system under conventional solution conditions. For instance, Fang *et al.* found a Mn–Ce heterometallic POM $[\{\alpha\text{-}P_2W_{15}O_{56}\}_6\{Ce_3Mn_2(\mu_3\text{-}O)_4(\mu_2\text{-}OH)_2\}_3(\mu_2\text{-}OH)_2(H_2O)_2(PO_4)]^{47-}$ (Fig. 14a and b)[120] by using a Mn–Ce heterometallic cluster $[Ce^{IV}_3Mn^{IV}_2O_6(O_2CMe)_{7.5}(NO_3)_3]\cdot(HO_2C\text{-}Me)_{0.5}(H_2O)_2$[186,187] to react with the $[\alpha\text{-}P_2W_{15}O_{56}]^{12-}$ POA with the additional addition of NaH_2PO_4, which is a gigantic hexa-Dawson poly(POM) cluster with crystallographic C_2 symmetry constructed from six trivacant Dawson $[\alpha\text{-}P_2W_{15}O_{56}]^{12-}$ POAs, three $[Ce_3Mn_2O_6(OH)_2]^{6+}$ core units and a central PO_4^{3-} group. Noticeably, each $[Ce_3Mn_2O_6(OH)_2]^{6+}$ core is sandwiched by two trivacant Dawson $[\alpha\text{-}P_2W_{15}O_{56}]^{12-}$ fragments forming a λ-shaped sandwich-type structure (Fig. 14a). Significantly, this finding not only demonstrates that the combination strategy of prefabricated TM–RE carboxylate clusters with lacunary POM precursors is a versatile tool to create neoteric molecule-based magnetic PTRHDMs,[120] but also may open the way to the preparation of organic–inorganic hybrid poly(PTRHDM) clusters by this straightforward metathesis reaction. In addition, by virtue of the step-by-step reaction, Ma *et al.* isolated a 3d–4f heterometallic 3-D Dawson cluster–organic framework $\{[Ce_4(H_2O)_{22}(dpdo)_5](Mn_2HP_2W_{15}O_{56})_2\}^{2-}$ (Fig. 14c and d) with self-penetrating (4,4,6)-connected net topology by reaction of the $[Mn_4(H_2O)_2(P_2W_{15}O_{56})_2]^{16-}$ precursor with the Ce^{3+} cation in the participation of dpdo (4,4′-bipyridine-*N*,*N*′-dioxide) under 160 °C hydrothermal conditions.[154] The fascinating structural feature is a self-penetrating (4,4,6)-connected network with $(4\cdot6^2\cdot8\cdot10^2)(4^2\cdot6\cdot8\cdot10^2)(4^2\cdot6^2\cdot8^9\cdot10^2)$ topology when each $[Mn_4(HP_2W_{15}O_{56})_2]^{14-}$ unit is considered as a six-connected node and each Ce^{3+} cation is viewed as a four-connected node.

3.4 PTRHDMs based on multi-vacant POM fragments

Completely different from most of the mono-, di- and tri-vacant POM fragments that not only can be isolated as pure POM precursors, but also can be *in situ* generated during the course of the preparation process, almost all the multivacant POM fragments except for hexavacant $[H_2P_2W_{12}O_{48}]^{12-}$ and hexadecavacant $[H_7P_8W_{48}O_{184}]^{33-}$[55] are *in situ* formed in the self-assembly of simple oxometalates or come from the degradation or rearrangement of lacunary POM precursors in the reaction procedure. In the process of exploiting PTRHDMs, tetravacant POM fragments have been observed. For example, Wang *et al.* reported a series of peculiar tetravacant Keggin PTRHDMs $[\{Ln^{III}Mn^{III}_4(\mu_3\text{-}O)_2(\mu_2\text{-}OH)_2(H_2O)(CO_3)\}(\beta\text{-}SiW_8O_{31})_2]^{11-}$ (Ln = Sm^{III}, Gd^{III}, Dy^{III}, Ho^{III}, Tm^{III}, Yb^{III}) (Fig. 15a),[149,166] in which a heterometallic appended cubane $\{Ln^{III}Mn^{III}_4(\mu_3\text{-}O)_2(\mu_2\text{-}OH)_2\text{-}(H_2O)(CO_3)\}^{7+}$ cluster (Fig. 15b) sandwiched by two diamagnetic tetravacant POM shells. They represent the first family of pure inorganic heterometallic appended cubane inserted POMs.

As we all know that phosphotungstates as one largest POM subclass not only can form the most famous plenary Dawson $[\alpha\text{-}P_2W_{18}O_{62}]^{6-}$ POA but also can derive some lacunary species such as monovacant $[\alpha\text{-}P_2W_{17}O_{61}]^{10-}$, trivacant $[\alpha\text{-}P_2W_{15}O_{56}]^{12-}$, hexavacant $[H_2P_2W_{12}O_{48}]^{12-}$ $\{P_2W_{12}\}$ and hexadecavacant $[H_7P_8W_{48}O_{184}]^{33-}$ $\{P_8W_{48}\}$, which may be the best candidates to incorporate more metal centers into fascinating high-nuclear or giant inorganic aggregates.[188–190] Especially, the typical hexavacant $\{P_2W_{12}\}$ precursor can be assembled into at least four types of aggregates with considerable sizes, including the $\{P_4W_{24}\}$ dimer, semi-opened $\{P_6W_{36}\}$ trimer, $\{P_6W_{39}\}$ trimer and crown-type $\{P_8W_{48}\}$ tetramer.[124,191–194] All of them exhibit strong reactivity on their inner surfaces with various electrophilic metal ions (such as TM and RE) and thus provide effective "reactors" for the assembly of huge clusters.[124] According to these characteristics, Wang and coworkers have obtained several excellent PTRHDMs.[124,131] In 2009, a supramolecular assembly $[Ce^{IV}_3Mn^{IV}_2O_6(OAc)_6(H_2O)_9]_2[Mn^{III}_2P_2W_{16}O_{60}]_3^{20-}$ (Fig. 15c) based on a triangular triple-Dawson-type subunit $[Mn^{III}_2P_2W_{16}O_{60}]_3^{24-}$ and bipyramid-like TM–Ln heterometallic cluster was isolated by introduction of the hexavacant precursor $\{P_2W_{12}\}$ into the HAc–NaAc buffer containing Ce^{4+} and Mn^{2+} cations.[124] The triangular triple-Dawson-type subunit $[Mn^{III}_2P_2W_{16}O_{60}]_3^{24-}$ (Fig. 15d) is

created by three di-Mn^{III} substituted $[Mn_2^{III}P_2W_{16}O_{60}]^{8-}$ fragments (Fig. 15e) through sharing six oxygen atoms. In 2010, Wang *et al.* took advantage of the reactions of $\{P_2W_{12}\}$ with TM and Ln cations assisted with tartrate or dimethylammonium chloride resulting in the isolation of another two heterometallic aggregates $[K_3\subset\{GdCo(H_2O)_{11}\}_2\{P_6W_{41}O_{148}(H_2O)_7\}]^{13-}$ (Fig. 15g) and $[K_3\subset\{GdMn(H_2O)_{10}\}\{H\text{-}MnGd_2(Tart)O_2(H_2O)_{15}\}\{P_6W_{42}O_{151}(H_2O)_7\}]^{11-}$ (Fig. 15j).[131] Both contain a crown-type POA shell $\{P_6W_{39}\}$ (Fig. 15f and i) formed by three $\{P_2W_{12}\}$ units connected by three $\{WO(H_2O)\}$ linkers. Furthermore, the former exhibits a one-dimensional chain-like structure composed of di-Co-containing $\{P_6W_{39}\}$ aggregates and $[Gd(H_2O)_7]^{3+}$ bridging units (Fig. 15h), nevertheless, in the latter, neighboring $[\{HMn^{II}Gd_2(Tart)O_2(H_2O)_{15}\}\{P_6W_{42}O_{151}(H_2O)_7\}]^{19-}$ are linked to the 1-D chain *via* sharing $[Gd(H_2O)_6]^{3+}$ connectors (Fig. 15k) and then the 1-D chains are bridged by $[Mn(H_2O)_4]^{2+}$ cations constructing a 2-D porous framework (Fig. 15l). In 2012, Kortz's group chose the cyclic $\{P_8W_{48}\}$ POA with a large central cavity, which was reported by Contant and Tézé in 1985,[195] as the precursor to react with Fe^{3+} and Ln cations in a simple one-pot reaction in pH = 4 aqueous medium in the presence of hydrogen peroxide, leading to a horseshoe-shaped PTRHDM $[Fe_{16}O_2(OH)_{23}(H_2O)_9P_8W_{49}O_{189}Ln_4(H_2O)_{19}]^{11-}$ (Ln = Eu^{III}, Gd^{III}) (Fig. 15o),[144] which comprises an unprecedented open 49-tungsto-8-phosphate ring $\{P_8W_{49}\}$ (Fig. 15m) with a central $[Fe_{16}O_2(OH)_{23}(H_2O)_9]^{21+}$ guest (Fig. 15n). This inorganic ring opening is unprecedented in POM chemistry, and will most likely have interesting and important consequences for synthetic chemists working in this area.[144]

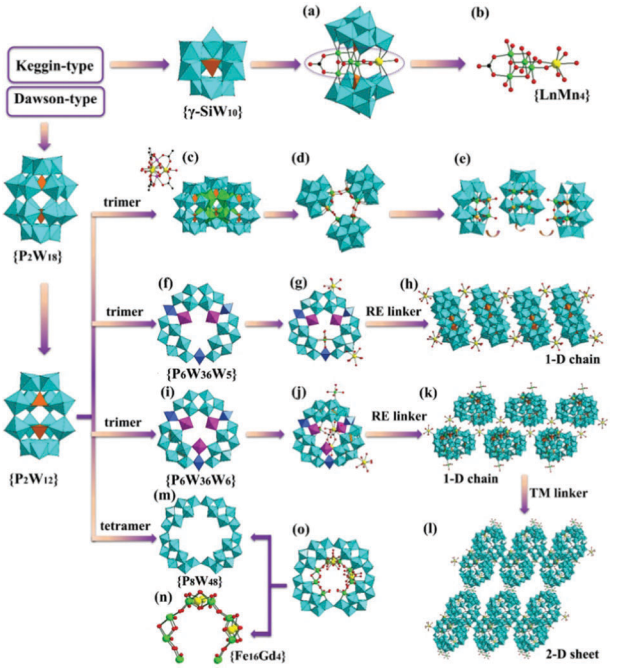

Fig. 15 (a) The structure of $[\{Ln^{III}Mn_4^{III}(\mu_3\text{-}O)_2(\mu_2\text{-}OH)_2(H_2O)(CO_3)\}(\beta\text{-}SiW_8O_{31})_2]^{13-}$. (b) The connection mode of the heterometallic appended cubane cluster $\{Ln^{III}Mn_4^{III}(\mu_3\text{-}O)_2(\mu_2\text{-}OH)_2(H_2O)(CO_3)\}^{7+}$. (c) The structure of $[Ce_3^{IV}Mn_2^{IV}O_6(OAc)_6(H_2O)_9]_2[Mn_2^{III}P_2W_{16}O_{60}]_3^{20-}$. (d) The structure of the triangular trimer $[Mn_2^{III}P_2W_{16}O_{60}]_3^{24-}$. (e) Three di-$Mn^{III}$ substituted $[Mn_2^{III}P_2W_{16}O_{60}]^{8-}$ fragments. (f) The structure of $[P_6W_{41}O_{148}(H_2O)_7]^{20-}$. (g) The structure of $[K_3\subset\{GdCo(H_2O)_{11}\}_2\{P_6W_{41}O_{148}(H_2O)_7\}]^{13-}$. (h) The 1-D chain-like structure of $[K_3\subset\{GdCo(H_2O)_{11}\}_2(P_6W_{41}O_{148}(H_2O)_7\}]^{13-}$. (i) The structure of $[P_6W_{42}O_{151}(H_2O)_7]^{20-}$. (j) The structure of $[K_3\subset\{GdMn^{II}(H_2O)_{10}\}\{HMn^{II}Gd_2(Tart)O_2(H_2O)_{15}\}\{P_6W_{42}O_{151}(H_2O)_7\}]^{11-}$. (k) The 1-D chain of $[\{HMn^{II}Gd_2(Tart)O_2(H_2O)_{15}\}\{P_6W_{42}O_{151}(H_2O)_7\}]^{19-}$. (l) The 2-D sheet structure of $[K_3\subset\{GdMn^{II}(H_2O)_{10}\}\{HMn^{II}Gd_2(Tart)O_2(H_2O)_{15}\}\{P_6W_{42}O_{151}(H_2O)_7\}]^{11-}$. (m) The structure of the open 49-tungsto-8-phosphate ring $\{P_8W_{49}\}$. (n) The structure of the central $[Fe_{16}O_2(OH)_{23}(H_2O)_9]^{21+}$ guest. (o) The structure of $[P_8W_{49}O_{189}Fe_{16}O_2(OH)_{23}(H_2O)_9Eu_4(H_2O)_{20}]^{11-}$. ($WO_6$: turquiose, XO_4: light orange, O: red, Ln: yellow; TM: bright green.)

3.5 PTRHDMs based on other POM fragments

In comparison with the lacunary Keggin and Dawson PTRHDMs, the research and investigation on PTRHDMs based on other structure type POM fragments remain underdeveloped. In this section, we will provide some typical examples to be discussed herein.

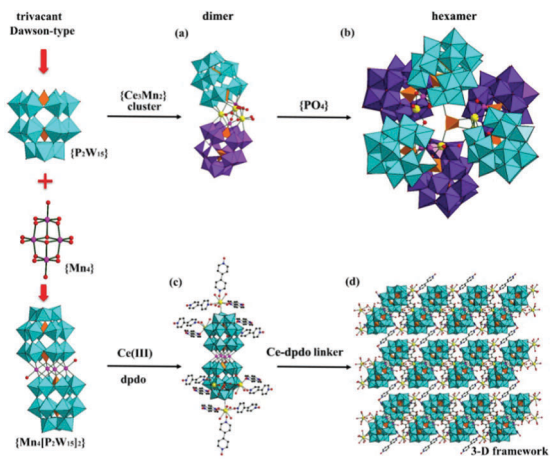

Fig. 14 (a) The λ-shaped sandwich-type subunit formed by a $[Ce_3Mn_2O_6(OH)_2]^{6+}$ core encapsulated by two tri-vacant Dawson $[\alpha\text{-}P_2W_{15}O_{56}]^{12-}$ fragments. (b) The structure of $[\{\alpha\text{-}P_2W_{15}O_{56}\}_6\{Ce_3Mn_2(\mu_3\text{-}O)_4(\mu_2\text{-}OH)_2\}_3(\mu_2\text{-}OH)_2(H_2O)_2(PO_4)]^{47-}$. (c) The structure of $\{[Ce_4(H_2O)_{22}(dpdo)_5](Mn_2HP_2W_{15}O_{56})_2\}^{2-}$. (d) The 3-D framework of $[Ce_4(H_2O)_{22}(dpdo)_5](Mn_2HP_2W_{15}O_{56})_2^{2-}$. ($WO_6$: turquiose, XO_4: light orange, Ce, yellow, O: red, Mn: pink, N: blue.)

As we know, the Preyssler-type $[Na(H_2O)P_5W_{30}O_{110}]^{14-}$ ($\{P_5W_{30}\}$) POA (Fig. 16a) is a rare species, which can be deemed as a hexavacant Keggin $\{PW_6\}$ fragment (Fig. 16b), encapsulating an open λ-shaped $\{P_4W_{24}\}$ unit (Fig. 16c) derived from the combination of two hexavacant Dawson $\{P_2W_{12}\}$ fragments through sharing two oxygen atoms (Fig. 16d). It has been little investigated[196–198] since it was discovered in 1970 by Preyssler,[199] mainly because it is comparatively difficult for the large scale preparation. However, it is bulky and has high negative surface charges, which is more favorable to construct new hybrids including $\{P_5W_{30}\}$ (Fig. 16e and f) and TM–Ln heterometallic ions. Recently, Yang's team selected it as the candidate and obtained two 3-D organic–inorganic PTRHDMs $[\{Sm_6Mn(\mu\text{-}H_2O)_2(OCH_2COO)_7(H_2O)_{18}\}\{Na(H_2O)P_5W_{30}O_{110}\}]^{8-}$ (Fig. 16g) and $[\{Sm_4Cu_2(gly)_2(ox)(H_2O)_{24}\}\{NaP_5W_{30}O_{110}\}]^{2-}$ (Fig. 16i).[155] The former displays one interesting 3-D framework (Fig. 16h) built by three types of subunits $\{P_5W_{30}\}$, $[Sm_2Mn(\mu\text{-}H_2O)_2(OCH_2COO)_2(H_2O)_5]^{4+}$ and $[Sm_4(OCH_2COO)_5(H_2O)_{13}]^{2+}$ whereas the

latter manifests another intriguing 3-D architecture (Fig. 16j) created by three types of subunits $\{P_5W_{30}\}$, $[SmCu(gly)(H_2O)_8]^{4+}$ and $[Sm_2(ox)(H_2O)_8]^{4+}$. Both represent the first 3-D PTRHDMs constructed from $\{P_5W_{30}\}$ subunits and TM/Ln–carboxylate–Ln connectors.

Obviously, during the past ten years, considerable attention has been concentrated on lacunary POT-based TRHDMs; however, explorations on POMB- or POV-based TRHDMs are very rare chiefly because it is comparatively difficult to prepare lacunary POMB or POV precursors in contrast to POTs. Under the continuously persisting efforts of synthetic chemists, only a few POMB-based TRHDMs and POV-based TRHDMs have been found. For example, Wang's group reported the first POMB-based TRHDM $(C_5H_9NO_2)_2[La(H_2O)_7CrMo_6H_6O_{24}]\cdot 11H_2O$ (Fig. 17a),[113] which exhibits a 1-D chain-like structure consisting of Anderson-type hexamolybdochromate $[CrMo_6H_6O_{24}]^{3-}$ covalently linked by the bridging $[La(H_2O)_7]^{3+}$ ions (Fig. 17b). It is worth pointing out that the Cr^{3+} ion is encapsulated in the center of Anderson-type $[CrMo_6H_6O_{24}]^{3-}$ POA and serves as a heteroatom of the hexamolybdochromate in this compound. In 2012, Li and his collaborators reported another two Anderson-type 3d–4f heterometallic POMBs $[\{CuTb(bmaed)(H_2O)_3\}_2\{IMo_6O_{24}\}]Cl\cdot 2MeOH\cdot 8H_2O$ (Fig. 17c) and $[\{CuTb(bmaed)(H_2O)_2\}_2\{AlMo_6O_{18}(OH)_6\}_2]\cdot MeOH\cdot 10H_2O$ (Fig. 17d) (bmaed = *N*,*N*′-bis(3-methoxysalicylidene) ethylenediamine).[142] The former comprises two $[CuTb(bmaed)(H_2O)_3]^{3+}$ cationic units and one A-type Anderson $[IMo_6O_{24}]^{5-}$[200] POA and the latter is composed of two $[CuTb(bmaed)(H_2O)_2]^{3+}$ cationic units and two B-type Anderson $[AlMo_6O_{24}H_6]^{3-}$[201] POAs. Generally speaking, both A- and B-type Anderson POAs possess the same molecular structure, but six oxygen atoms in the B-type Anderson unit are OH^- groups, which carry the less negative charge of the B-type Anderson POA.[201] In contrast to Anderson-type POMB-based TRHDMs, the report on Evans–Showell-type POM $[Co_2Mo_{10}H_4O_{38}]^{6-}$[202,203] as a building block is very rare.[204] In 2014, only two purely inorganic Evans–Showell-type POMB-based TRHDMs $[Ln(H_2O)_7][Ln(H_2O)_5][Co_2Mo_{10}H_4O_{38}]\cdot 5H_2O$ (Ln = Gd^{III}, Tb^{III}) (Fig. 17e) were made by An *et al.* by reaction of the $[Co_2Mo_{10}H_4O_{38}]^{6-}$ precursor with Gd^{3+} or Tb^{3+} cations in the 85 °C water–acetonitrile solution,[164] which are all built up of Evans–Showell-type $[Co_2Mo_{10}H_4O_{38}]^{6-}$ POAs bridged by Gd^{3+} or Tb^{3+} cations to form a 3-D racemic framework (Fig. 17f). Furthermore, by decreasing the reaction temperature, two 0-D chiral POMs $[Ln(H_2O)_6][Co_2Mo_{10}H_4O_{38}]^{3-}$ (Ln = Gd^{III}, Tb^{III}) (Fig. 17g) were got, in which one $[Co_2Mo_{10}H_4O_{38}]^{6-}$ POA is supported by a $[Ln(H_2O)_6]^{3+}$ cation.[164] Otherwise, during the course of the search for POMB-based TRHDMs, the ε-Keggin POMB precursors are selected as the starting materials. For instance, a POM–cyanometalate 3-D multilayered coordination network $[\varepsilon\text{-}PMo_{12}O_{37}(OH)_3\{La(H_2O)_5(Fe(CN)_6)_{0.25}\}_4]\cdot 12H_2O$ (Fig. 17h) was synthesized by Ohkoshi *et al.* by making use of the reaction of the mixed-valent ε-Keggin $[\varepsilon\text{-}PMo^V_8Mo^{VI}_4O_{36}(OH)_4\{La(H_2O)_4\}_4]^{5+}$[205] with $[Fe^{II}(CN)_6]^{4-}$ under typical bench conditions at room temperature and ambient pressure,[146] which constitutes the first example of a cyanometalate bonded to a POM unit.

Recently, a family of organic–inorganic hybrid POV-based TRHDMs $[\{La_2(DMF)_5(H_2O)_4\}\{MnV_{13}O_{38}\}]^-$ (Fig. 18a), $[\{Ce_2(DMF)_2(H_2O)_7\}\{MnV_{13}O_{38}\}]^-$ (Fig. 18c), $[\{K(H_2O)_2\}_2\{Nd(DMF)(H_2O)_3\}\{MnV_{13}O_{38}\}]^{2-}$ (Fig. 18e), $\{RE_2(C_6H_5NO_2)_3(H_2O)_6\}\{[MnV_{13}O_{38}]\}^-$ (RE = La^{III}, Ce^{III}) (Fig. 18g) and $[\{Pr(C_6H_5NO_2)(H_2O)_{3.5}\}\{Pr_{0.5}(H_2O)_2\}\{MnV_{13}O_{38}\}]^{2.5-}$ (Fig. 18b, d, f, h and j) were obtained by Wang's group by reaction of preformed $[MnV_{13}O_{38}]^{7-}$[206] POA

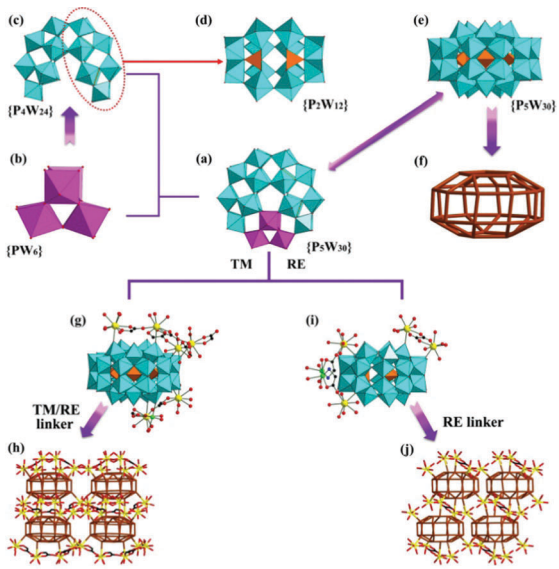

Fig. 16 (a) Side view of the $\{P_5W_{30}\}$ POA. (b) The hexavacant Keggin $\{PW_6\}$ fragment. (c) The open λ-shaped $\{P_4W_{24}\}$ unit. (d) The hexavacant Dawson $\{P_2W_{12}\}$ fragment. (e) Top view of the $\{P_5W_{30}\}$ POA. (f) The simplified graphic of the $\{P_5W_{30}\}$ POA. (g) The structural unit of $[\{Sm_6Mn(\mu\text{-}H_2O)_2(OCH_2COO)_7(H_2O)_{18}\}\{Na(H_2O)P_5W_{30}O_{110}\}]^{8-}$. (h) The 3-D framework of $[\{Sm_6Mn(\mu\text{-}H_2O)_2(OCH_2COO)_7(H_2O)_{18}\}\{Na(H_2O)P_5W_{30}O_{110}\}]^{8-}$. (i) The structural unit of $[\{Sm_4Cu_2(gly)_2(ox)(H_2O)_{24}\}\{NaP_5W_{30}O_{110}\}]^{2-}$. (j) The 3-D framework of $[\{Sm_4Cu_2(gly)_2(ox)(H_2O)_{24}\}\{NaP_5W_{30}O_{110}\}]^{2-}$.

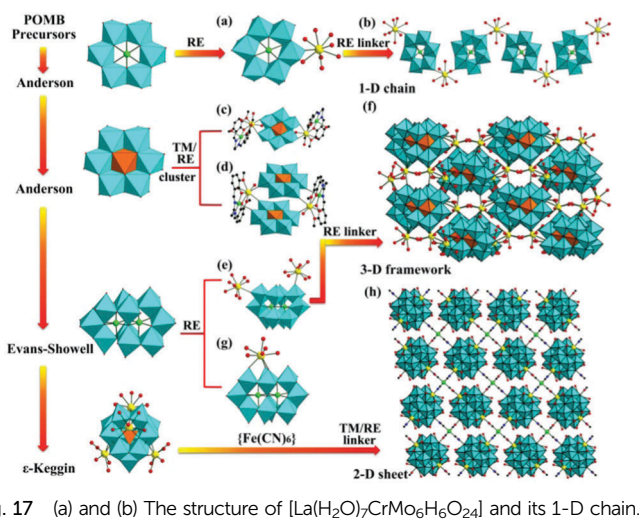

Fig. 17 (a) and (b) The structure of $[La(H_2O)_7CrMo_6H_6O_{24}]$ and its 1-D chain. (c) The molecular structure of $[\{CuTb(bmaed)(H_2O)_3\}_2\{IMo_6O_{24}\}]^+$. (d) The molecular structural unit of $[\{CuTb(bmaed)(H_2O)_2\}_2\{AlMo_6O_{18}(OH)_6\}_2]$. (e) $[Ln(H_2O)_7][Ln(H_2O)_5][Co_2Mo_{10}H_4O_{38}]$ (Ln = Gd^{III}, Tb^{III}). (f) The 3-D framework of $[Ln(H_2O)_7][Ln(H_2O)_5][Co_2Mo_{10}H_4O_{38}]$ (Ln = Gd^{III}, Tb^{III}). (g) The molecular structure of $[Ln(H_2O)_6][Co_2Mo_{10}H_4O_{38}]^{3-}$. (h) The POM–cyanometalate 3-D multilayered coordination network of $[\varepsilon\text{-}PMo_{12}O_{37}(OH)_3\{La(H_2O)_5(Fe(CN)_6)_{0.25}\}_4]\cdot 12H_2O$. ($MoO_6$: turquoise, XO_4: light orange, O: red, TM: bright green, Ln: yellow, N: blue, C: black.)

with RE cations in the conventional aqueous solution.[163] Their common structural feature is that they consist of a 1-D infinitely extended chain architecture built by alternative $[MnV_{13}O_{38}]^{7-}$ building blocks and RE–organic coordination linkages (Fig. 18d). They represent the first extended organic–inorganic hybrids created by $[MnV_{13}O_{38}]^{7-}$ POAs and RE cations.

4. Application fields

4.1 Magnetic properties

POMs can allow multinuclear spin-coupled magnetic centers (TM or RE) to encapsulate into their skeletons often through μ-oxo/hydroxo groups, which signifies that various shapes, sizes and types of magnetic clusters can be stabilized by POM ligands,[78,207,208] which has opened up a promising avenue for us to not only fabricate aesthetic structures but also deeply explore their fascinating magnetic behaviors. Moreover, nonmagnetic POA frameworks not only ensure an effective magnetic isolation of *in situ* generated TM or RE clusters from each other so that intermolecular interactions are usually negligible, offering a good opportunity for probing magnetic exchange interactions and electron delocalization in highly symmetrical clusters, but also can control the magnitude of magnetic couplings.[41,75–78] Because PTRHDMs contain TM and RE centers in their structures, their magnetic properties have attracted increasing interest due to the presence of exchange interactions between spin carriers in the solid-state chemistry and material science.[147,209,210] Although plenty of TM–Ln complexes have already been reported in the past two decades,[211–215] apart from the isotropic Gd^{III} cation with a $^8S_{7/2}$ single-ion ground state, the nature and magnitude of the exchange interactions of RE cations between themselves and with other magnetic groups and the evolution of the magnetic properties along the RE series are not well understood,[216] mainly because the orbital contribution, the ligand field effect and the spin–orbit coupling of most RE ions increase the complexity of the quantitative interpretation of the magnetic data.[216,217] Moreover, the $^{2S+1}$L group term of the $4f^n$ configuration for a RE cation often splits into $^{2S+1}L_J$ spectroscopic levels by interelectronic repulsion and spin–orbit coupling. Each of these states further splits into Stark sublevels by the crystal field perturbation.[216] Therefore, the magnetic properties of many PTRHDMs have been preliminarily studied[111,115,127,128,131,132,137,143,147,148,150,152,154,158–165] and their magnetic information is shown in Table S2 (ESI†). In this section, we will discuss some typical examples.

In 2008, Fang *et al.* investigated the magnetic properties of $[\{\alpha\text{-}P_2W_{16}O_{57}(OH)_2\}\{Ce^{IV}Mn^{IV}_6O_9(O_2CCH_3)_8\}]^{8-}$ (Fig. 19a)[119] and $[\{\alpha\text{-}P_2W_{15}O_{56}\}_6\{Ce_3Mn_2(\mu_3\text{-}O)_4(\mu_2\text{-}OH)_2\}_3(\mu_2\text{-}OH)_2(H_2O)_2(PO_4)]^{47-}$ (Fig. 19c)[120] by means of variable-temperature magnetic susceptibility measurements. The magnetic susceptibility of the former measured from 2 to 290 K indicates the AFM coupling between the S = 3/2 Mn^{IV} centers, affording a singlet ground state. The fitting of the experiment susceptibility data to the Curie–Weiss expression in the temperature range of 290 to 50 K results in the Weiss constant of −38 K. In the $\{Ce^{IV}Mn^{IV}_6O_9(O_2CCH_3)_8\}$ cluster, Mn1 and Mn1′, Mn2′ and Mn3′, Mn2 and Mn3 are respectively linked together by an acetate ligand, a μ_2-O atom and a μ_3-O atom; Mn1′ and Mn2′, Mn1 and Mn2 are respectively combined together *via* two acetate ligands and a

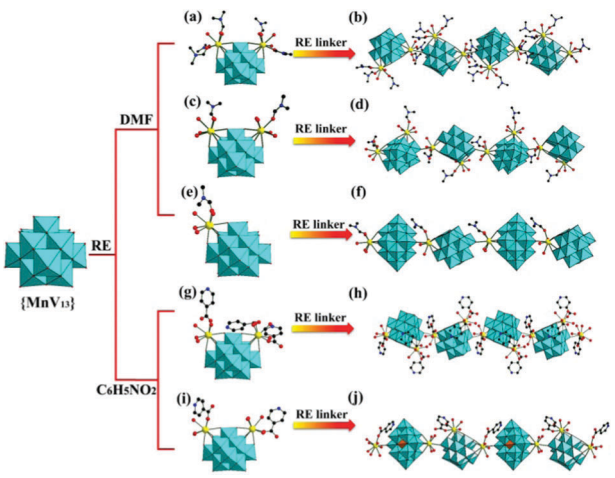

Fig. 18 (a) and (b) The structural unit of $[\{La_2(DMF)_5(H_2O)_4\}\{MnV_{13}O_{38}\}]^-$ and its 1-D chain. (c) and (d) The structural unit of $[\{Ce_2(DMF)_2(H_2O)_7\}\{MnV_{13}O_{38}\}]^-$ and its 1-D chain. (e) and (f) The structural unit of $[\{K(H_2O)_2\}_2\{Nd(DMF)(H_2O)_3\}\{MnV_{13}O_{38}\}]^{2-}$ and its 1-D chain. (g) and (h) The structural unit of $\{Ln_2(C_6H_5NO_2)_3(H_2O)_6\}\{[MnV_{13}O_{38}]\}^-$ (Ln = La^{III}, Ce^{III}) and its 1-D chain. (i) and (j) The structural unit of $[\{Pr(C_6H_5NO_2)(H_2O)_{3.5}\}\{Pr_{0.5}(H_2O)_2\}\{MnV_{13}O_{38}\}]^{2.5-}$ and its 1-D chain. (VO_6: turquoise, MnO_4: light orange, O: red, Ln: yellow, N: blue. C: black.)

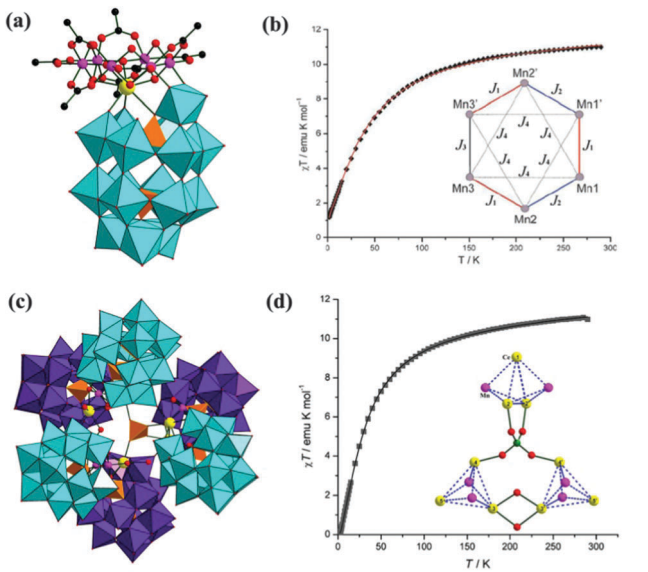

Fig. 19 (a) The structure of $[\{\alpha\text{-}P_2W_{16}O_{57}(OH)_2\}\{Ce^{IV}Mn^{IV}_6O_9(O_2CCH_3)_8\}]^{8-}$. (b) Temperature dependence of $\chi_M T$ at 0.1 Tesla (gray squares: experimental data; red solid line: best fit to the isotropic Heisenberg model). Inset: The magnetic exchange model. (c) The structure of $[\{\alpha\text{-}P_2W_{15}O_{56}\}_6\{Ce_3Mn_2(\mu_3\text{-}O)_4(\mu_2\text{-}OH)_2\}_3\ (\mu_2\text{-}OH)_2(H_2O)_2(PO_4)]^{47-}$. (d) Temperature dependence of $\chi_M T$ at 0.1 Tesla (gray squares: experimental data; black solid line: the best fit to the isotropic Heisenberg model). Inset: Connectivity between $\{Ce^{IV}_3Mn^{IV}_2\}$ cores and the central phosphate units. [(b) is reprinted with permission from ref. 119. Copyright 2008 The Royal Society of Chemistry; (d) is reprinted with permission from ref. 120. Copyright 2008 Wiley-VCH Verlag GmbH & Co. KGaA, Weinheim.]

μ_3-O atom, while Mn3 and Mn3′ are bridged together through an acetate ligand, a μ_3-O atom and an O–W–O linker, based on these three bridging modes, the magnetic exchange constants of three types of exchange pathways are defined as J_1, J_2 and J_3, respectively (Fig. 19b). In addition, the magnetic exchange constants of next-nearest neighboring Mn^{IV} centers (Mn1 and Mn2′, Mn1 and Mn3, Mn2′ and Mn3, Mn1′ and Mn2, Mn1′ and Mn3′, Mn3′ and Mn2) *via* O–Ce–O bridges are all defined as J_4. An isotropic Heisenberg spin Hamiltonian $\left(H = -2\sum JS_iS_j\right)$ based on these three interactions and a small next-nearest neighbor coupling constant (J_4) leads to a best fit of the low-field susceptibility data with J_1 = −4.2 cm^{-1}, J_2 = −4.6 cm^{-1}, J_3 = +0.4 cm^{-1}, J_4 = −0.5 cm^{-1} and a uniform g factor of g_{iso} = 2.06, which further consolidate the dominant AFM interactions within the $\{Ce^{IV}Mn^{IV}_6O_9(O_2CCH_3)_8\}$ cluster in $[\{\alpha\text{-}P_2W_{16}O_{57}(OH)_2\}\{Ce^{IV}Mn^{IV}_6O_9(O_2CCH_3)_8\}]^{8-}$.[119] In the case of $[\{\alpha\text{-}P_2W_{15}O_{56}\}_6\{Ce_3Mn_2(\mu_3\text{-}O)_4(\mu_2\text{-}OH)_2\}_3(\mu_2\text{-}OH)_2(H_2O)_2(PO_4)]^{47-}$, this aggregate can be viewed as three independent antiferromagnetically coupled Mn^{IV} (S = 3/2) dimers with an overall singlet ground state (Fig. 19d). Albeit slight geometry differences exist between independent $\{Ce_3Mn_2\}$ cores of dimers, a simple model on the basis of three identical Mn···Mn coupling interactions can explain its magnetic behavior. An isotropic Heisenberg model $H = -2\sum JS_iS_j$ yields a nearly perfect fit to the experimental data with J = −5.1 cm^{-1} and g_{iso} = 1.98.[120]

In 2009, Mialane *et al.* deeply probed the magnetic properties of a $\{GdCu_3(OH)_3(O(W))\}$ cubane inserted germanotungstate $\{[Cu(en)_2(H_2O)][(Cu(en)(OH))_3Gd(SiW_{11}O_{39})(H_2O)]\}_2\cdot 20H_2O$ (Fig. 20a) by the variable-temperature magnetic susceptibility measurement and an established magnetic model.[126] In this structure, two magnetic $\{GdCu_3(OH)_3(O(W))\}$ cubane subunits (Fig. 20b) are well isolated by two nonmagnetic $[SiW_{11}O_{39}]^{8-}$ moieties, which provides a good opportunity to quantitatively analyze the magnetic exchange interactions. The χ_MT (9.25 cm^3 K mol^{-1}) related to one cubane subunit and one isolated $[Cu(en)_2(H_2O)]^{2+}$ group at room temperature is slightly lower than the theoretical value (cm^3 K mol^{-1}) expected for four non-interacting S = 1/2 Cu^{2+} ions and one S = 7/2 Gd^{3+} ion (Fig. 20c). With the decrease in temperature, the χ_MT declines to the minimum at 30 K and then rapidly increases up to 2 K, indicating the coexistence of AFM and ferromagnetic (FM) coupling interactions. To evaluate the magnetic coupling interactions between magnetic centers in the cubane subunit, the magnetic coupling constants between the Cu^{II} centers (Cu1 and Cu2, Cu1 and Cu3, Cu2 and Cu3) are regarded as equivalent (J_1) and the magnetic coupling constants between the Gd^{III} and three Cu^{II} centers (Gd and Cu1, Gd and Cu2, Gd and Cu3) are also viewed as identical (J_2). Based on the Hamiltonian: $H = -J_1(S_{Cu1}S_{Cu2} + S_{Cu1}S_{Cu3} + S_{Cu2}S_{Cu3}) - J_2(S_{Gd}S_{Cu1} + S_{Gd}S_{Cu1} + S_{Gd}S_{Cu3}) + Ng^2\beta^2/4k$, the best fit of the χ_MT *vs.* T plot affords J_1 = −81.0 cm^{-1}, J_2 = +0.06 cm^{-1} and g = 2.01 and leads to a S = 4 ground state arising from a FM coupling between the S = 7/2 spin of the Gd^{III} center and the S = 1/2 spin of the antiferromagnetically coupled $\{Cu_3\}$ fragment. Moreover, the magnetization *vs.* field experiment performed at 2 K confirms the nature of the ground state (Fig. 20c, inset). In order to validate the above results, the paramagnetic Gd^{III} center was replaced by a diamagnetic La^{III} center, and 2-D $[Cu(en)_2][(Cu(en)(OH))_3La(SiW_{11}O_{39})]\cdot 20H_2O$ can be obtained and its magnetic properties have also been studied (Fig. 20d). The χ_MT value of one cubane subunit and one isolated $[Cu(en)_2(H_2O)]^{2+}$ ion decreases with lowering the temperature down to 25 K, where a plateau is reached and then the χ_MT slightly decreases from 15 K to 2 K, which indicates the AFM magnetic interactions within the cubane subunit. The decrease of the χ_MT below 15 K is assigned to small intercubane magnetic interactions. The simulation on the basis of the Hamiltonian: $H = -J(S_{Cu1}S_{Cu2} + S_{Cu1}S_{Cu3} + S_{Cu2}S_{Cu3}) + Ng^2\beta^2/4k$ gives J = −71.0 cm^{-1} and g = 2.00. This decrease of the χ_MT below 15 K in $[Cu(en)_2][(Cu(en)(OH))_3La(SiW_{11}O_{39})]\cdot 20H_2O$ further proves that the magnetic interactions between Gd^{III} and Cu^{II} ions are FM in $\{[Cu(en)_2(H_2O)][(Cu(en)(OH))_3Gd(SiW_{11}O_{39})(H_2O)]\}_2\cdot 20H_2O$.[126]

Additionally, Reinoso's group measured the magnetism of two sandwich-type PTRHDMs $[\{Ce(H_2O)_2\}_2Mn_2(B\text{-}\alpha\text{-}GeW_9O_{34})_2]^{8-}$[129] and $[\{Ce^{IV}(OAc)\}Cu^{II}_3(H_2O)(B\text{-}\alpha\text{-}GeW_9O_{34})_2]^{11-}$.[133] The former contains a unique $\{Ce^{III}_2Mn^{III}_2O_{20}\}$ rhomblike subunit (Fig. 21a). The χ_MT at 300 K of 8.2 cm^3 K mol^{-1} agrees with that expected for two uncoupled high-spin Mn^{III} ions and two uncoupled Ce^{III} ions. Upon lowering the temperature, the χ_MT gradually decreases until 60 K, which is attributed to the AFM interactions between the paramagnetic centers. By further lowering the temperature, the χ_MT increases to a maximum and this signifies the dominant $Ce^{III}\cdots Mn^{III}$ FM interaction (Fig. 21b). For this rhomblike magnetic motif, two different J and J' values are expected. J is always greater than J', furthermore, octahedral Mn^{III} ions that are connected *via* oxo or

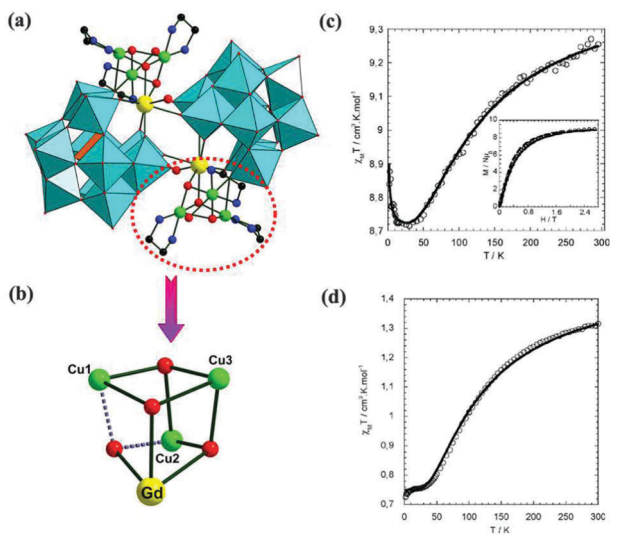

Fig. 20 (a) The structure of $\{[Cu(en)_2(H_2O)][(Cu(en)(OH))_3Gd(SiW_{11}O_{39})(H_2O)]\}_2\cdot 20H_2O$. (b) The $\{GdCu_3(OH)_3(O(W))\}$ cubane unit. (c) Temperature dependence of χ_MT for $\{[Cu(en)_2(H_2O)][(Cu(en)(OH))_3Gd(SiW_{11}O_{39})(H_2O)]\}_2\cdot 20H_2O$ and the solid line is generated by the best fitting result; Inset: M *vs.* H plot at 2 K. Dashed line: Brillouin function for a S = 4 spin and a S = 1/2 isolated Cu^{2+} ion. (d) Temperature dependence of χ_MT for $[Cu(en)_2][(Cu(en)(OH))_3La(SiW_{11}O_{39})]\cdot 20H_2O$. The solid line is generated by the best fitting results. [(c) and (d) are reprinted with permission from ref. 126. Copyright 2009 The Royal Society of Chemistry.]

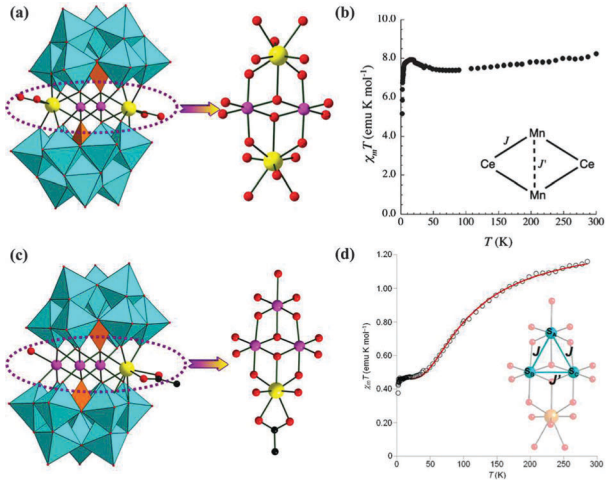

Fig. 21 (a) The molecular structure of $[\{Ce(H_2O)_2\}_2Mn_2(B\text{-}\alpha\text{-}GeW_9O_{34})_2]^{8-}$ and the central $\{Ce^{III}_2Mn^{III}_2O_{20}\}$ cluster. (b) Temperature dependence of the $\chi_M T$ plot for $[\{Ce(H_2O)_2\}_2Mn_2(B\text{-}\alpha\text{-}GeW_9O_{34})_2]^{8-}$. Inset: The schematic representation of the magnetic exchange pathways in the $\{Ce^{III}_2Mn^{III}_2O_{20}\}$ cluster. (c) The molecular structure of $[\{Ce^{IV}(OAc)\}Cu^{II}_3(H_2O)(B\text{-}\alpha\text{-}GeW_9O_{34})_2]^{11-}$ and the central $\{Ce^{IV}Cu^{II}_3O_{18}\}$ cluster. (d) Temperature dependence of $\chi_M T$ for $[\{Ce^{IV}(OAc)\}Cu^{II}_3(H_2O)(B\text{-}\alpha\text{-}GeW_9O_{34})_2]^{11-}$ and the solid red line represents the best fit to a triangular model. Inset: Scheme for the magnetic exchange pathways within the Cu_3 cluster. [(b) is reprinted with permission from ref. 129. Copyright 2009 American Chemical Society; (d) is reprinted with permission from ref. 133. Copyright 2011 American Chemical Society.]

hydroxo bridges display AFM interactions based on analogous systems.[218–220] Thus, J' must be negative in this system, as a result, the dominant FM interactions must be due to J being positive. The coexistence of AFM and FM interactions is further validated by the M–H plot at 2 K. The feature of the M–H plot in the $\{Ce^{III}_2Mn^{III}_2O_{20}\}$ cluster suggests a ground state with six unpaired electrons ($S = 3$), intermediate between the pure FM and AFM energy levels and also influenced by the spin frustration anticipated for this rhomblike arrangement with competing magnetic interactions.[129] In contrast, the latter consists of a central $\{Ce^{IV}Cu^{II}_3O_{18}\}$ rhomblike cluster (Fig. 21c). Its magnetic susceptibility is also measured (Fig. 21d). The $\chi_M T$ at 300 K of 1.16 cm^3 K mol^{-1} is consistent with the expected value for three non-interacting Cu^{II} ions and a diamagnetic Ce^{IV} ion. Upon cooling, the $\chi_M T$ decreases to 40 K and then reaches a plateau (40–3 K). After that, an additional decrease is observed. The first-step decrease is derived from AFM interactions within a $\{Ce^{IV}Cu^{II}_3O_{18}\}$ rhomblike cluster whereas the second-step decrease may be owing to the intermolecular interactions. The plateau originates from the paramagnetic ground state of the Cu_3 trimer. To explore its magnetic behavior, the magnetic core in the $\{Ce^{IV}Cu^{II}_3O_{18}\}$ rhomblike cluster is considered as an isosceles Cu_3 triangle; two different magnetic exchange pathways exist (J and J') (inset in Fig. 21d), the fitting using $H = -2J(S_AS_B + S_AS_C) - 2J'S_BS_C$ Hamiltonian affords $J = -23.6$ cm^{-1}, $J' = -68.8$ cm^{-1} and $g = 2.22$. The AFM interactions of $Cu_B\cdots Cu_C$ centers are much stronger than those of $Cu_A\cdots Cu_B$ and $Cu_A\cdots Cu_C$ centers.[133]

In recent years, an aspect of this interesting research field has been focused on the construction of new PTRHDMs with SMM behavior. SMM properties largely rely on their intrinsic magnetic characteristics, such as the high-spin ground state (S) and magnetocrystalline anisotropy (D), which lead to a spin-reversal barrier (U_{eff}) for the slow relaxation of magnetization, $U_{eff} = |D|S^2$ and $|D|(S^2 - 1/4)$ for a SMM with integer and half integer spins, respectively.[221–224] D must be negative in order to give rise to this spin-reversal barrier. For Ln ions, their significant magnetic anisotropy arises from the large unquenched orbital angular momentum, which may result in the appearance of the SMM behavior.[225] To date, several POM-based SMMs have been reported.[226–232] Although some efforts have been paid on the construction of high-spin and anisotropic TM–Ln heterometallic clusters encapsulated by lacunary diamagnetic POM fragments, few of them exhibit SMM properties. In 2012, Li *et al.* reported two Anderson-type PTRHDM SMMs $[\{CuTbL(H_2O)_3\}_2\{IMo_6O_{24}\}]Cl{\cdot}2MeOH{\cdot}8H_2O$ (Fig. 22a) and $[\{CuTbL(H_2O)_2\}_2\{AlMo_6O_{18}(OH)_6\}_2]{\cdot}MeOH{\cdot}10H_2O$ (Fig. 22c) (L = *N*,*N*′-bis(3-methoxysalicylidene)ethylenediamine), which are stabilized by Schiff-base ligands.[142] Their alternating-current (ac) susceptibilities were undertaken under the zero direct-current field to investigate their SMM behaviors. Obvious maximum values in the out-of-phase (χ'') ac susceptibilities are observed below 10 K in two Anderson-type PTRHDMs, suggesting the characteristic of SMMs (Fig. 22b and d).[233–236] From the frequency dependence of the ac data, the relaxation time (τ) of the systems has been evaluated and plotted in a semilogarithmic scale as a function of T^{-1}.[142] In addition, the characteristic time of the quantum tunneling of magnetization (QTM) is rapid (*ca.* 1.1×10^{-3} s), interpreting the nonexistence of M *versus* H hysteresis at the sweeping rate used in a typical magnetometer. The energy gap (U_{eff}) related to the thermally activated mechanism of relaxation has been calculated by using the experimental data above 4 K. Their U_{eff} are 17.1 and 20.8 K, respectively. Compared with the expected values of around 10^{-9}–10^{-11} s for SMMs, both τ_0 are obviously larger. Both τ_0 are apparently increased by the

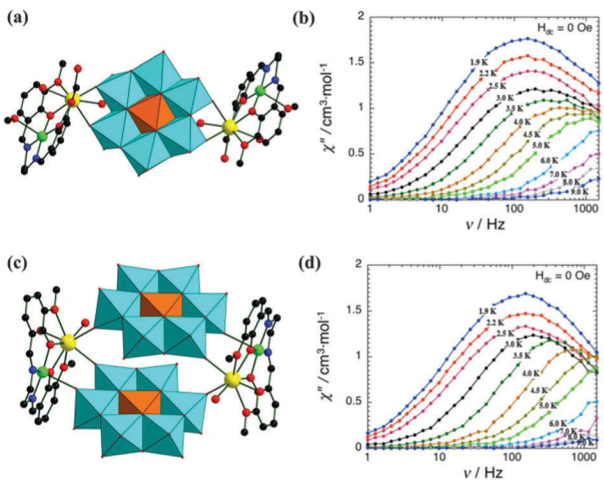

Fig. 22 (a) The molecular structure of $[\{CuTbL(H_2O)_3\}_2\{IMo_6O_{24}\}]Cl{\cdot}2MeOH{\cdot}8H_2O$. (b) The frequency-dependent out-of-phase (χ'') ac susceptibility under zero dc field for $[\{CuTbL(H_2O)_3\}_2\{IMo_6O_{24}\}]Cl{\cdot}2MeOH{\cdot}8H_2O$. (c) The molecular structure of $[\{CuTbL(H_2O)_2\}_2\{AlMo_6O_{18}(OH)_6\}_2]{\cdot}MeOH{\cdot}10H_2O$. (d) The frequency-dependent out-of-phase (χ'') ac susceptibility under zero dc field for $[\{CuTbL(H_2O)_2\}_2{\cdot}\{AlMo_6O_{18}(OH)_6\}_2]{\cdot}MeOH{\cdot}10H_2O$. [(b) and (d) are reprinted with permission from ref. 142. Copyright 2012 American Chemical Society.]

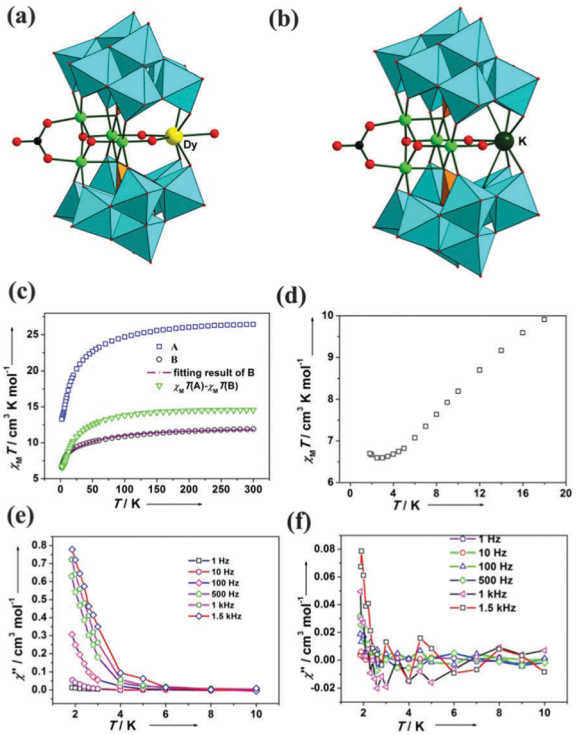

Fig. 23 (a) The molecular structure of $K_7Na_6[\{Dy^{III}Mn^{III}_4(\mu_3\text{-}O)_2(\mu_2\text{-}OH)_2(H_2O)\ (CO_3)\}(\beta\text{-}SiW_8O_{31})_2]\cdot 21H_2O$ (**A**). (b) The molecular structure of $K_9Na_6[\{KMn^{III}_4\ (\mu_3\text{-}O)_2(\mu_2\text{-}OH)_2(CO_3)\}(\beta\text{-}SiW_8O_{31})_2]\cdot 22H_2O$ (**B**). (c) The temperature dependence of $\chi_M T$ plots for **A** (square), **B** (circle) and $\chi_M T$(**A**)–$\chi_M T$(**B**) (triangle), respectively. (d) The low-temperature dependence of $\chi_M T$(**A**)–$\chi_M T$(**B**). (e) The temperature-dependent out-of-phase (χ'') ac susceptibility under zero direct-current (dc) field for **A**. (f) The temperature-dependent out-of-phase (χ'') ac susceptibility under zero dc field for **B**. [(c–f) are reprinted with permission from ref. 149. Copyright 2013 The Royal Society of Chemistry.]

presence of QTM, revealing that the acquired U_{eff} must be taken as a lower limit of the real thermal energy gaps.[142]

To continue and deepen the research in this special field, in 2013, Wang's group reported another $\{Dy^{III}Mn^{III}_4\}$ encapsulated PTRHDM $K_7Na_6[\{Dy^{III}Mn^{III}_4(\mu_3\text{-}O)_2(\mu_2\text{-}OH)_2(H_2O)(CO_3)\}(\beta\text{-}SiW_8O_{31})_2]\cdot 21H_2O$ (**A**) (Fig. 23a) showing the SMM-like slow magnetic relaxation feature,[149] Its $\chi_M T$ value gradually decreases from 300 K to 1.8 K, which is attributed to the large orbital contribution of Dy^{III} ions and the dominant AFM coupling within Mn^{III} centers (Fig. 23c). In order to evaluate the coupling nature between Dy^{III} and Mn^{III} ions, $K_9Na_6[\{KMn^{III}_4(\mu_3\text{-}O)_2(\mu_2\text{-}OH)_2(CO_3)\}(\beta\text{-}SiW_8O_{31})_2]\cdot 22H_2O$ (**B**) (Fig. 23b) was synthesized with a similar core structure to **A** and its variable-temperature susceptibility has been measured and then $\chi_M T$(**A**)–$\chi_M T$(**B**) was calculated (Fig. 23c). At room temperature, the $\chi_M T$(**A**)–$\chi_M T$(**B**) value of 14.5 emu K mol^{-1} is in good agreement with the magnetic contribution of a Dy^{III} ion. Upon cooling, it decreases to a minimum value at about 3 K, implying the AFM coupling between the Dy^{III} and Mn^{III} ions. Below 3 K, it gradually increases, which can be attributed to the arrangement of the net spins between $\{Mn^{III}_4\}$ and Dy^{III} ions along the applied field (Fig. 23d). The AC susceptibilities of **A** (Fig. 23e) and **B** (Fig. 23f) were performed, but no peak was observed in the out of phase (χ'') for both. The strongly frequency-dependent signals (χ'') below 4 K for **A** indicate the SMM-like slow relaxation while the frequency-dependent signals (χ'') below 2.5 K for **B** reveal the slow magnetization relaxation behaviour.

4.2 Photoluminescence

Classical inorganic and organic luminescent materials have been widely exploited and realized because of their diversiform functionalities and applications in display, lighting, sensing, and optical devices.[81,237–239] RE-based complexes can reveal fascinating photoluminescence properties in areas such as lasers, light-emitting diodes, cathode rays, plasma displays, optical fibers, optical amplifiers, NIR-emitting materials and sensory probes,[240,241] which are related to the properties of RE ions: (i) compared with other elements, RE ions have a characteristic 4f electronic structure, large atomic magnetic moment, and strong spin coupling; (ii) the shielding of the 4f electrons by the outer 5s and 5p electrons results in well-defined absorption and emission bands;[242] (iii) their high colour purity and potentially high internal quantum efficiency;[241,243] (iv) each RE ion exhibits narrow and characteristic 4f–4f transitions; (v) fluorescence life can span from nanoseconds to microseconds. Additionally, the atomic properties of RE ions are maintained in the complexes. Furthermore, photoexcitation of the O → M (M = Mo, W) ligand to metal charge transfer (LMCT) bands of the POM lattices can result in intramolecular energy transfer from O → M excited states to excited energy levels of RE ions,[244] then to sensitize the RE emission. Besides, the photoluminescence behavior of some RE-containing POMs and the molecular mechanisms of intramolecular energy transfer processes have been investigated by Yamase and other groups.[22,245–248] As a consequence, the solid-state photoluminescence properties of some typical PTRHDMs have been investigated at room temperature.[136,138,139,141,145,147,155,157,162,168] In addition, their photoluminescence data have been listed in Table S3 (ESI†). These photoluminescence research studies may provide some candidates for the discovery of new light-emitting materials. Herein, several typical examples are highlighted. In 2014, Zhao *et al.* investigated the photoluminescence properties of $[Eu(H_2O)_8]_2[Fe_4(H_2O)_8(thr)_2][B\text{-}\beta\text{-}SbW_9O_{33}]_2\cdot 22H_2O$ and its solid-state emission spectrum under excitation at 310 nm exhibits five characteristic emission bands at 564, 594, 618, 648, and 700 nm, which are respectively attributed to $^5D_0 \rightarrow {}^7F_0$, $^5D_0 \rightarrow {}^7F_1$, $^5D_0 \rightarrow {}^7F_2$, $^5D_0 \rightarrow {}^7F_3$ and $^5D_0 \rightarrow {}^7F_4$ transitions derived from the Eu^{III} cations (Fig. 24a).[162] In general, the $^5D_0 \rightarrow {}^7F_0$ transition is strictly forbidden in a symmetric field. But the weak $^5D_0 \rightarrow {}^7F_0$ emission at 564 nm is seen in this compound, indicating that the Eu^{III} cations dwell in the lower symmetric ligand field. In addition, the intensity ratio of the $^5D_0 \rightarrow {}^7F_2/{}^5D_0 \rightarrow {}^7F_1$ transitions is usually functioned as a criterion of examining the local chemical microenvironments and the site symmetry of the Eu^{III} cations,[249] that is, the $^5D_0 \rightarrow {}^7F_1$ transition is dominant in a centrosymmetric environment whereas the $^5D_0 \rightarrow {}^7F_2$ transition is the strongest in a noncentrosymmetric field.[250,251] Here, the intensity ratio of the $^5D_0 \rightarrow {}^7F_2/{}^5D_0 \rightarrow {}^7F_1$ transitions is 4.7, which further suggests the low site symmetry of the Eu^{III} cations, which coincides with the

distorted monocapped square antiprism geometry of Eu^{III} cations. Moreover, its luminescence decay curve was also measured (Fig. 24b) and fitted by the single exponential function [$I = A\exp(-t/\tau)$]. The lifetime τ is 0.097 ms, which is much shorter than those of $K_{13}[Eu(SiW_{11}O_{39})_2]$ (2.440 ms) and $Na_{0.5}Cs_{4.5}[Eu(\alpha\text{-}SiW_{11}O_{39})(H_2O)_2]\cdot 23H_2O$ (0.39 ms),[86] principally because aqueous ligands on Eu^{3+} cations in $[Eu(H_2O)_8]_2[Fe_4(H_2O)_8(thr)_2][B\text{-}\beta\text{-}SbW_9O_{33}]_2\cdot 22H_2O$ are able to boost the radiationless deactivation of the $^5D_0$ state and partly quench the luminescence emission.[86] Just recently, Zhao *et al.* also intensively probed the luminescence beheviors of a Tb^{III}-containing PTRHDM $[Tb(H_2O)_8]_2[Fe_4(H_2O)_8(L\text{-}thr)_2(B\text{-}\beta\text{-}AsW_9O_{33})_2]\cdot 20H_2O$,[168] which almost is isomorphous to $[Eu(H_2O)_8]_2[Fe_4(H_2O)_8(thr)_2][B\text{-}\beta\text{-}SbW_9O_{33}]_2\cdot 22H_2O$.[162] This Tb^{III}-containing PTRHDM illustrates four apparent emission bands centered at 509, 549, 590 and 625 nm when it is excited at 379 nm (Fig. 24c). Those emission bands appearing at 549, 590 and 625 nm correspond to the $^5D_4 \rightarrow {}^7F_5$, $^5D_4 \rightarrow {}^7F_4$ and $^5D_4 \rightarrow {}^7F_3$ characteristic transitions of the Tb^{III} cations. In order to understand the broad emission band at 509 nm, they measured the photoluminescence spectrum of the starting material $K_{14}[As_2W_{19}O_{67}(H_2O)]$ under excitation at 379 nm (Fig. 24d), which displays an obvious emission band at 509 nm originating from the $^3T_{1u} \rightarrow {}^1A_{1g}$ transitions of the O $\rightarrow$ W ligand-to-metal charge transfer of POT skeletons.[22,252] Thus, the emission band appearing at 509 nm in the luminescence spectrum of $[Tb(H_2O)_8]_2[Fe_4(H_2O)_8(L\text{-}thr)_2(B\text{-}\beta\text{-}AsW_9O_{33})_2]\cdot 20H_2O$ must stem from the $^3T_{1u} \rightarrow {}^1A_{1g}$ transitions of the O $\rightarrow$ W ligand-to-metal charge transfer. However, the decay curve of $[Tb(H_2O)_8]_2[Fe_4(H_2O)_8(L\text{-}thr)_2(B\text{-}\beta\text{-}AsW_9O_{33})_2]\cdot 20H_2O$ cannot be fitted to a single exponential function, but a double exponential function as $I = A_1\exp(-t/\tau_1) + A_2\exp(-t/\tau_2)$ with the luminescent lifetimes τ_1 of 1.69 μs (9.20%) and τ_2 of 12.74 μs (90.80%) (Fig. 24e), which conflicts with the fact that one crystallographically unique Tb^{III} cation exists in the structure and a lifetime should be observed. For the sake of searching the origin of the second lifetime, the decay curve of the precursor $K_{14}[As_2W_{19}O_{67}(H_2O)]$ was also recorded (Fig. 24f), which exhibits two lifetimes with τ_1 and τ_2 of 0.87 μs (24.83%) and 8.83 μs (75.17%). Therefore, the two lifetimes of $[Tb(H_2O)_8]_2[Fe_4(H_2O)_8(L\text{-}thr)_2(B\text{-}\beta\text{-}AsW_9O_{33})_2]\cdot 20H_2O$ is due to the common contribution of the Tb^{III} cations and the O $\rightarrow$ W ligand-to-metal charge transfer transitions. These results also confirm that the intramolecular transfer of the O $\rightarrow$ W LMCT energy to the Tb^{III} center indeed occurred in the course of the emission process.[168] This observation agrees well with the previous reports on intramolecular transfer from POM to the Tb^{III} ions by Yamase and Boskovic.[253,254]

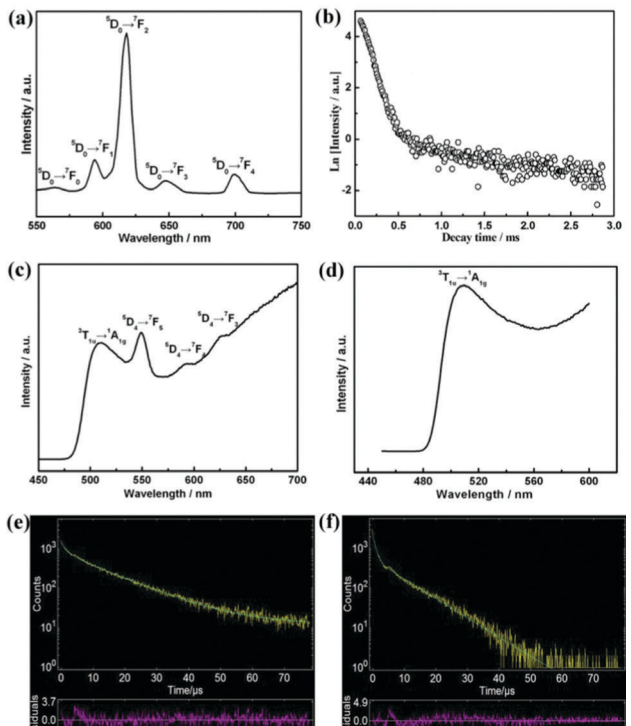

Fig. 24 (a) and (b) The emission spectrum and luminescence decay curve of $[Eu(H_2O)_8]_2[Fe_4(H_2O)_8(thr)_2][B\text{-}\beta\text{-}SbW_9O_{33}]_2\cdot 22H_2O$ at room temperature. (c) and (e) The emission spectrum and luminescence decay curve of $[Tb(H_2O)_8]_2[Fe_4(H_2O)_8(L\text{-}thr)_2(B\text{-}\beta\text{-}AsW_9O_{33})_2]\cdot 20H_2O$ at room temperature. (d) and (f) The emission spectrum and luminescence decay curve of $K_{14}[As_2W_{19}O_{67}(H_2O)]$ at room temperature. [(a) and (b) are reprinted with permission from ref. 162. Copyright 2014 American Chemical Society; (c–f) are reprinted with permission from ref. 168. Copyright 2015 The Royal Society of Chemistry.]

4.3 Electrochemical and electrocatalytic properties

As known to all, modern civilization has become more dependent on fossil fuels of finite supply and uneven global distribution, resulting in two problematic consequences: (i) poor fossil resources of the country and vulnerability of nation states to fossil-fuel imports; and (ii) carbon dioxide emissions caused by global warming. In other words, in recent years, carbon dioxide emissions caused by global warming, energy shortage and environmental problems have become the focus of world attention. Interestingly, the battery, which can enable the wireless revolution of iPads, cell phones, laptop computers and digital cameras, provides the impetus for us to find another electrochemical technology that enables modern civilization to secure a sustainable, distributed energy supply for all people and reduce the imprint on air pollution of the internal combustion engine and coal-fired power plants. It is generally known that each cell of the battery stores electrical energy as chemical energy in two electrodes separated by an electrolyte that transfers the ionic component of the chemical reaction inside the cell and forces the electronic component outside the battery. So the selection of the electrode materials and electrolyte has become a vital step. POMs, as a large and rapidly growing class, can undergo a reversible multielectron redox process, and can be utilized as the chemically bulk-modified carbon paste electrodes (CPEs) with many advantages of being inexpensive, easy to handle, and easy to prepare, so they have attracted much attention in electrochemical applications and the manufacture of chemically modified electrodes.[255–257] Additionally, extensive studies have shown that POMs are capable of delivering the electrons to other species, thus serving as powerful electron reservoirs for multielectron reductions and electrocatalytic processes.[18,258] In this context, multifarious electrochemical and electrocatalytic research

studies about PTRHDMs have been investigated to date.[114,116,117,121,124,151,154,157,162,163,165,166,169] For instance, in 2009, Wang's group studied the electrochemical and electrocatalytic properties of a triple-Dawson-type PTRHDM $Na_{20}[Ce_3^{IV}Mn_2^{IV}O_6(OAc)_6(H_2O)_9]_2[Mn_2^{III}P_2W_{16}O_{60}]_3{\cdot}21H_2O$ that was dissolved in pH = 4.0 acetate buffer solution (1×10^{-4} mmol L^{-1}) by virtue of cyclic voltammetry at a scan rate of 150 mV s^{-1} (the working electrode: glassy carbon; the reference electrode: Ag/AgCl; the counter electrode: platinum wire).[124] As shown in Fig. 25a, its cyclic voltammogram (CV) displays five pairs of redox waves with the mean peak potentials of 0.819, 0.368, −0.503, −0.669 and −0.847 V in the potential region of 1.15 to −1.1 V. The first oxidation peak I (0.926 V) and its reduction counterpart I′ (0.712 V) correspond to the redox procedure of the Mn centers.[259,260] The second oxidation peak II (0.496 V) and its reduction counterpart II′ (0.240 V) are ascribed to the redox procedure of Ce^{IV}/Ce^{III} ions.[261,262] The remaining three pairs of redox peaks (III: −0.504 V, IV: −0.676 V, V: −0.898 V, III′: −0.502, IV′: −0.662, V′: −0.796 V) are all attributed to the redox procedure of W^{VI} centers.[263,264] What's more, its electrocatalytic activity towards the reduction of NO_2^- was also examined in the same buffer solution (Fig. 25b). Upon the addition of nitrite, the reduction peak currents of W-based waves increase, in the meantime, the corresponding oxidation peak currents decrease, indicating that nitrite was reduced by the reduced POM species.[124,265] In 2014, Zhao and co-workers explored the solid-state electrochemistry behaviour of $[Pr(H_2O)_8]_2[Fe_4(H_2O)_8(thr)_2][B\text{-}\beta\text{-}SbW_9O_{33}]_2{\cdot}22H_2O$-CPE and its electrocatalytic activities towards BrO_3^- and H_2O_2 reduction in 0.5 mol L^{-1} $Na_2SO_4 + H_2SO_4$ aqueous solution by means of a modified CPE at room temperature.[162] Its CV shows four groups of redox peaks between −1.0 and 1.0 V with mean peak potentials of −0.693 V (I–I′), −0.407 V (II–II′), 0.166 V (III–III′) and 0.445 V (VI–VI′) (the reference electrode is Ag/AgCl) (Fig. 25c). The I–I′, II–II′, III–III′ redox waves are attributed to the redox process of the W^{VI} centers and the peak with the mean peak potential 0.445 V is assigned to the redox process of the Fe^{III}-centers.[173,266] Moreover, the variation of the cathodic peak current of the W^{VI}-based wave (I′) with the scan rate was also investigated (Fig. 25d). When the scan rate varies between 80 and 320 mV s^{-1}, the peak current (I_{pc}) is proportional to the scan rate, revealing that the redox process succumbs to the surface-controlled procedure. For the purpose of evaluating its electrocatalytic activities toward the reduction of BrO_3^- and H_2O_2, cyclic voltammetry measurements in the 0.5 mol L^{-1} acidic sulfate medium (pH = 1.91) containing different concentrations of $NaBrO_3$ or H_2O_2 were carried out at room temperature (Fig. 25e and f). With the addition of bromate or hydrogen peroxide, the cathodic current of the W^{VI}-based wave gradually increases, meanwhile, the corresponding anodic oxidation peak current declines. But, the Fe^{III}-based reduction peak is less influenced. These results indicate that $[Pr(H_2O)_8]_2[Fe_4(H_2O)_8(thr)_2][B\text{-}\beta\text{-}SbW_9O_{33}]_2{\cdot}22H_2O$-CPE illustrates the evident electrocatalytic activities towards the reduction of BrO_3^- and H_2O_2 and the reduction processes of BrO_3^- and H_2O_2 are mainly controlled by the reduced species of tungsten–oxo clusters.[162] Additionally, as well as

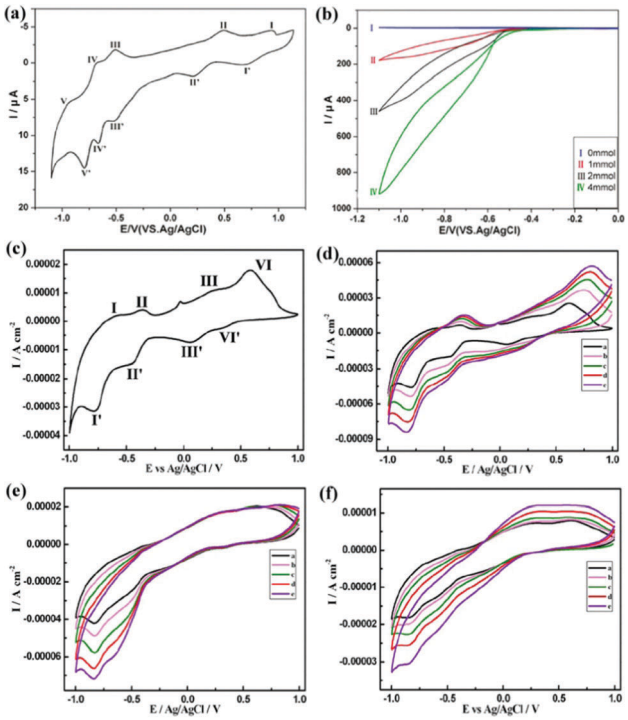

Fig. 25 (a) The CV of $Na_{20}[Ce_3^{IV}Mn_2^{IV}O_6(OAc)_6(H_2O)_9]_2[Mn_2^{III}P_2W_{16}O_{60}]_3{\cdot}21H_2O$ (1×10^{-4} mmol L^{-1}) in the pH = 4.0 acetate buffer solution. Scan rate: 150 mV s^{-1}. (b) The variation of CVs of $Na_{20}[Ce_3^{IV}Mn_2^{IV}O_6(OAc)_6(H_2O)_9]_2[Mn_2^{III}P_2W_{16}O_{60}]_3{\cdot}21H_2O$ (1×10^{-4} mmol L^{-1}) in the pH = 4.0 acetate buffer solution with different concentrations of NO_2^- [(I) 0.0, (II) 1.0, (III) 2.0, and (IV) 4.0 mmol L^{-1}], scan rate: 150 mV s^{-1}. (c) The CV of $[Pr(H_2O)_8]_2[Fe_4(H_2O)_8(thr)_2][B\text{-}\beta\text{-}SbW_9O_{33}]_2{\cdot}22H_2O$-CPE in the pH = 1.91 $Na_2SO_4 + H_2SO_4$ solution. Scan rate: 80 mV s^{-1}. (d) CVs of $[Pr(H_2O)_8]_2[Fe_4(H_2O)_8(thr)_2][B\text{-}\beta\text{-}SbW_9O_{33}]_2{\cdot}22H_2O$-CPE in the pH = 1.91 $Na_2SO_4 + H_2SO_4$ solution at variable scan rates ((a) 80; (b) 140; (c) 200; (d) 260; (e) 320 mV s^{-1}). (e) The variation of CVs of $[Pr(H_2O)_8]_2[Fe_4(H_2O)_8\ (thr)_2][B\text{-}\beta\text{-}SbW_9O_{33}]_2{\cdot}22H_2O$-CPE in the pH = 1.91 $Na_2SO_4 + H_2SO_4$ solution with different concentrations of BrO_3^- [(a) 3×10^{-3}; (b) 7×10^{-3}; (c) 1.1×10^{-2}; (d) 1.5×10^{-2}; (e) 1.9×10^{-2} mmol L^{-1}], scan rate: 80 mV s^{-1}. (f) The variation of CVs of $[Pr(H_2O)_8]_2[Fe_4(H_2O)_8(thr)_2][B\text{-}\beta\text{-}SbW_9O_{33}]_2{\cdot}22H_2O$-CPE in the pH = 1.91 $Na_2SO_4 + H_2SO_4$ solution with different concentrations of H_2O_2 [(a) 5.88×10^{-3}; (b) 1.37×10^{-2}; (c) 2.16×10^{-2}; (d) 2.94×10^{-2}; (e) 3.72×10^{-2} mmol L^{-1}], scan rate: 80 mV s^{-1}. [(a) and (b) are reprinted with permission from ref. 124. Copyright 2009 American Chemical Society; (c–f) are reprinted with permission from ref. 162. Copyright 2014 American Chemical Society.]

its electrocatalytic reduction towards inorganic anions – iodate that is ascribed to W-centers, Ma *et al.* investigated the electrocatalytic oxidation of $Na_2[Ce_4(H_2O)_{22}(dpdo)_5](Mn_2HP_2W_{15}O_{56})_2{\cdot}8H_2O$ towards the biological molecules – ascorbic acid and dopamine that are assigned to Ce and/or Mn centers.[154] Upon addition of ascorbic acid and dopamine, the anodic peak currents of the Mn(II) and Ce(III) wave apparently increase, indicating that $Na_2[Ce_4(H_2O)_{22}(dpdo)_5](Mn_2HP_2W_{15}O_{56})_2{\cdot}8H_2O$ can catalyze the oxidation of ascorbic acid and dopamine.[154] In other words, PTRHDMs may function as potential electrocatalytic materials in the future.

4.4 Photocatalytic properties

Because some POMs exhibit photocatalytic activities in the degradation of organic components under UV or visible irradiation by oxidation of organic materials,[267] Niu *et al.* selectively

explored photodegradation reactions of rhodamine-B upon 500 W Hg lamp irradiation with the participation of some phosphotungstate-/arsenotungstate-based TM–RE heterometallic derived materials as photocatalysts.[138,145] Experimental results demonstrate that these PTRHDMs to some extent inhibit the photodegradation of rhodamine-B, the main reasons of which can be interpreted as follows: (a) these PTRHDMs can serve as absorbers of Hg lamp irradiation; (b) the formation of hydrogen-bonds between rhodamine-B substrates ($N(C_2H_5)_2$, COOH) and PTRHDMs (the nitrogen atoms of organoamine ligands, surface oxygen atoms of POMs) or the weak π–π stacking interactions between phenyl cycles on rhodamine-B substrates and pyridine cycles on organic ligands enhances the chemical stability of rhodamine-B substrates in solution, which make the photodegradation of rhodamine-B substrates become slow.[138,145] It is extremely clear that the photocatalytic investigation of the degradation of organic components remains largely unexplored. Furthermore, the research on the photocatalytic hydrogen evolution *via* water splitting with PTRHDMs as catalysts is still virgin.

5. Outlook and conclusions

This review mainly compiles those reported results on PTRHDMs made in the past decade with an emphasis on synthesis, structural aspects and some related properties. In this view, we initially retrospect the simplified history of POM chemistry and summarize the structural types of POM anions, such as Keggin, Wells–Dawson, Linqvist, Anderson–Evans, Weakley, Finke, Sliverton, and Stranberg. Besides the familiar Keggin- and Dawson-type PTRHDMs, the PTRHDMs based on Anderson–Evans- and Evans–Showell-type POM fragments are also a new highlight in this field. What's more, Wang's group has reported the first series of POV-based PTRHDMs. Since the RE ions or TM ions were firstly introduced in POM chemistry, the chemistry of RESPs and TMSPs is still booming to date. With the development of POM chemistry, the RE and TM ions were simultaneously introduced into the POM system in 2004, hitherto, the synthesis and exploration of neotype PTRHDMs have shown a huge development potential. Furthermore, on the basis of the results in this review, we can see that two methods (CASS and HT) and five main synthetic strategies are very effective in the preparation of PTRHDMs, but the introduction of other synthetic methods, such as the mixed solvent diffusion method, ionothermal synthesis, high-temperature solid-state reaction and microwave synthesis, may break through the bottleneck in the preparation chemistry of PTRHDMs and will bring about a great development prospect of PTRHDM chemistry.

Subsequently, we discussed the reasons for introduction of TM and RE cations into POMs. Based on the above mentioned structures and properties, they all can be seen as products by means of ''bottom-up approaches'', that is, the chemical properties of POM building blocks, metal ions and organic ligands are utilized to self-organize or self-assemble into PTRHDMs with multifuctionlities of POM, metal ions and organic components. According to the differences of the POM building blocks, we divided the reported PTRHDMs into five categories.

(1) Apparently, the amount of the PTRHDMs based on monovacant POM fragments is much more than others, however, due to the space limitation of the monovacant site of POM fragments, only one RE ion can be captured into the monovacant position, which not only impedes the formation of RE clusters but also leads to the marginalization of the TM ions in the periphery of POM fragments. While the characteristic and the structural stability of this kind of PTRHDMs may also provide a useful moment for the introduction of rigid nitrogen–organic ligands to obtain PTRHDM cluster–organic frameworks, which will have similar potential applications to metal–organic frameworks (MOFs).

(2) The PTRHDMs based on di-vacant POM building blocks are more inclined to form the oligomeric structures, such as monomer, dimer, trimer, hexamer and dodecamer. However, most of them are purely inorganic and few have extended structures. Hence, the importing additional metal–organic complexes may greatly increase the structural diversity of this type of PTRHDMs.

(3) According to the reported results, undoubtedly, the sandwich-type PTRHDMs almost are TM_4-sandwiched POMs with RE cosmetics as linkers, which result in 1-, 2- and 3-D expanded structures. Additionally, only Cu^{II}, Fe^{III} and $Mn^{II/III/IV}$ ions as TM cations are used. So, other TM cations, even noble metals, can maybe be employed in this branch. Moreover, the exploration and discovery of RE-sandwiched multivacant POM derivatives with TM/TM-organic connectors are very interesting.

(4) Moreover, the occurrence of PTRHDMs based on POMB and POV building units will greatly widen the research scope of this field, so the introduction of other structural types of POM anions such as polyoxoniobates or polyoxotantates may be worth considering.

Then, we highlight the robustness of such TM–RE cations and their versatile functionality allowing for magnetic, photoluminescence, and electrochemical properties in the final PTRHDMs.

(i) Albeit several POM-based SMMs have been obtained, their magnetic application investigations are still very limited. So other applications of magnetic PTRHDMs, such as devices, biological sensing and imaging and biological therapy, should also be developed.

(ii) To date, PTRHDMs with special fluorescence performances have not been discovered and there is almost no in-depth study about the photoluminescence properties of PTRHDMs. As a result, profound investigations on the luminescence behaviors and luminescence mechanisms and how to improve luminescence performances and enhance quantum yield to discover PTHRDMs with outstanding photoluminescence properties may also be a challenging research field.

(iii) New types of energy storage systems are needed due to the increasing demand and the accelerating consumption of energy threatening the development of society and the economy. It is worth noting that a battery is a better energy storage device. What's more, many POMs, such as Keggin and Dawson POM anions, can give rise to mixed-valence species, which make them greatly attractive in the preparation of modified

electrodes and in the application of electrocatalysis. So the requirement of cheap and non-toxic electrodes offers an excellent opportunity for the synthesis of PTRHDMs.

(iv) As we know, one of the important application fields is catalysis, however, the exploration of the catalysis of PTRHDMs is hardly a blank to date. This subject is worth exploring because PTRHDMs have multiple Lewis acid and alkali active sites and functional cooperativity of multicomponents.

It can be concluded with confidence that the persistent and dedicated efforts of chemists over the past ten years have revealed a vast and beautiful array of PTRHDMs, which may in fact just be the reason why the PTRHDM research field has flourished in recent years. Of course, many more interesting species and functionalities remain to be explored and examined, predicting that this area of POM chemistry still has great growing opportunities in the future.

Abbreviations

POM	Polyoxometalate
POA	Polyoxoanion
POT	Polyoxotungstate
POMB	Polyoxomolybdate
POV	Polyoxovanadate
TM	Transition-metal
RE	Rare-earth
Ln	Lanthanide
TMSP	Transition-metal substituted polyoxometalate
RESP	Rare-earth substituted polyoxometalate
PTRHDM	POM-based TM–RE heterometallic derived material
TRHDM	TM–RE heterometallic derived material
ICCC	International conference on coordination chemistry
HSAB	Hard and soft acids and bases
CASS	Conventional aqueous solution synthesis
HT	Hydrothermal technique
DMSO	Dimethyl sulfoxide
NMP	*N*-Methyl pyrrolidone
dap	1,2-Diaminopropane
bmaed	*N*,*N*′-Bis(3-methoxysalicylidene)-ethylenediamine
2,2′-bpy	2,2′-Bipyridine
TMC	Transition-metal complex
HOAc	Acetic acid
Ox	Oxalate
SMM	Single molecule magnet
en	Ethylenediamine
CPE	Carbon paste electrode
dpdo	4,4′-Bipyridine-*N*,*N*′-dioxide
thr	Threonine
DMF	*N*,*N*-Dimethylformamide
C_6H_5NO	Isonicotinic acid
CV	Cyclic voltammogram
pzda	Pyrazine-2,3-dicarboxylate
AFM	Antiferromagnetic
FM	Ferromagnetic
QTM	The quantum tunneling of magnetization
ac	Alternating-current
dc	Direct-current

Acknowledgements

This work was supported by the Natural Science Foundation of China (no. 21571016, 91122028, 21571048, 21301049, U1304208), the Natural Science Foundation of China for Distinguished Young Scholars (no. 20725101), the 973 Program (no. 2014CB932101), Program for Science & Technology Innovation Talents in Universities of Henan Province (no. 16HASTIT001), the Natural Science Foundation of Henan Province (no. 142300410451), the Postdoctoral Foundation of Henan Province (2014025), 2014 Special Foundation for Scientific Research Project of Henan University (XXJC20140001), 2012 Young Backbone Teachers Foundation from Henan Province (2012GGJS-027) and the Students Innovative Pilot Plan of Henan University (15NA002).

Notes and references

1 M. T. Pope, *Heteropoly and Isopoly Oxometalates*, Springer, Berlin, 1983.
2 H. Lv, J. Song, Y. V. Geletii, J. W. Vickers, J. M. Sumliner, D. G. Musaev, P. Kögerler, P. F. Zhuk, J. Bacsa, G. Zhu and C. L. Hill, *J. Am. Chem. Soc.*, 2014, **136**, 9268.
3 C. L. Hill and C. M. Prosser-McCartha, *Coord. Chem. Rev.*, 1995, **143**, 407.
4 Q. Chen and J. Zubieta, *Coord. Chem. Rev.*, 1992, **114**, 107.
5 J. T. Rhule, C. L. Hill, D. A. Judd and R. F. Schinazi, *Chem. Rev.*, 1998, **98**, 327.
6 J. Berzelius, *Pogg. Ann.*, 1826, **6**, 369.
7 P. Putaj and F. Lefebvre, *Coord. Chem. Rev.*, 2011, **255**, 1642.
8 J. F. Keggin, *Proc. R. Soc. London, Ser. A*, 1934, **144**, 75.
9 E.-B. Wang, C.-W. Hu and L. Xu, *Introduction of Polyacid Chemistry*, Chemical Industry Press, Beijing, 1998.
10 M. T. Pope and A. Müller, *Angew. Chem., Int. Ed. Engl.*, 1991, **30**, 34.
11 C. L. Hill, *Chem. Rev.*, 1998, **98**, 1.
12 L. C. W. Baker and D. C. Glick, *Chem. Rev.*, 1998, **98**, 3.
13 Y. P. Jeannin, *Chem. Rev.*, 1998, **98**, 51.
14 P. Gouzerh and A. Proust, *Chem. Rev.*, 1998, **98**, 77.
15 I. A. Weinstock, *Chem. Rev.*, 1998, **98**, 113.
16 I. V. Kozhevnikov, *Chem. Rev.*, 1998, **98**, 171.
17 N. Mizuno and M. Misono, *Chem. Rev.*, 1998, **98**, 199.
18 M. Sadakane and E. Steckhan, *Chem. Rev.*, 1998, **98**, 219.
19 A. Müller, F. Peters, M. T. Pope and D. Gatteschi, *Chem. Rev.*, 1998, **98**, 239.
20 E. Coronado and C. J. Gómez-García, *Chem. Rev.*, 1998, **98**, 273.
21 W. G. Klemperer and C. G. Wall, *Chem. Rev.*, 1998, **98**, 297.
22 T. Yamase, *Chem. Rev.*, 1998, **98**, 307.
23 D. E. Katsoulis, *Chem. Rev.*, 1998, **98**, 359.
24 A. Proust, *Actual. Chim.*, 2000, 55.
25 S. Reinoso, P. Vitoria, L. S. Felices, A. Montero, L. Lezama and J. M. Gutiérrez-Zorrilla, *Inorg. Chem.*, 2007, **46**, 1237.
26 J. J. Borrás-Almenar, E. Coronado, A. Müller and M. T. Pope, *Polyoxometalate Molecular Science*, Kluwer Academic Publishers, Dordrecht, The Netherlands, 2003.
27 H. Lv, Y. V. Geletii, C. Zhao, J. W. Vickers, G. Zhu, Z. Luo, J. Song, T. Lian, D. G. Musaev and C. L. Hill, *Chem. Soc. Rev.*, 2012, **41**, 7572.
28 T. Okuhara, N. Mizuno and M. Misono, *Adv. Catal.*, 1996, **41**, 113.
29 G. Chottard, C. L. Hill, M. S. Weeks and R. F. Schinazi, *J. Med. Chem.*, 1990, **33**, 2767.
30 A. Banerjee, B. S. Bassil, G.-V. Röschenthaler and U. Kortz, *Chem. Soc. Rev.*, 2012, **41**, 7590.

31 T. Yamase and P. V. Prokop, *Angew. Chem., Int. Ed.*, 2002, **41**, 466.
32 Y. Wang and I. A. Weinstock, *Chem. Soc. Rev.*, 2012, **41**, 7479.
33 A. Proust, B. Matt, R. Villanneau, G. Guillemot, P. Gouzerh and G. Izzet, *Chem. Soc. Rev.*, 2012, **41**, 7605.
34 S.-T. Zheng and G.-Y. Yang, *Chem. Soc. Rev.*, 2012, **41**, 7623.
35 H. N. Miras, J. Yan, D. L. Long and L. Cronin, *Chem. Soc. Rev.*, 2012, **41**, 7403.
36 P. C. Yin, D. Li and T. B. Liu, *Chem. Soc. Rev.*, 2012, **41**, 7368.
37 R. Yu, X.-F. Kuang, X.-Y. Wu, C.-Z. Lu and J. P. Donahue, *Coord. Chem. Rev.*, 2009, **253**, 2872.
38 D.-Y. Du, L.-K. Yan, Z.-M. Su, S.-L. Li, Y.-Q. Lan and E.-B. Wang, *Coord. Chem. Rev.*, 2013, **257**, 702.
39 V. E. Simmons and L. C. W. Baker, *Proc. VII I.C.C.C.*, Stockholm, 1962, p. 195.
40 L. C. W. Baker and V. E. Simmons, *Proc. IX I.C.C.C.*, St. Moritz, 1966, p. 421.
41 J.-W. Zhao, C.-M. Wang, J. Zhang, S.-T. Zheng and G.-Y. Yang, *Chem. – Eur. J.*, 2008, **14**, 9223.
42 (*a*) N. Haraguchi, Y. Okaue, T. Isobe and Y. Matsuda, *Inorg. Chem.*, 1994, **33**, 1015; (*b*) A. Tézé and G. Hervé, *Inorganic Syntheses*, John Wiley and Sons, New York, 1990, vol. 27, p. 90.
43 P. J. Domaille, *Inorganic Syntheses*, John Wiley and Sons, New York, 1990, vol. 27, p. 101.
44 A. Tézé and G. Hervé, *Inorganic Syntheses*, John Wiley and Sons, New York, 1990, vol. 27, p. 88.
45 N. H. Nsouli, B. S. Bassil, M. H. Dickman, U. Kortz, B. Keita and L. Nadjo, *Inorg. Chem.*, 2006, **45**, 3858.
46 U. Kortz, M. G. Savelieff, B. S. Bassil and M. H. Dickman, *Angew. Chem., Int. Ed.*, 2011, **40**, 3384.
47 P. J. Domaille, *Inorganic Syntheses*, John Wiley and Sons, New York, 1990, vol. 27, p. 100.
48 G. Hervé and A. Tézé, *Inorg. Chem.*, 1977, **16**, 2115.
49 A. J. Gaunt, I. Maya, R. Copping, A. I. Bhatt, D. Collison, O. D. Fox, K. T. Holman and M. T. Pope, *Dalton Trans.*, 2003, 3009.
50 C. Tourné, A. Revel, G. Tourné and M. Vendrell, *C. R. Seances Acad. Sci., Ser. C*, 1973, **277**, 643.
51 M. Bosing, I. Loose, H. Pohlmann and B. Krebs, *Chem. – Eur. J.*, 1997, **3**, 1232.
52 B. Botar, T. Yamase and E. Ishikawa, *Inorg. Chem. Commun.*, 2000, **3**, 579.
53 R. G. Finke, M. W. Droege and P. J. Domaille, *Inorg. Chem.*, 1987, **26**, 3886.
54 R. Contant, *Inorganic Syntheses*, John Wiley and Sons, New York, 1990, vol. 27, p. 108.
55 R. Contant, *Inorganic Syntheses*, John Wiley and Sons, New York, 1990, vol. 27, p. 110.
56 J. Fischer, L. Ricard and R. Weiss, *J. Am. Chem. Soc.*, 1976, **98**, 3050.
57 L. M. Rodriguez-Albelo, A. R. Ruiz-Salvador, A. Sampieri, D. W. Lewis, A. Gómez, B. Nohra, P. Mialane, J. Marrot, F. Sécheresse, C. Mellot-Draznieks, R. N. Biboum, B. Keita, L. Nadjo and A. Dolbecq, *J. Am. Chem. Soc.*, 2009, **131**, 16078.
58 D.-Y. Du, J.-S. Qin, Y.-G. Li, S.-L. Li, Y.-Q. Lan, X.-L. Wang, K.-Z. Shao, Z.-M. Su and E.-B. Wang, *Chem. Commun.*, 2011, **47**, 2832.
59 Y. Kikukawa, S. Yamaguchi, K. Tsuchida, Y. Nakagawa, K. Uehara, K. Yamaguchi and N. Mizuno, *J. Am. Chem. Soc.*, 2008, **130**, 5472.
60 D.-Y. Du, J.-S. Qin, T.-T. Wang, S.-L. Li, Z.-M. Su, K.-Z. Shao, Y.-Q. Lan, X.-L. Wang and E.-B. Wang, *Chem. Sci.*, 2012, **3**, 705.
61 C.-Y. Sun, S.-X. Liu, D.-D. Liang, K.-Z. Shao, Y.-H. Ren and Z.-M. Su, *J. Am. Chem. Soc.*, 2009, **131**, 1883.
62 N. Mizuno, K. Yamaguchi and K. Kamata, *Coord. Chem. Rev.*, 2005, **249**, 1944.
63 D. C. Duncan, R. C. Chambers, E. Hecht and C. L. Hill, *J. Am. Chem. Soc.*, 1995, **117**, 681.
64 M. W. Droege and R. G. Finke, *J. Mol. Catal.*, 1991, **69**, 323.
65 N. I. Kuznetsova, L. I. Kuznetsova and V. A. Likholobov, *J. Mol. Catal. A: Chem.*, 1996, **108**, 135.
66 I. C. M. S. Santos, M. M. Q. Simões, M. M. M. S. Pereira, R. R. L. Mar-tins, M. G. P. M. S. Neves, J. A. S. Cavaleiro and A. M. V. Cavaleiro, *J. Mol. Catal. A: Chem.*, 2003, 195–253.
67 T. Yamase, E. Ishikawa, Y. Asai and S. Kanai, *J. Mol. Catal. A: Chem.*, 1996, **114**, 237.
68 E. Ishikawa and T. Yamase, *J. Mol. Catal. A: Chem.*, 1999, **142**, 61.
69 R. Ben-Daniel, A. M. Khenkin and R. Neumann, *Chem. – Eur. J.*, 2000, **6**, 3722.
70 M. D. Ritorto, T. M. Anderson, W. A. Neiwert and C. L. Hill, *Inorg. Chem.*, 2004, **43**, 44.
71 N. Mizuno, C. Nozaki, I. Kiyoto and M. Misono, *J. Am. Chem. Soc.*, 1998, **120**, 9267.
72 N. Mizuno, C. Nozaki, I. Kiyoto and M. Misono, *J. Catal.*, 1999, **182**, 285.
73 N. Mizuno, I. Kiyoto, C. Nozaki and M. Misono, *J. Catal.*, 1999, **184**, 171.
74 N. Mizuno, Y. Seki, Y. Nishiyama, I. Kiyoto and M. Misono, *J. Catal.*, 1999, **184**, 550.
75 J. M. Clemente-Juan and E. Coronado, *Coord. Chem. Rev.*, 1999, **193–195**, 361.
76 J. M. Clemente-Juan, E. Coronado, A. Forment-Aliaga, J. R. Galán-Mascarós, C. Giménez-Saiz and C. J. Gómez-García, *Inorg. Chem.*, 2004, **43**, 2689.
77 N. Zamstein, A. Tarantul and B. Tsukerblat, *Inorg. Chem.*, 2007, **46**, 8851.
78 U. Kortz, A. Müller, J. van Slageren, J. Schnack, N. S. Dalal and M. Dressel, *Coord. Chem. Rev.*, 2009, **253**, 2315.
79 O. Oms, A. Dolbecq and P. Mialane, *Chem. Soc. Rev.*, 2012, **41**, 7497.
80 R. G. Pearson, *J. Am. Chem. Soc.*, 1963, **85**, 3533.
81 K. Binnemans, *Chem. Rev.*, 2009, **109**, 4283.
82 (*a*) V. Chandrasekhar, P. Bag and E. Colacio, *Inorg. Chem.*, 2013, **52**, 4562; (*b*) C. H. Huang, *Rare Earth Coordination Chemistry: Fundamentals and Applications*, John Wiley & Sons (Asia) Pte Ltd., Clementi Loop, Singapore, 2010.
83 G. A. Barbieri, *Atti R. Accad. Naz. Lincei, Mem. Cl. Sci. Fis., Mat. Nat.*, 1914, **11**, 805.
84 R. D. Peacock and T. J. R. Weakley, *J. Chem. Soc. A*, 1971, 1836.
85 M. Sadakane, M. H. Dickman and M. T. Pope, *Angew. Chem., Int. Ed.*, 2000, **39**, 2914.
86 P. Mialane, L. Lisnard, A. Mallard, J. Marrot, E. Antic-Fidancev, P. Aschehoug, D. Vivien and F. Sécheresse, *Inorg. Chem.*, 2003, **42**, 2102.
87 A. J. Gaunt, I. May, M. J. Sarsfield, D. Collison, M. Helliwell and I. S. Denniss, *Dalton Trans.*, 2003, 2767.
88 R. Copping, A. J. Gaunt, I. May, M. J. Sarsfield, D. Collison, M. Helliwell, I. S. Denniss and D. C. Apperley, *Dalton Trans.*, 2005, 1256.
89 B. Gao, S.-X. Liu, L.-H. Xie, M. Yu, C.-D. Zhang, C.-Y. Sun and H.-Y. Cheng, *J. Solid State Chem.*, 2006, **179**, 1681.
90 Y. Liu, S.-X. Liu, R.-G. Cao, H.-M. Ji, S.-W. Zhang and Y.-H. Ren, *J. Solid State Chem.*, 2008, **181**, 2237.
91 N. Jiang, L. Xu, F.-Y. Li, G.-G. Gao and L.-H. Fan, *Inorg. Chem. Commun.*, 2008, **11**, 24.
92 Y.-G. Li, L. Xu, G.-G. Gao, N. Jiang, H. Liu, F.-Y. Li and Y.-Y. Yang, *CrystEngComm*, 2009, **11**, 1512.
93 F. Hussain, A. Degonda, S. Sandriesser, T. Fox, S. S. Mal, U. Kortz and G. R. Patzke, *Inorg. Chim. Acta*, 2010, **363**, 4324.
94 F. Hussain, S. Sandriesser, M. Speldrich and G. R. Patzke, *J. Solid State Chem.*, 2011, **184**, 214.
95 J.-Y. Niu, M.-L. Wei, J.-P. Wang and D.-B. Dang, *Eur. J. Inorg. Chem.*, 2004, 160.
96 J.-P. Wang, X.-Y. Duan, X.-D. Du and J.-Y. Niu, *Cryst. Growth Des.*, 2006, **6**, 2266.
97 J.-P. Wang, J.-W. Zhao, X.-Y. Duan and J.-Y. Niu, *Cryst. Growth Des.*, 2006, **6**, 507.
98 J. Y. Niu, K. H. Wang, H. N. Chen, J. W. Zhao, P. T. Ma, J. P. Wang, M. X. Li, Y. Bai and D. B. Dang, *Cryst. Growth Des.*, 2009, **9**, 4362.
99 K. Wassermann, M. H. Dickman and M. T. Pope, *Angew. Chem., Int. Ed. Engl.*, 1997, **36**, 1445.
100 R. C. Howell, F. G. Perez and L. C. Francesconi, *Angew. Chem., Int. Ed.*, 2001, **40**, 4031.
101 (*a*) K. Fukaya and T. Yamase, *Angew. Chem., Int. Ed.*, 2003, **42**, 654; (*b*) N. V. Izarova, M. N. Sokolov, F. M. Dolgushin, M. Y. Antipin, D. Fenske and V. P. Fedin, *C. R. Chim.*, 2005, **8**, 1922; (*c*) N. V. Izarova, M. N. Sokolov, D. G. Samsonenko, A. Rothenberger, D. Y. Naumov, D. Fenske and V. P. Fedin, *Eur. J. Inorg. Chem.*, 2005, 4985; (*d*) N. V. Izarova, M. N. Sokolov, D. G. Samsonenko, A. Rothenberger, D. Fenske and V. P. Fedin, *Russ. Chem. Bull.*, 2008, **57**, 78.
102 B. S. Bassil, M. H. Dickman, I. Römer, B. von der Kammer and U. Kortz, *Angew. Chem., Int. Ed.*, 2007, **46**, 6192.
103 F. Hussain, F. Conrad and G. R. Patzke, *Angew. Chem., Int. Ed.*, 2009, **48**, 9088.

104 X.-J. Feng, H.-Y. Han, Y.-H. Wang, L.-L. Li, Y.-G. Li and E.-B. Wang, *CrystEngComm*, 2013, **15**, 7267.
105 J.-J. Wei, L. Yang, P.-T. Ma, J.-P. Wang and J.-Y. Niu, *Cryst. Growth Des.*, 2013, **13**, 3554.
106 T. Yamase, H. Fujita and K. Fukushima, *Inorg. Chim. Acta*, 1988, **151**, 15.
107 J. Liu, E.-B. Wang, Y.-S. Zhou and C.-W. Hu, *Acta Pharmacol. Sin.*, 1998, **33**, 544.
108 C.-D. Wu, C.-Z. Lu, H.-H. Zhang and J.-S. Huang, *J. Am. Chem. Soc.*, 2002, **124**, 3836.
109 J.-H. Xu, S. Zhao, W. Chen, M. Wang and Y.-F. Song, *Chem. – Eur. J.*, 2012, **18**, 4775.
110 P. Mialane, A. Dolbecq, E. Rivière, J. Marrot and F. Sécheresse, *Eur. J. Inorg. Chem.*, 2004, 33.
111 W.-L. Chen, Y.-G. Li, Y.-H. Wang, E.-B. Wang and Z.-M. Zhang, *Dalton Trans.*, 2008, 865.
112 G.-L. Xue, B. Liu, H.-M. Hu, J.-H. Yang, J.-W. Wang and F. Fu, *J. Mol. Struct.*, 2004, **690**, 95.
113 H.-Y. An, Y. Lan, Y.-G. Li, E.-B. Wang, N. Hao, D.-R. Xiao, L.-Y. Duan and L. Xu, *Inorg. Chem. Commun.*, 2004, **7**, 356.
114 W.-L. Chen, Y.-G. Li, Y.-H. Wang and E.-B. Wang, *Eur. J. Inorg. Chem.*, 2007, 2216.
115 A. Merca, A. Müller, J. van Slageren, M. Läge and B. Krebs, *J. Cluster Sci.*, 2007, **18**, 711.
116 S. Chang, Y.-F. Qi, E.-B. Wang, Y.-G. Li and H. Jin, *J. Cluster Sci.*, 2007, **18**, 781.
117 W.-L. Chen, Y.-G. Li, Y.-H. Wang, E.-B. Wang and Z.-M. Su, *Dalton Trans.*, 2007, 4293.
118 H.-J. Pang, C.-J. Zhang, D.-M. Shi and Y.-G. Chen, *Cryst. Growth Des.*, 2008, **8**, 4476.
119 X.-K. Fang and P. Kögerler, *Chem. Commun.*, 2008, 3396.
120 X.-K. Fang and P. Kögerler, *Angew. Chem., Int. Ed.*, 2008, **47**, 8123.
121 Z.-M. Zhang, Y.-G. Li, W.-L. Chen, E.-B. Wang and X.-L. Wang, *Inorg. Chem. Commun.*, 2008, **11**, 879.
122 J.-P. Wang, Q.-X. Yan, X.-D. Du and J.-Y. Niu, *J. Cluster Sci.*, 2008, **19**, 491.
123 J.-F. Cao, S.-X. Liu, R.-G. Cao, L.-H. Xie, Y.-H. Ren, C.-Y. Gao and L. Xu, *Dalton Trans.*, 2008, 115.
124 Y.-W. Li, Y.-G. Li, Y.-H. Wang, X.-J. Feng, Y. Lu and E.-B. Wang, *Inorg. Chem.*, 2009, **48**, 6452.
125 B. Li, J.-W. Zhao, S.-T. Zheng and G.-Y. Yang, *J. Cluster Sci.*, 2009, **20**, 503.
126 B. Nohra, P. Mialane, A. Dolbecq, E. Rivière, J. Marrot and F. Sécheresse, *Chem. Commun.*, 2009, 2703.
127 S. Reinoso, M. Giménez-Marqués, J. R. Galán-Masarós, P. Vitoria and J. M. Gutiérrez-Zorrilla, *Angew. Chem., Int. Ed.*, 2010, **49**, 8384.
128 D.-Y. Du, J.-S. Qin, S.-L. Li, X.-L. Wang, G.-S. Yang, Y.-G. Li, K.-Z. Shao and Z.-M. Su, *Inorg. Chim. Acta*, 2010, **363**, 3823.
129 S. Reinoso and J. R. Galán-Mascarós, *Inorg. Chem.*, 2010, **49**, 377.
130 J. D. Compain, P. Mialane, A. Dolbecq, I. M. Mbomekallé, J. Marrot, F. Sécheresse, C. Duboc and E. Rivière, *Inorg. Chem.*, 2010, **49**, 2851.
131 S. Yao, Z.-M. Zhang, Y.-G. Li, Y. Lu, E.-B. Wang and Z.-M. Su, *Cryst. Growth Des.*, 2010, **10**, 135.
132 D.-Y. Du, J.-S. Qin, S.-L. Li, Y.-Q. Lan, X.-L. Wang and Z.-M. Su, *Aust. J. Chem.*, 2010, **63**, 1389.
133 S. Reinoso, J. R. Galán-Mascarós and L. Lezama, *Inorg. Chem.*, 2011, **50**, 9587.
134 W.-D. Wang, X.-X. Li, W.-H. Fang and G.-Y. Yang, *J. Cluster Sci.*, 2011, **22**, 87.
135 L. J. Chen, D. Y. Shi, Y. Wang, H. L. Cheng, Z. D. Geng, J. W. Zhao, P. T. Ma and J. Y. Niu, *J. Coord. Chem.*, 2011, **64**, 400.
136 D. Y. Shi, L. J. Chen, J. W. Zhao, Y. Wang, P. T. Ma and J. Y. Niu, *Inorg. Chem. Commun.*, 2011, **14**, 324.
137 Z.-M. Zhang, Y.-G. Li, S. Yao and E.-B. Wang, *Dalton Trans.*, 2011, **40**, 6475.
138 J. Y. Niu, S. W. Zhang, H. N. Chen, J. W. Zhao, P. T. Ma and J. P. Wang, *Cryst. Growth Des.*, 2011, **11**, 3769.
139 S. W. Zhang, J. W. Zhao, P. T. Ma, H. N. Chen, J. Y. Niu and J. P. Wang, *Cryst. Growth Des.*, 2012, **12**, 1263.
140 J. W. Zhao, D. Y. Shi, L. J. Chen, Y. Z. Li, P. T. Ma, J. P. Wang and J. Y. Niu, *Dalton Trans.*, 2012, **41**, 10740.
141 S. W. Zhang, J. W. Zhao, P. T. Ma, J. Y. Niu and J. P. Wang, *Chem. – Asian J.*, 2012, **7**, 966.
142 X. J. Feng, W. Z. Zhou, Y. G. Li, H. S. Ke, J. K. Tang, R. Clérac, Y. H. Wang, Z. M. Su and E. B. Wang, *Inorg. Chem.*, 2012, **51**, 2722.
143 X. K. Fang, K. McCallum, H. D. Pratt, T. M. Anderson, K. Dennis and M. Luban, *Dalton Trans.*, 2012, **41**, 9867.
144 A. H. Ismail, B. S. Bassil, G. H. Yassin, B. Keita and U. Kortz, *Chem. – Eur. J.*, 2012, **18**, 6163.
145 D.-Y. Shi, J.-W. Zhao, L.-J. Chen, P.-T. Ma, J.-P. Wang and J.-Y. Niu, *CrystEngComm*, 2012, **14**, 3108.
146 J. D. Compain, K. Nakabayashi and S. Ohkoshi, *Inorg. Chem.*, 2012, **51**, 4897.
147 J. W. Zhao, J. Luo, L. J. Chen, J. Yuan, H. Y. Li, P. T. Ma, J. P. Wang and J. Y. Niu, *CrystEngComm*, 2012, **14**, 7981.
148 S. Yao, J.-H. Yan, Y.-C. Yu and E.-B. Wang, *Inorg. Chem. Commun.*, 2012, **23**, 70.
149 H.-H. Wu, S. Yao, Z.-M. Zhang, Y.-G. Li, Y. Song, Z.-J. Liu, X.-B. Han and E.-B. Wang, *Dalton Trans.*, 2013, **42**, 342.
150 H.-Y. Zhao, J.-W. Zhao, B.-F. Yang, H. He and G.-Y. Yang, *CrystEngComm*, 2013, **15**, 5209.
151 J. W. Zhao, D. Y. Shi, L. J. Chen, P. T. Ma, J. P. Wang, J. Zhang and J. Y. Niu, *Cryst. Growth Des.*, 2013, **13**, 4368.
152 H.-Y. Zhao, J.-W. Zhao, B.-F. Yang, H. He and G.-Y. Yang, *CrystEngComm*, 2013, **15**, 8186.
153 H.-Y. Zhao, J.-W. Zhao, B.-F. Yang, H. He and G.-Y. Yang, *Cryst. Growth Des.*, 2013, **13**, 5169.
154 T.-T. Yu, H.-Y. Ma, C.-J. Zhang, H.-J. Pang, S.-B. Li and H. Liu, *Dalton Trans.*, 2013, **42**, 16328.
155 Y.-Y. Li, J.-W. Zhao, Q. Wei, B.-F. Yang, H. He and G.-Y. Yang, *Chem. – Asian J.*, 2014, **9**, 858.
156 J. Luo, J. W. Zhao, J. Yuan, Y. Z. Li, L. J. Chen, P. T. Ma, J. P. Wang and J. Y. Niu, *Inorg. Chem. Commun.*, 2013, **27**, 13.
157 J. L. Zhang, J. Li, L. J. Li, H. Z. Zhao, P. T. Ma, J. W. Zhao and L. J. Chen, *Spectrochim. Acta, Part A*, 2013, **114**, 360.
158 Y. Y. Li, S. B. Tian, Y. Z. Li, J. W. Zhao, P. T. Ma and L. J. Chen, *Inorg. Chim. Acta*, 2013, **405**, 105.
159 H.-J. Pang, C. J. Gómez-García, J. Peng, H.-Y. Ma, C.-J. Zhang and Q.-Y. Wu, *Dalton Trans.*, 2013, **42**, 16596.
160 J. Wang, J.-W. Zhao, H.-Y. Zhao, B.-F. Yang, H. He and G.-Y. Yang, *CrystEngComm*, 2014, **16**, 252.
161 H.-Y. Zhao, J.-W. Zhao, B.-F. Yang, H. He and G.-Y. Yang, *CrystEngComm*, 2014, **16**, 2230.
162 J.-W. Zhao, J. Cao, Y.-Z. Li, J. Zhang and L.-J. Chen, *Cryst. Growth Des.*, 2014, **14**, 6217.
163 D. Liu, Y. Lu, H.-Q. Tan, T.-T. Wang and E.-B. Wang, *Cryst. Growth Des.*, 2015, **15**, 103.
164 H.-Y. An, Y. Hu, L. Wang, E.-L. Zhou, F. Fei and Z.-M. Su, *Cryst. Growth Des.*, 2015, **15**, 164.
165 J.-W. Zhao, Y.-Z. Li, F. Ji, J. Yuan, L.-J. Chen and G.-Y. Yang, *Dalton Trans.*, 2014, **43**, 5694.
166 Y.-Z. Chen, Z.-J. Liu, Z.-M. Zhang, H.-Y. Zhou, X.-T. Zheng and E.-B. Wang, *Inorg. Chem. Commun.*, 2014, **46**, 155.
167 Y. Lü, Y.-G. Chen and X.-M. Li, *Inorg. Chem. Commun.*, 2014, **45**, 33.
168 L. J. Chen, F. Zhang, X. Ma, J. Luo and J. W. Zhao, *Dalton Trans.*, 2015, **44**, 12598.
169 L. J. Chen, J. Cao, X. H. Li, X. Ma, J. Luo and J. W. Zhao, *CrystEngComm*, 2015, **17**, 5002.
170 (*a*) P. J. Hagrman, D. Hagrman and J. Zubietua, *Angew. Chem., Int. Ed.*, 1999, **38**, 2638; (*b*) J.-W. Zhao, H.-P. Jia, J. Zhang, S.-T. Zheng and G.-Y. Yang, *Chem. – Eur. J.*, 2007, **13**, 10030; (*c*) J. Gopalakrishnan, *Chem. Mater.*, 1995, **7**, 1265; (*d*) D. Hagrman, C. Sangregorio, C. J. O'Connor and J. Zubieta, *J. Chem. Soc., Dalton Trans.*, 1998, 3707; (*e*) H. Jin, Y. Qi, E. Wang, Y. Li, C. Qin, X. Wang and S. Chang, *Eur. J. Inorg. Chem.*, 2006, 4541; (*f*) A. Rabenau, *Angew. Chem., Int. Ed. Engl.*, 1985, **24**, 1026.
171 R. D. Peacock and T. J. R. Weakley, *J. Chem. Soc. A*, 1971, 1836.
172 U. Kortz, G. S. Masha, S. B. Bassem and H. D. Michael, *Angew. Chem., Int. Ed.*, 2001, **18**, 2284.
173 U. Kortz, M. G. Savelieff, B. S. Bassil, B. Keita and L. Nadjo, *Inorg. Chem.*, 2002, **41**, 783.
174 M. Bösing, I. Loose, H. Pohlmann and B. Krebs, *Chem. – Eur. J.*, 1997, **3**, 1232.
175 T. J. R. Weakley, H. T. J. Evans, J. S. Showell, G. F. Tourné and C. M. Tourné, *J. Chem. Soc., Chem. Commun.*, 1973, 139.
176 X. Zhang, T. M. Anderson, Q. Chen and C. L. Hill, *Inorg. Chem.*, 2011, **40**, 418.

177 T. M. Anderson, X. Zhang, K. I. Hardcastle and C. L. Hill, *Inorg. Chem.*, 2002, **41**, 2477.
178 U. Kortz, I. M. Mbomekalle, B. Keita, L. Nadjo and P. Berthet, *Inorg. Chem.*, 2002, **41**, 6412.
179 L. Ruhlmann, J. Canny, R. Contant and R. Thouvenot, *Inorg. Chem.*, 2002, **41**, 3811.
180 I. M. Mbomekalle, B. Keita, M. Nierlich, U. Kortz, P. Berthet and L. Nadjo, *Inorg. Chem.*, 2003, **42**, 5143.
181 I. M. Mbomekalle, B. Keita, L. Nadjo, W. A. Neiwert, L. Zhang, K. I. Hardcastle, C. L. Hill and T. M. Anderson, *Eur. J. Inorg. Chem.*, 2003, 3924.
182 L. Ruhlmann, J. Canny, J. Vaissermann and R. Thouvenot, *Dalton Trans.*, 2004, 794.
183 Y. Hou, L. Xu, M. J. Cichon, S. Lense, K. I. Hardcastle and C. L. Hill, *Inorg. Chem.*, 2010, **49**, 4125.
184 U. Kortz, S. Nellutla, A. C. Stowe, N. S. Dalal, U. Rauwald, W. Danquah and D. Ravot, *Inorg. Chem.*, 2004, **43**, 2308.
185 T. Lis, *Acta Crystallogr., Sect. B: Struct. Crystallogr. Cryst. Chem.*, 1980, **36**, 2042.
186 A. J. Tasiopoulos, T. A. O'Brien, K. A. Abboud and G. Christou, *Angew. Chem., Int. Ed.*, 2004, **43**, 345.
187 A. J. Tasiopoulos, P. L. Milligan, Jr., K. A. Abboud, T. A. O'Brien and G. Christou, *Inorg. Chem.*, 2007, **46**, 9678.
188 B. Godin, Y.-G. Chen, J. Vaissermann, L. Ruhlmann, M. Verdaguer and P. Gouzerh, *Angew. Chem., Int. Ed.*, 2005, **44**, 3072.
189 S. S. Mal and U. Kortz, *Angew. Chem., Int. Ed.*, 2005, **44**, 3777.
190 M. Zimmermann, N. Belai, R. J. Butcher, M. T. Pope, E. V. Chubarova, M. H. Dickman and U. Kortz, *Inorg. Chem.*, 2007, **46**, 1737.
191 M. H. Alizadeh, S. P. Harmalker, Y. Jeannin, J. Martin-Frère and M. T. Pope, *J. Am. Chem. Soc.*, 1985, **107**, 2662.
192 F. Hussain, U. Kortz, B. Keita, L. Nadjo and M. T. Pope, *Inorg. Chem.*, 2006, **45**, 761.
193 Z. M. Zhang, S. Yao, Y. G. Li, Y. H. Wang, Y. F. Qi and E. B. Wang, *Chem. Commun.*, 2008, 1650.
194 Z. M. Zhang, S. Yao, Y. F. Qi, Y. G. Li, Y. H. Wang and E. B. Wang, *Dalton Trans.*, 2008, 3051.
195 R. Contant and A. Tézé, *Inorg. Chem.*, 1985, **24**, 4610.
196 S. Q. Liu, D. G. Kurthe, H. Möhwald and D. Volkmer, *Adv. Mater.*, 2002, **14**, 225.
197 S. Cardona-Serra, J. M. Clemente-Juan, E. Coronado, A. Gaita-Ariño, A. Camón, M. Evangelisti, F. Luis, M. J. Martínez-Pérez and J. Sesé, *J. Am. Chem. Soc.*, 2012, **134**, 14982.
198 M. Rahimizadeh, T. Bazazan, A. Shiri, M. Bakavoli and H. Hassani, *Chin. Chem. Lett.*, 2011, **22**, 435.
199 C. Preyssler, *Bull. Soc. Chim. Fr.*, 1970, 30.
200 M. Filowitz, R. K. C. Ho, W. G. Klemperer and W. Shum, *Inorg. Chem.*, 1979, **18**, 93.
201 V. Shivaiah, M. Nagaraju and S. K. Das, *Inorg. Chem.*, 2003, **42**, 6604.
202 G. A. Tsigdinos, PhD thesis, Boston University, 1961.
203 A. L. Nolan, R. C. Burns and G. A. Lawrance, *Dalton Trans.*, 1996, 2629.
204 U. Lee and H. C. Joo, *Acta Crystallogr., Sect. E: Struct. Rep. Online*, 2010, **66**, i10.
205 P. Mialane, A. Dolbecq, L. Lisnard, A. Mallard, J. Marrot and F. Sécheresse, *Angew. Chem., Int. Ed.*, 2002, **41**, 2398.
206 C. M. Flynn and M. T. Pope, *J. Am. Chem. Soc.*, 1969, **92**, 85.
207 *Polyoxometalate Chemistry: From Topology via Self-Assembly to Applications*, ed. M. T. Pope and A. Müller, Kluwer, Dordrecht, The Netherlands, 2001.
208 *Comprehensive Coordination Chemistry II*, ed. J. A. McCleverty and T. J. Meyer, Elsevier Ltd, Oxford, UK, 2004.
209 O. Kahn, *Adv. Inorg. Chem.*, 1995, **43**, 179.
210 A. C. Rizzi, R. Calvo, R. Baggio, M. T. Garland, O. Peña and M. Perec, *Inorg. Chem.*, 2002, **41**, 5609.
211 T. Sanada, T. Suzuki, T. Yoshida and S. Kaizaki, *Inorg. Chem.*, 1998, **37**, 4712.
212 R. E. P. Winpenny, *Chem. Soc. Rev.*, 1998, **27**, 447.
213 J. P. Costes, F. Dahan, A. Dupuis and J. P. Laurent, *Inorg. Chem.*, 1997, **36**, 3429.
214 A. Figuerola, J. Ribas, M. LIunell, D. Casanova, M. Maestro, S. Alvarez and C. Diaz, *Inorg. Chem.*, 2005, **44**, 6939.
215 M. Li, Y. Lan, A. M. Ako, W. Wernsdorfer, C. E. Anson, G. Buth, A. K. Powell, Z. Wang and S. Gao, *Inorg. Chem.*, 2010, **49**, 11587.
216 M. L. Kahn, J. Sutter, S. Golhen, P. Guionneau, L. Ouahab, O. Kahn and D. Chasseau, *J. Am. Chem. Soc.*, 2000, **122**, 3413.
217 C. Benelli and D. Gatteschi, *Chem. Rev.*, 2002, **102**, 2369.
218 X.-Y. Zhang, C. J. O'Connor, G. B. Jameson and M. T. Pope, *Inorg. Chem.*, 1996, **35**, 30.
219 P. Mialane, C. Duboc, J. Marrot, E. Rivière, A. Dolbecq and F. Sécheresse, *Chem. – Eur. J.*, 2006, **12**, 1950.
220 Z. Zhang, E. Wang, W. Chen and H. Tan, *Aust. J. Chem.*, 2007, **60**, 284.
221 Q. Wu, Y.-G. Li, Y.-H. Wang, E.-B. Wang, Z.-M. Zhang and R. Clérac, *Inorg. Chem.*, 2009, **48**, 1606.
222 R. Sessoli, D. Gatteschi, A. Caneschi and M. A. Novak, *Nature*, 1993, **365**, 141.
223 D. Gatteschi and R. Sessoli, *Angew. Chem., Int. Ed.*, 2003, **42**, 268.
224 H. Oshio, M. Nihei, A. Yoshida, H. Nojiri, M. Nakano, A. Yamaguchi, Y. Karaki and H. Ishimoto, *Chem. – Eur. J.*, 2005, **11**, 843.
225 P. Zhang, Y. N. Guo and J. K. Tang, *Coord. Chem. Rev.*, 2013, **257**, 1728.
226 M. A. AlDamen, J. M. Clemente-Juan, E. Coronado, C. MartíGastaldo and A. Gaita-Ariño, *J. Am. Chem. Soc.*, 2008, **130**, 8874.
227 M. A. AlDamen, S. J. Cardona-Serra, M. Clemente-Juan, E. Coronado, A. Gaita-Ariño, C. Martí-Gastaldo, F. Luis and O. Montero, *Inorg. Chem.*, 2009, **48**, 3467.
228 C. Ritchie, A. Ferguson, H. Nojiri, H. N. Miras, Y. F. Song, D. L. Long, E. Burkholder, M. Murrie, P. Kögerler, E. K. Brechin and L. Cronin, *Angew. Chem., Int. Ed.*, 2008, **47**, 5609.
229 J. D. Compain, P. Mialane, A. Dolbecq, I. M. Mbomekallé, J. Marrot, F. Sécheresse, E. Rivière, G. Rogez and W. Wernsdorfer, *Angew. Chem., Int. Ed.*, 2009, **48**, 3077.
230 X. K. Fang, M. Speldrich, H. Schilder, R. Cao, K. P. O'Halloran, C. L. Hill and P. Kögerler, *Chem. Commun.*, 2010, **46**, 2760.
231 M. Ibrahim, Y. Lan, B. S. Bassil, Y. X. Xiang, A. Suchopar, A. K. Powell and U. Kortz, *Angew. Chem., Int. Ed.*, 2011, **50**, 4708.
232 C. Ritchie, M. Speldrich, R. W. Gable, L. Sorace, P. Kögerler and C. Boskovic, *Inorg. Chem.*, 2011, **50**, 7004.
233 J. P. Costes, F. Dahan and W. Wernsdorfer, *Inorg. Chem.*, 2006, **45**, 5.
234 J. P. Costes, M. Auchel, F. Dahan, V. Peyrou, S. Shova and W. Wernsdorfer, *Inorg. Chem.*, 2006, **45**, 1924.
235 S. Osa, T. Kido, N. Matsumoto, N. Re, A. Pochaba and J. Mrozinski, *J. Am. Chem. Soc.*, 2004, **126**, 420.
236 T. Kajiwara, M. Nakano, S. Takaishi and M. Yamashita, *Inorg. Chem.*, 2008, **47**, 8604.
237 Y. J. Cui, Y. F. Yue, G. D. Qian and B. L. Chen, *Chem. Rev.*, 2012, **112**, 1126.
238 S. V. Eliseeva and J. C. G. Bunzli, *Chem. Soc. Rev.*, 2010, **39**, 189.
239 L. D. Carlos, R. A. S. Ferreira, V. de Zea Bermudez, B. Julián-López and P. Escribano, *Chem. Soc. Rev.*, 2011, **40**, 536.
240 L. Armelao, S. Quici, F. Barigelletti, G. Accorsi, G. Bottaro, M. Cavazzini and E. Tondello, *Coord. Chem. Rev.*, 2010, **254**, 487.
241 J. C. G. Buünzli and C. Piguet, *Chem. Soc. Rev.*, 2005, **34**, 1048.
242 G. J. Sopasis, M. Orfanoudaki, P. Zarmpas, A. Philippidis, M. Siczek, T. Lis, J. R. O'Brien and C. J. Milios, *Inorg. Chem.*, 2012, **51**, 1170.
243 Y. Li, F.-K. Zheng, X. Liu, W.-Q. Zou, G.-C. Gou, C.-Z. Lu and J.-S. Huang, *Inorg. Chem.*, 2006, **45**, 6308.
244 C. Ritchie, V. Baslon, E. G. Moore, C. Reber and C. Boskovic, *Inorg. Chem.*, 2012, **51**, 1142.
245 T. Yamase, T. Kobayashi, M. Sugeta and H. Naruke, *J. Phys. Chem. A*, 1997, **101**, 5046.
246 T. Yamase and H. Naruke, *J. Chem. Soc., Dalton Trans.*, 1991, 285.
247 I. Creaser, M. C. Heckel, R. J. Neitz and M. T. Pope, *Inorg. Chem.*, 1993, **32**, 1573.
248 X. Wang, Y. Guo, Y. Li, E. Wang, C. Hu and N. Hu, *Inorg. Chem.*, 2003, **42**, 4135.
249 T. Zhang, C. Spitz, M. Antonietti and C. F. J. Faul, *Chem. – Eur. J.*, 2005, **11**, 1001.
250 A. F. Kirby and F. S. Richardson, *J. Phys. Chem.*, 1983, **87**, 2544.
251 J. W. Stouwdam and F. C. J. M. van Veggel, *Nano Lett.*, 2002, **2**, 733.
252 T. Ito, H. Yashiro and T. Yamase, *Langmuir*, 2006, **22**, 2806.
253 T. Yamase and H. Naruke, *J. Phys. Chem. B*, 1999, **103**, 8850.
254 C. Ritchie, E. G. Moore, M. Speldrich, P. Kögerler and C. Boskovic, *Angew. Chem., Int. Ed.*, 2010, **49**, 7702.
255 J. E. Toth and F. C. Anson, *J. Am. Chem. Soc.*, 1989, **111**, 2444.
256 X.-L. Wang, Z.-H. Kang, E.-B. Wang and C.-W. Hu, *Mater. Lett.*, 2002, **56**, 393.

257 Z. Zhang, Y. Qi, C. Qin, Y. Li, E. Wang, X. Wang, Z. Su and L. Xu, *Inorg. Chem.*, 2007, **46**, 8162.
258 X. Wang, E. Wang, Y. Lan and C. Hu, *Electroanalysis.*, 2002, **14**, 1116.
259 R. Neumann and M. Gara, *J. Am. Chem. Soc.*, 1995, **117**, 5066.
260 B. Keita, P. Mialane, F. Sécheresse, P. Oliveira and L. Nadjo, *Electrochem. Commun.*, 2007, **9**, 164.
261 M. Sadakane, M. H. Dickman and M. T. Pope, *Inorg. Chem.*, 2001, **40**, 2715.
262 F. L. Sousa, F. A. Almeida, A. M. V. Cavaleiro, J. Klinowski and H. I. S. Nogueira, *Chem. Commun.*, 2004, 2656.
263 A. M. Todea, A. Merca, H. Bögge, J. V. Slageren, M. Dressel, L. Engelhardt, M. Luban, T. Glaser, M. Henry and A. Müller, *Angew. Chem., Int. Ed.*, 2007, **46**, 6106.
264 L. H. Bi, U. Kortz, S. Nellutla, A. C. Stowe, J. Tol, N. S. Dalal, B. Keita and L. Nadjo, *Inorg. Chem.*, 2005, **44**, 896.
265 B. Keita, Y. W. Lu, L. Nadjo and R. Contant, *Electrochem. Commun.*, 2000, **2**, 720.
266 N. Anwar, M. Vagin, F. Laffir, G. Armstrong, C. Dickinson and T. McCormac, *Analyst*, 2012, **137**, 624.
267 (*a*) H. Fu, Y. G. Li, Y. Lu, W. L. Chen, Q. Wu, J. X. Meng, X. L. Wang, Z. M. Zhang and E. B. Wang, *Cryst. Growth Des.*, 2011, **11**, 458; (*b*) C. C. Chen, W. Zhao, P. X. Lei, J. C. Zhao and N. Serpone, *Chem. – Eur. J.*, 2004, **10**, 1956; (*c*) Q. Wu, W. L. Chen, D. Liu, C. Liang, Y. G. Li, S. W. Lin and E. B. Wang, *Dalton Trans.*, 2011, **40**, 56; (*d*) W. L. Chen, B. W. Chen, H. Q. Tan, Y. G. Li, Y. H. Wang and E. B. Wang, *J. Solid State Chem.*, 2010, **183**, 310.